İSTANBUL TECHNICAL UNIVERSITY ★ INSTITUTE OF SCIENCE AND TECHNOLOGY

INTERACTIVE COMPUTER-AIDED CONTROLLER DESIGN FOR MECHATRONIC SYSTEMS

M.Sc. Thesis by
Burak DEMİREL

Department : Mechatronics Engineering

Programme : Mechatronics Engineering

Thesis Supervisor: Prof. Dr. Levent GÜVENÇ

SEPTEMBER 2009

İSTANBUL TECHNICAL UNIVERSITY ★ INSTITUTE OF SCIENCE AND TECHNOLOGY

INTERACTIVE COMPUTER-AIDED CONTROLLER DESIGN FOR MECHATRONIC SYTEMS

M.Sc. Thesis by
Burak DEMİREL
(518071005)

Date of submission : 25 September 2009
Date of defence examination: 29 September 2009

Supervisor (Chairman) : Prof. Dr. Levent GÜVENÇ (ITU)
Members of the Examining Committee : Assis. Prof. Dr. Ümit SÖNMEZ (ITU)
Prof. Dr. Elbrus CAFEROV (ITU)

SEPTEMBER 2009

İSTANBUL TEKNİK ÜNİVERSİTESİ ★ FEN BİLİMLERİ ENSTİTÜSÜ

MEKATRONİK SİSTEMLER İÇİN İNTERAKTİF BİLGİSAYAR DESTEKLİ KONTROLCÜ TASARIMI

YÜKSEK LİSANS TEZİ
Burak DEMİREL
(518071005)

Tezin Enstitüye Verildiği Tarih : 25 Eylül 2009
Tezin Savunulduğu Tarih : 29 Eylül 2009

Tez Danışmanı : Prof. Dr. Levent GÜVENÇ (İTÜ)
Diğer Jüri Üyeleri : Yrd. Doç. Dr. Ümit SÖNMEZ (İTÜ)
Prof. Dr. Elbrus CAFEROV (İTÜ)

EYLÜL 2009

FOREWORD

First of all, I would like to express my deep appreciation and sincere thanks to my advisor, Prof. Dr. Levent Güvenç, for his constant guidance and support throughout the course of this research. He introduced me to the area of parameter space analysis of linear systems and the advanced control techniques in Mechatronics and also taught me most of the subjects in this thesis. I have greatly benefited from him as a role-model of an excellent teacher and researcher.

I would like also to thank Yrd. Doç. Dr Ümit Sönmez, Prof. Dr. İbrahim Eksin and Yrd. Doç. Dr. Osman Kaan Erol who have played an important role in my personal and scientific life. Special thanks to all member of the Mechatronics Research Laboratories (MEKAR) for their friendship, support, and creating pleasant working environment. I also want to thank Mr. Mümin Tolga Emirler for his valuable comments on this thesis and helping me to draw some figures in this thesis.

Additionally, I would like to acknowledge the financial support from the Scientific and Technical Research Council of Turkey (TÜBİTAK) under the National Scholarship Programme for Master of Science Students and thank the all program managers.

Finally, I would like to thank my parents Şükrü and Bahar for their support and patience, and my brother Serdar for his never-ending helps.

September 2009

Burak Demirel

Mechatronics Engineering

TABLE OF CONTENTS

Page

ABBREVIATIONS

AFM : Atomic Force Microscope
BIBO : Boundary-Input-Boundary-Output
CRB : Complex Root Boundary
GM : Gain Margin
GUI : Graphical User Interface
IMP : Internal Model Principle
IRB : Infinity Root Boundary
LTI : Linear Time Invariant
MIMO : Multi-Input-Multi-Output
MP : Minimum Phase
NMP : Non-minimum Phase
OPTC : Optimal Precision Tracking Controller
PD : Proportional-plus-Derivative
PI : Proportional-plus-Integral
PID : Proportional-plus-Integral-plus-Derivative
PM : Phase Margin
PTC : Precision Tracking Controller
RRB : Real Root Boundary
SISO : Single-Input-Single-Output
ZPET : Zero Phase Error Tracking

LIST OF TABLES

Page

LIST OF FIGURES

Page

INTERACTIVE COMPUTER–AIDED CONTROLLER DESIGN FOR MECHATRONIC SYSTEMS

SUMMARY

A novel interactive software tool based on MATLAB to analyze and design of controllers for mechatronic systems is presented in this master thesis. The toolbox includes four different control strategies such as classical control, preview control, model regulator control and repetitive control. The synthesis technique behind some of these mentioned strategies is based on mapping Hurwitz stability, *D*-stability or the frequency domain specifications of weighted sensitivity minimization and gain/phase margin bound to the chosen controller parameter space.

In classical control, we can use both parametric robust control techniques and analytical solution procedure. As distinct from abovementioned robust control method, the analytical solution procedure used to design classical controllers like lead, lag, lead-lag compensator in frequency domain is basically relied on the analytical solution of phase margin design. By this way, the unique controller parameters can be calculated for the desired crossover frequency and phase margin.

In preview control, we deal with synthesis of three different kinds of discrete-time feedforward controllers such as zero phase error tracking (ZPET) controller, precision tracking controller (PTC) and optimal precision tracking controller (OPTC). The parameters of ZPET and PTC are calculated by using some symbolic manipulations in this work. Besides, we benefit from the Big-Bang Big-Crunch optimization method to minimize the cost function when designing OPTC.

To design both model regulator and repetitive control, we use a design method based on mapping a frequency domain mixed sensitivity bound into chosen controller parameter space. The solution procedure results in graphical solution regions (2-D plots with colour filling showing where the specifications are met) in controller parameter space. Hence, the user can focus on analyzing the graphical results without making some tedious calculations.

The effectiveness of proposed methods was demonstrated by carrying out a design and simulation study for several examples and case studies.

MEKATRONİK SİSTEMLER İÇİN İNTERAKTİF BİLGİSAYAR DESTEKLİ KONTROLCÜ TASARIMI

ÖZET

Bu yüksek lisans tezinde mekatronik sistemler için kontrolcü tasarımında ve analizinde kullanılmak üzere geliştirilen MATLAB tabanlı interaktif bir yazılım anlatılmıştır. Bu MATLAB tabanlı yazılım; klasik kontrol, öngörülü kontrol, model regülasyonu kontrolü ve tekrarlamalı kontrol gibi kontrol stratejilerini içermektedir. Bu belirtilen kontrol stratejilerinin temelindeki sentez tekniği, Hurwitz karalılığına, *D*-karalılığına veya ağırlıklandırılmış duyarlılık minimizasyonunun frekans tanım bölgesindeki özelliklerine ve seçili kontrolcü parametre uzayındaki genlik/faz kazancının sınırına dayalı olarak gerçekleştirilmiştir.

Klasik kontrolcü tasarımında, hem parametrik dayanıklı (robust) kontrol teknikleri hem de frekans tanım bölgesinde tasarım için analitik çözüm prosedürü kullanılmıştır. Yukarıda belirtilenin dayanıklı kontrol metodu haricinde, frekans tanım bölgesine bağlı analitik çözüm tekniği faz ilerlemeli, faz gerilemeli ve faz ilerlemeli-gerilemeli kompanzatör tasarımında kullanılmıştır. Bu frekans tanım bölgesindeki tasarım temel olarak faz kazancı tasarımının analitik çözümüne dayanmaktadır. Bu yolla kontrol parametreleri kazanç eğrisinin kesim frekansı ve faz kazancı için tasarlanmıştır.

Öngörülü kontrolcü tasarımında, üç farklı ayrık zamanlı ileri yol kontrolcü sentezi ile uğraşılmıştır. Bu kontrolcüler, sıfır faz hatası takipli kontrolcü (ZPET), hassas takipli kontrolcü (PTC) ve optimal hassas takipli kontrolcü (OPTC)'dir. Bu çalışmada ZPET ve PTC'nin parametreleri sembolik manipülasyonlar kullanılarak hesaplanmıştır. Bununla birlikte, OPTC tasarlanırken amaç fonksiyonu minimize edecek parametre değeri Büyük Patlama Büyük Çökme optimizasyon yöntemiyle elde edilmiştir.

Hem model regülatörü hem de tekrarlamalı kontrolcü tasarlanırken, frekans tanım bölgesindeki robust performans sınırlarını seçili kontrolcü parametre uzayına eşleştirilmesine dayalı bir tasarım metodu kullanılmıştır. Çözüm prosedürüyle kontrolcü parametre uzayında grafiksel çözüm bölgeleri elde edilmiştir. Böylece can sıkıcı hesaplamalarla uğraşmadan grafiksel sonuçların analizine odaklanılabilinir.

Önerilen yöntemlerin etkinliğini, çeşitli örnek ve durum çalışmaları için yürütülen tasarım ve benzetim çalışmalarıyla gösterilmiştir.

1. INTRODUCTION

1.1 Background

Rapid developing societies produce new challenges requiring novel engineering approaches. Engineers must overcome such challenges and also provide more effective solutions to classical and latest engineering problems. This can be achieved by utilizing different relevant advances produced in technology. Moreover, a new way of addressing the engineering problems has to be applied, not considering only isolated engineering specialities. In this context, it can be considered of the creation of a novel engineering philosophy, namely called Mechatronics.

Mechatronics is the synergetic combination of mechanical systems, electronics, control systems and computers (see Figure 1.1) [1]. Its name comes from the combination of two words: MECHAnics and ElecTRONICS[1]. The most important element in mechatronics is the integration of these areas through the design process. An industrial robot system is a prime example of a mechatronic system including aspects of mechanics, electronics and computing [1]. Mechatronic systems play an important role in many different business sectors like automotive systems, aerospace systems, medical, materials processing, manufacturing process, defence systems, chemical systems and consumer products [2].

The fundamental characteristic of mechatronics engineering and the key for being successful in mechatronic researches is to establish a balance between two sets of skills: modelling/analysis skills and experimentation/hardware implementation skills. In this thesis, we focus on totally improving the modelling/analysis skills. For this purpose, Control of Mechatronic Systems (COMES) Toolbox has been developed as a toolbox for MATLAB and aims being a user-friendly and user-extensible, software-based, mathematical analysis framework for control of mechatronic systems. This toolbox includes five different kinds of control methodology, which are widely used in mechatronic systems, like classical control, preview control,

[1] The term of "Mechatronics" was firstly created by Tetsuro Mori and Jiveshwar Sharma, who are the senior engineers of the Japanese company and American company in 1969 [1].

model regulator control, repetitive control and a multi-objective parameter space approach to robust control (including Hurwitz stability, *D*-stability, mapping frequency domain bounds, phase/gain margin). The final one (parameter space approach to robust control approach) is a general control strategy and it can be quietly applied to many different types of linear control systems (whose uncontrolled plant order is not important). These control systems can be used alone or can be used all in one. The general block diagram including the all advanced control techniques can be seen in Figure 1.2. In some applications, the combination of these control systems is able to perform an additional improvement to the performance of mechatronic systems. Additionally, the reader can check the explanation of abovementioned control methodologies and their well-known application areas of these control systems in the following chapters.

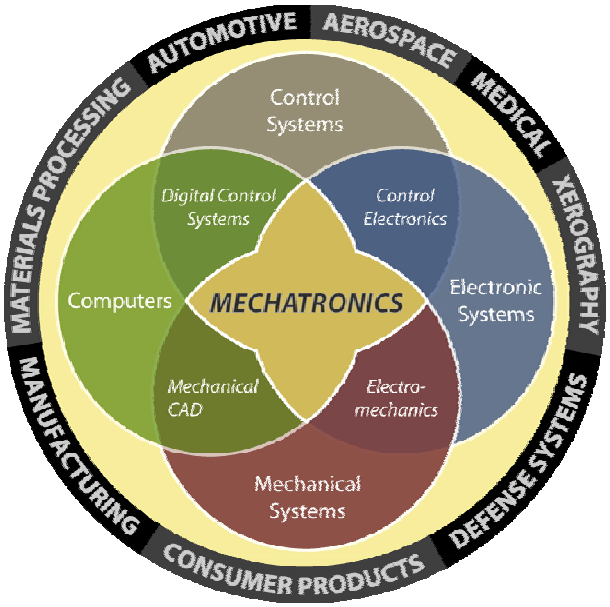

Figure 1.1 : Venn diagram of mechatronics, [1].

The COMES toolbox offers mechatronic engineers and control engineers an open and extensible environment, where to explore ideas, prototype and share new algorithms, and build applications for the analysis and simulation of mechatronic systems. Additionally, it is well suited for educational purpose. We are thinking of these tools to be a nice complement to text books and laboratories. The students are able to improve both their design skills and insight in control theory. Furthermore, these tools allow students to work at home or at their own place. We illustrate their use in the classical assignment of modelling, analysis, and design for various courses in automatic control. Until recently, many tools for control education and

engineering design have been developed for several years. Some of original works on computer-aided control engineering can be listed as follows. Schaufelberger and his team [3] have developed many interesting idea about the computer-aided education in the field of automatic control at ETH Zürich. Johansson et al [4] have developed an interactive design tool, which aims to design classical controllers like lead, lag or lead-lag compensator, in order to use in automatic control education. Additionally, Azemi et al [5] have gathered the all programs that are used in teaching the optimal control course and prepared a toolbox for MATLAB to design optimal controllers. Instead of the use of computer-aided control system design in the educational manner, they can be utilized to solve real engineering problems. Let us give you several examples about this use of toolboxes. Sienel et al [6] have created an interactive MATLAB-based robust control toolbox called PARADISE in order to design and analysis control systems by means of using the parameter space approaches to robust control. Similarly, Sakabe et al [7] have developed a MATLAB-based toolbox to design robust controller based on parameter space approach. Hyodo et al [8] have also improved the MATLAB-based toolbox for parametric robust control. In reference [9], a robust control toolbox which combines Robust Control Toolbox, LMI and μ-Analysis and Synthesis Toolbox is given. Vivero and Castro [10] have introduced novel software for MATLAB to analyze and design multivariable control systems. Boyle et al [11] have designed an interactive design program for the frequency domain analysis and design of multivariable feedback systems to be utilized with PC-MATLAB or Pro-MATLAB. Campa et al [12] have created a new multivariable design program for linear systems analysis and robust control synthesis.

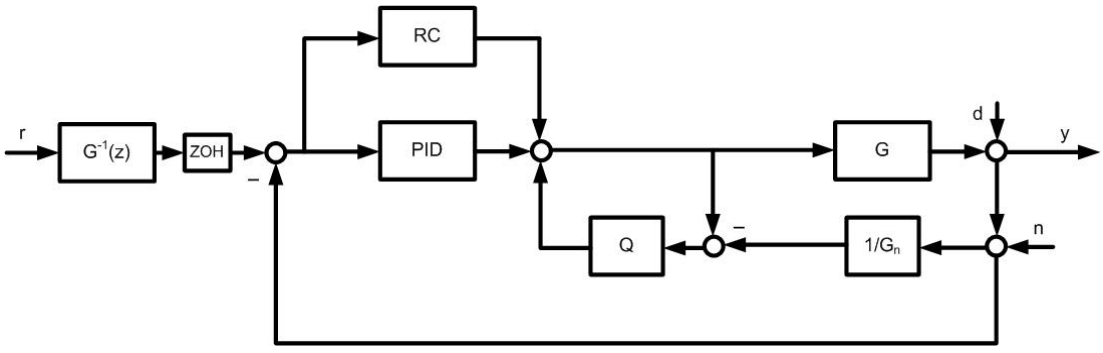

Figure 1.2 : The general block diagram of control systems including all advanced control techniques for mechatronics.

1.2 Thesis Overview and Contribution

The objective of this thesis is to develop an interactive MATLAB program with a graphical user interface (GUI) to synthesize various advanced control systems techniques for mechatronic systems. This toolbox includes four different type of control architecture such as classical control, preview control, model regulator control and repetitive control. Moreover, the core infrastructure of the novel toolbox is generally based on the parameter space approach to robust control. Using abovementioned parameter space methodology, the all kind of controller can be robustly designed instead of preview control because it is basically relied on a different strategy. The novel toolbox can also provide both powerful numerical and symbolic analysis methods to design chosen type of controller with desired specifications. Additionally, the toolbox enables the user to access easily all data and data structures. Thus, the desired data can be taken from the MATLAB workspace to use in a new assignment.

The content and contribution of respective chapters are outlined below.

Chapter 2 presents a brief review of classical (conventional) control techniques in both time-domain and frequency-domain. In general, trial and error procedure is used when designing a classical controller in frequency-domain. In contrast, the analytical solution procedure in frequency-domain has been developed and analyzed here. In order to demonstrate the ease of this solution procedure, a well-known example from literature is used. Moreover, an interactive MATLAB-based program with graphical user interface (GUI) has been developed to calculate easily the controller parameters of classical controllers like lead, lag, lag-lead, PI, PD and PID. Finally, the advantages and disadvantages of both analytical solution procedure and trial and error procedure are discussed.

Chapter 3 is dedicated to explaining a multi-objective parameter space approach to robust control and developing an interactive design tool based on MATLAB for determining controller parameter space regions corresponding to chosen constraints. In this chapter, robust design based on mapping Hurwitz stability, *D*-stability and the frequency specifications of weighted sensitivity minimization and phase and gain margin bound to a chosen controller parameter space is presented. As a part of multi-objective approach, the solution procedure is repeated for each case and the

intersection of these controller regions are determined. To easily determine the controller region, we have developed a MATLAB toolbox for robust parametric control via parameter space approach based on symbolic computation.

In *Chapter 4*, some basic information on preview control techniques are given, in detail. The need for the approximate inverse of a closed-loop system appears in preview control. Therefore, we have to focus on the non-minimum phase (NMP) zeros because the system's stability can be suffered from the presence of NMP zeros. Additionally, several methods can be used to design non-causal approximate inverse filters for discrete-time systems with NMP zeros such as zero phase error tracking (ZPET) control, precision tracking control (PTC), and optimal precision tracking control (OPTC) are investigated in this chapter. In order to calculate the abovementioned input shaping filters, an interactive program with graphical user interface (GUI) relied on MATLAB is created by the author. Then, these preview control techniques are applied to the tool positioning control problem in noncircular machining to illustrate the preview control methodologies and demonstrate the effectiveness of the COMES toolbox. Finally, it is shown that COMES toolbox is very useful for designing the ZPET, PTC and OPTC controllers. It reduces the design time.

Chapter 5 presents a summary of model regulator (disturbance observer) control systems. Firstly, the general model regulator architecture is given here. Then, robust design based on mapping robust performance frequency domain specifications to chosen disturbance observer parameters is presented. In addition, the front wheel steering-based vehicle yaw stability controller design problem is given as a numerical example in order to illustrate the usefulness of this methodology. COMES toolbox is used to determine the parameter space regions for several operating points. At the end of chapter, the advantages of the disturbance observer and usefulness of interactive MATLAB design tool are discussed.

In *Chapter 6*, we purpose a method to make parameter space design of repetitive controllers for satisfying a mixed sensitivity performance requirements. Firstly, the fundamental elements of repetitive control systems such as time advance, low-pass filter $q(s)$, dynamic compensator $b(s)$ and internal model principle are presented here. Then, the stability of repetitive control system investigated by using regeneration spectrum function and a necessary condition is created. To synthesize a robust

repetitive control system, a general procedure for mapping frequency domain specifications into controller parameter space is given in this chapter. In addition, high-speed atomic force microscope (AFM) scanner position control example is utilized to prove the usefulness and effectiveness of methodology. To determining the controller regions, a MATLAB-based toolbox is designed. Finally, the design steps of the abovementioned methodology are summarized and the advantages of use of this toolbox are discussed.

1.3 COMES: Control of Mechatronic System Toolbox

In this part of thesis, a new toolbox to design advanced control techniques for mechatronic systems is presented. The concept and basic usage of this toolbox is given here but the types of control architectures and how the toolbox can be used to solve the problem for these control architectures are explained in the following chapters. The latest version of COMES toolbox can be downloaded from this website: http://www.itu.edu.tr/~demirelbu. More details and examples can be found at this site and check the user manual for the additional information about toolbox.

1.3.1 Concept

COMES toolbox is an interactive MATLAB program to design advanced control systems for mechatronics. Moreover, this toolbox uses parameter space approaches when being able to design classical (conventional) controller, model regulator (disturbance observer) and repetitive controller. The aim is to design a user-friendly toolbox with graphical user interface (GUI), which hides all calculations from the user as much as possible. Hence, the user can focus on analyzing the graphical results rather than do the all complicated calculations. COMES toolbox uses both symbolic and numerical code to get the benefits from the world.

1.3.2 Architecture

The architecture of COMES toolbox being a Computer-aided Control System Design (CACSD) toolbox is driven by the following objectives: user friendliness, code maintenance and code efficiency. Therefore, the codes of this toolbox can divide into several subdivisions (modules). This shows the modularity of this toolbox. These

modules are also divided into even smaller parts to increase the speed of algorithms. The all individual subdivisions (modules) will be discussed in the following chapters.

1.3.3 Specifications

Our MATLAB toolbox for control of mechatronic systems includes four different kinds of control strategies:

- Classical Control
- Preview Control
- Model Regulator Control
- Repetitive Control

Instead of these control techniques, the toolbox also includes a general control methodology for robust control. Our MATLAB toolbox for robust parametric control synthesis is based on a parameter space approach accomplished by symbolic manipulation. Numerical simulation of frequency-domain characteristics is also available. A typical screenshot of our toolbox is shown Figure 1.3. Current version of our MATLAB toolbox supports robust controller synthesis in terms of following specifications:

- Hurwitz stability
- *D*-stability
- frequency-domain specifications of weighted sensitivity minimization like nominal performance, robust stability and robust performance
- gain/phase margin specification

We can achieve not only a single-objective controller synthesis but also multi-objective controller synthesis among the above specifications based on a parameter space approach accomplished by quantifier elimination.

1.3.4 Working with the toolbox

The main window can be activated at the MATLAB prompt with the command "comes", and then a check is performed of the MATLAB version (that must be 6.5 or greater) and of the presence in MATLAB path of the following toolboxes: Extended

Symbolic Math Toolbox and Mapping Toolbox. If the MATLAB version is lower than 6.5, an error line will occur at the MATLAB prompt.

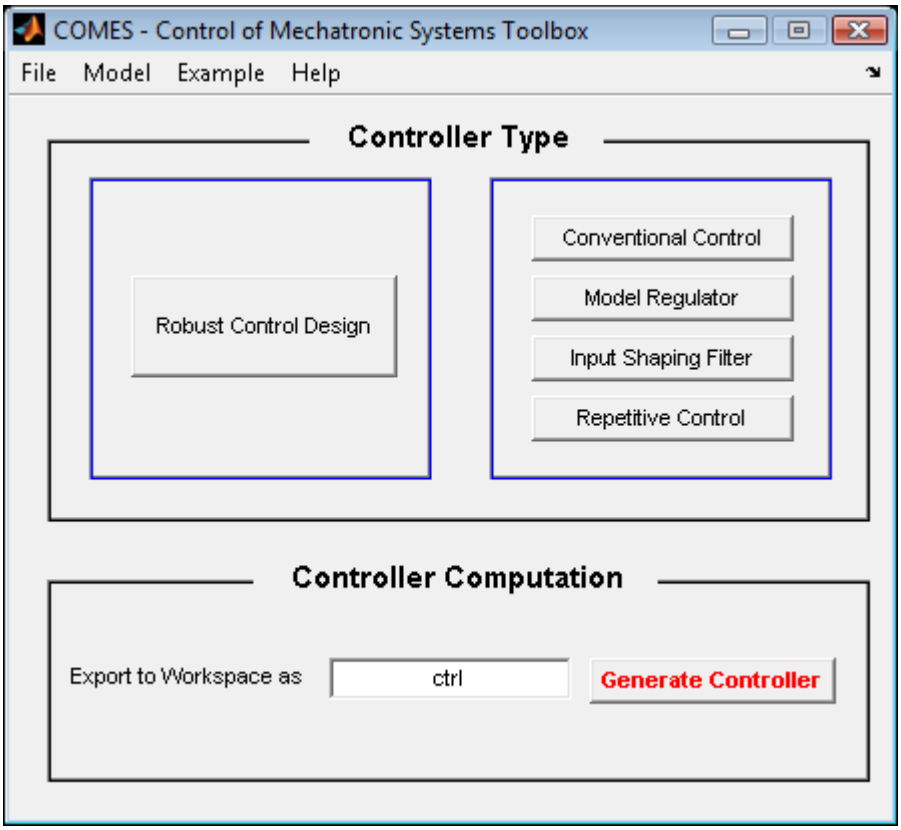

Figure 1.3 : The main window of our MATLAB toolbox.

A typical screenshot of our toolbox can be seen in Figure 1.3. All synthesis and analysis procedure can be achieved by using a GUI conveniently. In "Controller Type" section, four different kinds of control techniques can be chosen in order to design a desired control system. When pressing “Conventional Control” button as an example, the relavent GUI appears. Then, the all calculation can be done via this GUI. Instead of these four control techniques, ther exists another one. This one is the robust control design by using parameter space approach. In this section, symbolic computations required in handling parametric models and reducing design specifications to algebraic constraints are performed by using the "Extended Symbolic Math Toolbox" on MATLAB.

When synthesizing a control system, the data and controller parameters, which are calculated by means of COMES toolbox, are automatically sent to MATLAB workspace as a structure "COMES_wrkspc". The desired data such as controller parameters and parameter space plots can be chosen from this structure.

2. CLASSICAL CONTROL

2.1 Introduction to Classical Control

Classical (conventional) control techniques work best for single-input-single-output (SISO), linear time-invariant (LTI) systems where the required performance specifications are given in the time-domain and/or frequency-domain. In spite of the presence of a large number of advanced control techniques in the literature, classical control methods are widely used in the control of mechatronic systems because they can easily be implemented as real-time systems and their costs are relatively cheaper as compared to these more advanced techniques. In Chapter 2, classical control systems such as lead, lag, lead-lag compensators, PI, PD and PID controllers are examined and analytical solution techniques for the synthesis of these classical control systems are presented, in detail.

There are basically two different approaches to reshaping the transient response of a closed-loop control system. One of them is the root-locus design methodology and the other one is the frequency response design methodology. The root-locus design directly gives some valuable information on the transient response of the closed-loop control systems as one sees the closed-loop pole locations. In comparison, the frequency response design gives this information only indirectly. In the frequency domain, the transient response performance can be specified in terms of the phase margin, gain margin and the resonant peak magnitude for example all of which give an estimation of the system damping, gain crossover frequency, resonant frequency and bandwidth. These characteristics are related to the speed of the transient response and the static error constant which gives the steady state accuracy [13].

Trial and error procedures [14-19] are used extensively in designing conventional controllers like lead, lag or lead-lag compensator in the frequency-domain. The main drawback of the frequency response classical controller design method outlined above is the guessing and trial and error involved. The designer has to guess the phase lead (or phase lag) which will be needed at the new gain crossover frequency

whose location is not known before the design process is completed. Several trial and error cycles might be necessary before the desired phase margin is obtained. Experienced designers can usually guess the controller parameters, which will result in a desired level of performance of the closed-loop system after a few trials. However, students or inexperienced designers will be able to choose the correct parameters after many guesses. Indeed, the trial and error procedure is very heuristic and relies heavily on graphical methods. Additionally, it requires a lot of trial and error so that educated initial designs and understanding of specifications will reduce development time greatly.

The analytical solution procedure is generally obtained to design classical control systems by using the root-locus approach by Ross, Warren, Thaler and Wakeland [19-21]. However, it does not exist any analytical solution technique to design classical controllers using Bode and Nichols methods. Besides, Wakeland [22] presented an analytical solution technique to eliminate the trial and error procedure in the design of lead-lag compensator. Mitchell [23] improved this methodology for the lead and lag compensators, respectively. The analytical solution technique mentioned above is based upon the analytical solution of phase margin design. This can be just accomplished by solving a quadratic equation.

The primarily objective of this chapter is to present an analytical solution procedure for the design of single-input-single-output (SISO), linear time-invariant (LTI) closed-loop control systems by using the frequency response approach. For this purpose, a Graphical User Interface (GUI) based on MATLAB has been developed in order to analytically calculate the conventional controller parameters.

Outline of the Chapter: The organization of the rest of the chapter is as follows. Section 2.2 discusses lead compensation using frequency response approach. Section 2.2.1 gives some basic information on the basic design principle of phase-lead compensator. For the phase-lead compensator, the analytical solution procedure is given in Section 2.2.2. Special case of phase-lead compensator called Proportional-plus-Derivative (PD) Controller is investigated in Section 2.2.3. Section 2.3 discusses lag compensation using frequency response approach. Section 2.3.1 gives some basic information on the basic design principle of phase-lead compensator. For the phase-lead compensator, the analytical solution procedure is given in Section 2.3.2. Special case of phase-lead compensator called Proportional-plus-Integral (PI)

Controller is investigated in Section 2.3.3. In Section 2.4, the "Classical Control" section of COMES toolbox being an interactive design tool for MATLAB is demonstrated. Finally, Section 2.5 gives concluding comments on the frequency response approach to the control systems design.

2.2 Lead Compensation

Lead compensator is a first order filter whose phase angle Bode plot has a positive phase angle. It is utilized to add an extra phase lead (positive phase) to the control system. In addition, this compensator usually increases the phase margin of the open-loop control system. Thanks to lead compensation, the transient response of the system and small changes in steady state accuracy can be improved. Also, it may accentuate high frequency noise effect.

2.2.1 Characteristics of lead compensators

The basic phase lead compensator consists of a gain, one zero and one pole. The transfer function of a general lead compensator is given by

$$G_{lead}(s) = K_C \alpha \frac{Ts+1}{\alpha Ts+1} = K_C \frac{s+\frac{1}{T}}{s+\frac{1}{\alpha T}} \quad (0<\alpha<1) \qquad \textbf{(2.1)}$$

where α is called the attenuation factor of the lead compensator. It has a zero at s=-$1/T$ and a pole at s=-1/(αT). The zero is always located to the right of the pole in the complex plane because of 0<α<1. Moreover, the pole is located far to the left for a small value of α. The minimum value of α is limited by the physical construction of the lead compensator. The minimum value of α can be generally taken to be about 0.05 (This means that the maximum phase lead that may be produced by a lead compensator is about 65°) [13]. For a given value of α, the angle between the positive real axis and the tangent line drawn from the origin to the semi circle gives the maximum phase lead angle, ϕ_m. The frequency at the tangent is called ω_m. From Figure 2.1 the phase angle at ω=ω_m is ϕ_m, where

$$\sin\phi_m = \frac{\frac{1-\alpha}{2}}{\frac{1+\alpha}{2}} = \frac{1-\alpha}{1+\alpha} \qquad \textbf{(2.2)}$$

Equation **(1.2)** relates the maximum phase lead angle and the value of α. Figure 2.2 shows the Bode diagram of a lead compensator when K_C=1 and α=0.1. The corner frequencies of the lead compensator are ω=0.01 and ω=10.

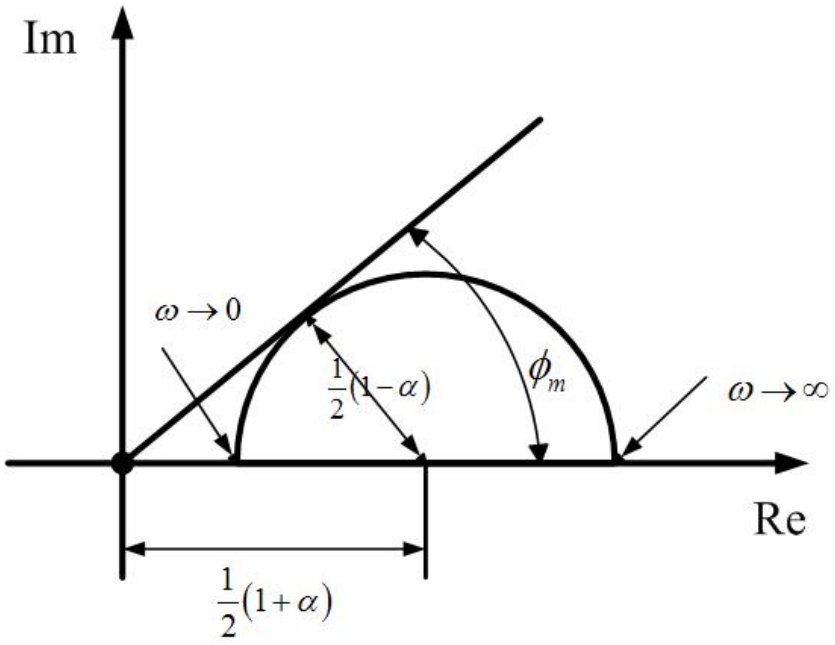

Figure 2.1 : Polar plot of a lead compensator.

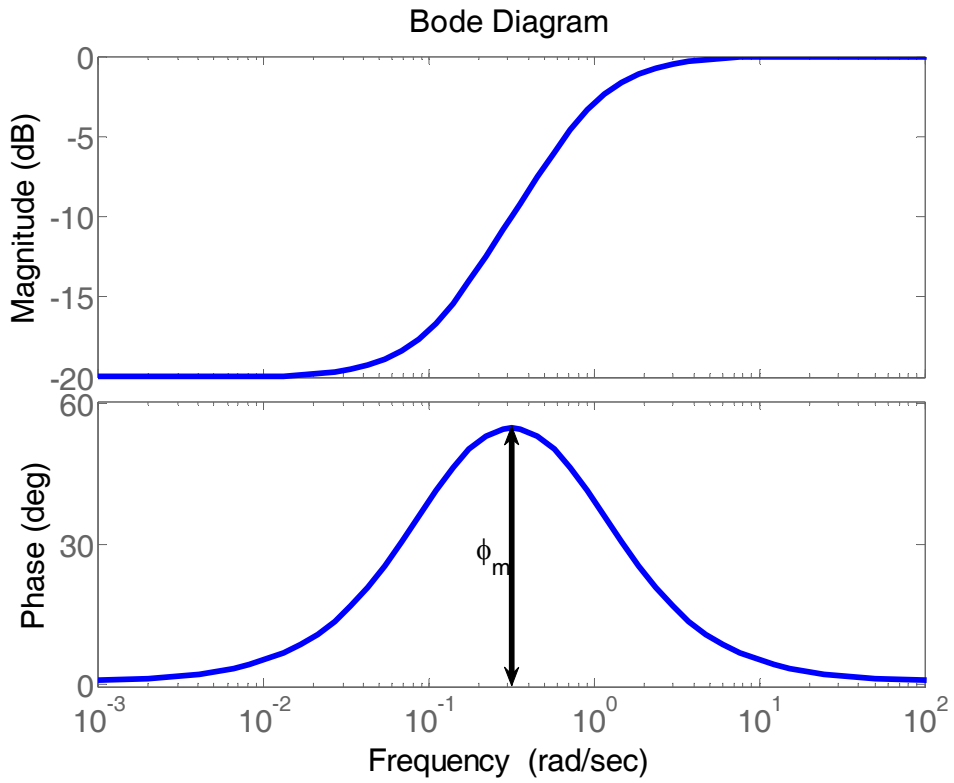

Figure 2.2 : Bode diagram of a phase-lead compensator (for K_C=1, α=0.1 and T=10).

2.2.2 Analytical lead compensator design in frequency domain

It is possible to do this phase margin based design in the frequency domain analytically as outlined below.

Step 1: Evaluate the compensator gain $K_C\alpha$ so that the desired velocity error constant K_v is obtained. Then, the compensator transfer function is rewritten as

$$C(s) = K_c\alpha \frac{\tau s + 1}{\alpha\tau s + 1} = K_c\alpha C_p(s) \tag{2.3}$$

$$C_p(s) = \frac{\tau s + 1}{\alpha\tau s + 1} \tag{2.4}$$

The rest of the procedure involves designing G_p for the desired phase margin. The designed $C_p(s)$ should result

$$\left| C_p\left(j\omega_{gc1}\right)\left[K_c\alpha G_p\left(j\omega_{gc1}\right)H\left(j\omega_{gc1}\right)\right]\right| = 1 \tag{2.5}$$

$$\theta = \angle\left(C_p\left(j\omega_{gc1}\right)\right) = \pi + \phi_m + \tau_d\omega - \angle\left(G_p\left(j\omega_{gc1}\right)H\left(j\omega_{gc1}\right)\right) \tag{2.6}$$

where ϕ_m is the desired phase margin and ω_{gc} is the gain crossover frequency. The gain margin obtained should be checked at the end of the design procedure. The equation above can be written as two equations involving phase angles and magnitudes, respectively. When the desired phase margin ϕ_m and the desired gain crossover frequency ω_{gc} are selected only two unknowns remain in two equations above. It is possible to solve for these two unknowns which are τ and α in the expression for $C_p(s)$ (or $C_p(j\omega)$).

$$\frac{1}{\alpha\tau} = \frac{\sin\theta}{\cos\theta - K_c\alpha\left|G_p\left(j\omega_{gc1}\right)H\left(j\omega_{gc1}\right)\right|}\omega_{gc1} \tag{2.7}$$

$$\frac{1}{\tau} = \frac{\sin\theta}{\dfrac{1}{K_c\alpha\left|G_p\left(j\omega_{gc1}\right)H\left(j\omega_{gc1}\right)\right|} - \cos\theta}\omega_{gc1} \tag{2.8}$$

The derivation of these two equations is skipped in this part because it is tedious. However, its derivation can be found in Appendix A.1. Their correctness might be verified by back substitution. By the way, some constraints must be satisfied for us to be able to use them, though.

Step 2: Generate the Bode diagram of open loop control system ($K_C\alpha G(s)H(s)$) and locate the gain crossover frequency ω_{gc}. Choose the new gain crossover frequency ω_{gc} subject to $K_C\alpha G(s)H(s)|_{s=j\omega}$ has magnitude lower than 0dB.

Step 3: Evaluate the angle θ using the equation seen below

$$\theta = \pi + \phi_m + \tau_d\omega - \angle\left(G_p\left(j\omega_{gc1}\right)H\left(j\omega_{gc1}\right)\right) \qquad \textbf{(2.9)}$$

Step 4: Evaluate $1/\tau$ and $1/(\alpha\tau)$ using the equations

Step 5: Draw Bode diagram of compensated system $C(s)G(s)H(s)$. Evaluate phase margin and gain margin.

It should not be forget that the constraints seen below must be ensured in order to calculate any controller parameters which are satisfied the desired performance in the frequency-domain by using analytical solution procedure.

Constraints: (for the phase lead compensation)

i. $\theta > 0^o$

Need for positive phase lead.

ii. $\left|G_p\left(j\omega_{gc1}\right)\right| > 1$

To be able to change the gain crossover frequency

iii. $\cos\theta > \dfrac{1}{\left|G_p\left(j\omega_{gc1}\right)\right|}$

Need for $1/\alpha\tau$ to be positive

An Example from Literature: Consider the system analyzed in [22]. The open-loop transfer function is given by

$$G(s) = \frac{1}{s(1+0.2s)(1+0.45s)} \qquad \textbf{(2.10)}$$

It is desired to design a compensator for the system **(2.10)** so that the static velocity error constant K_v is 4 sec^{-1}, the phase margin is at least 55° and gain crossover frequency is 4.25 rad/sec. By utilizing the Classical Controller Design part of COMES toolbox based on MATLAB, the lead compensator satisfied the desired design specifications in the frequency-domain will be able to design in this section.

In Figure 2.3, the general structure of GUI based on MATLAB is demonstrated. On the left side of Figure 2.3, the Bode magnitude and phase plots can be seen. In these plots, the blue curve denotes the uncompensated system and the red one denotes the compensated system. The type of controller which will be designed can be chosen from "Controller Type" option in the menu bar. According to the chosen controller type, the sections seen on the right side of Figure 2.3 can be activated or deactivated.

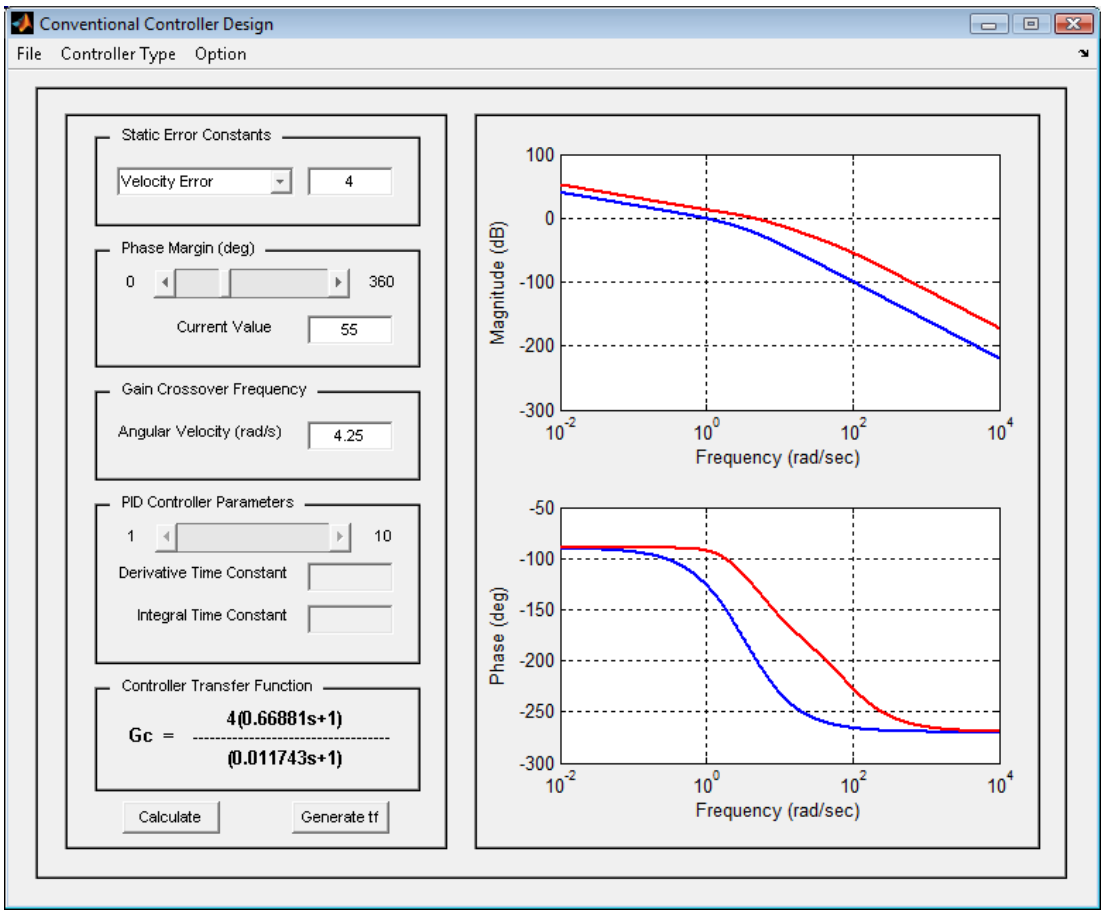

Figure 2.3 : Lead compensator design with the classical control part of COMES toolbox.

The Bode plots (with and without compensation) and the unit-step response of this phase lead compensated system are displayed on the following pages. Comparison of the unit-step response with the step responses for the root-locus based phase lead compensated system shows faster rise time, lower overshoot and lower settling time for this design. This is partially due to the different phase margin (PM) values ($\zeta \cong PM/100$). Furthermore, the design time can decrease by means of using COMES toolbox.

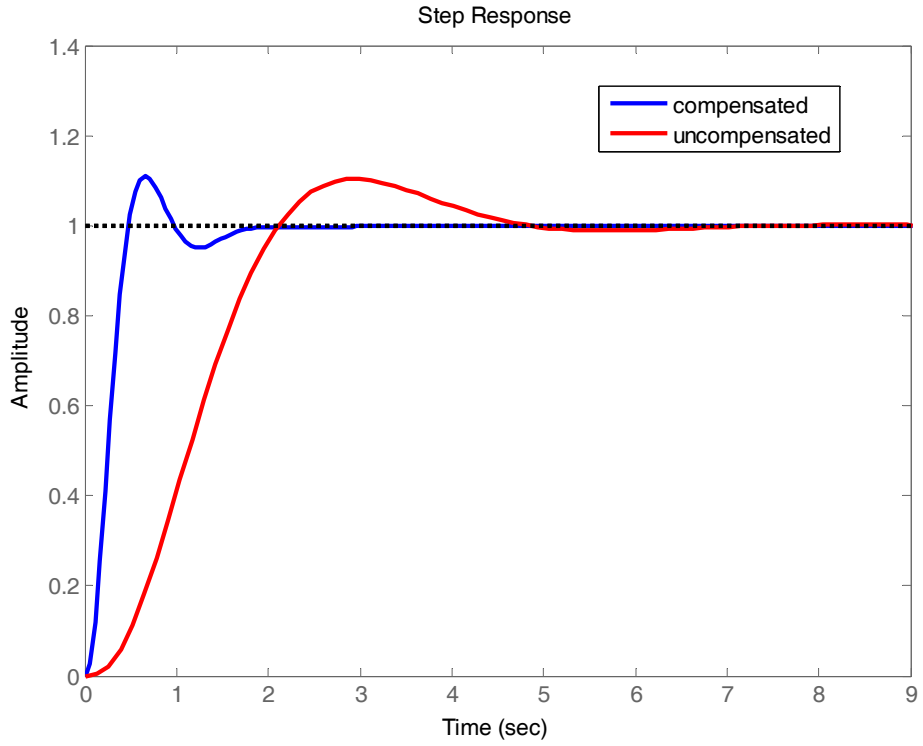

Figure 2.4 : Unit-step response of compensated and uncompensated systems.

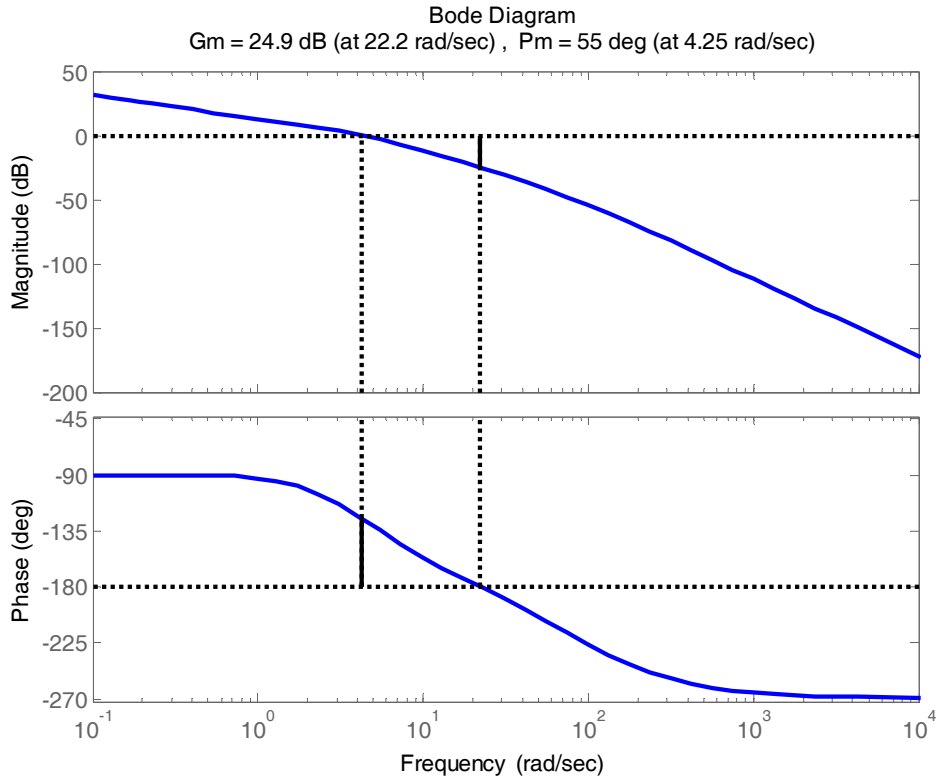

Figure 2.5 : Bode plots of open-loop control system with design specifications like GM, PM and gain crossover frequency.

2.2.3 Special case: PD control

Proportional-plus-derivative (PD) control is just a special case of phase lead control with the compensator pole at infinity.

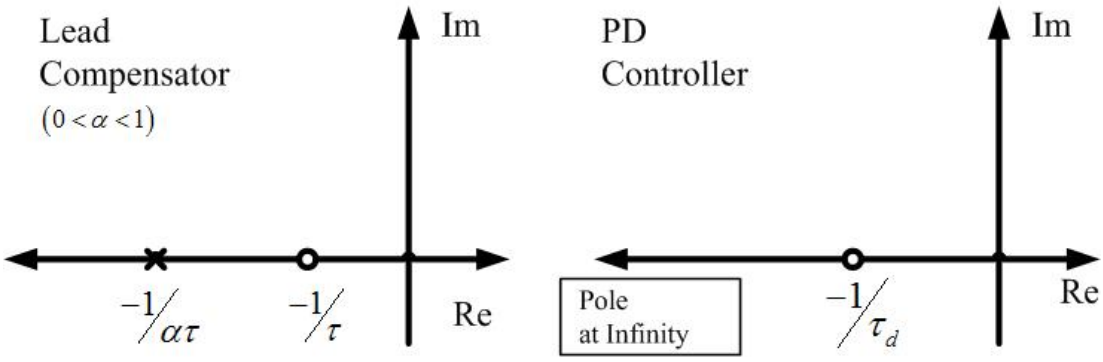

Figure 2.6 : The pole-zero location of phase lead compensator and PD controller.

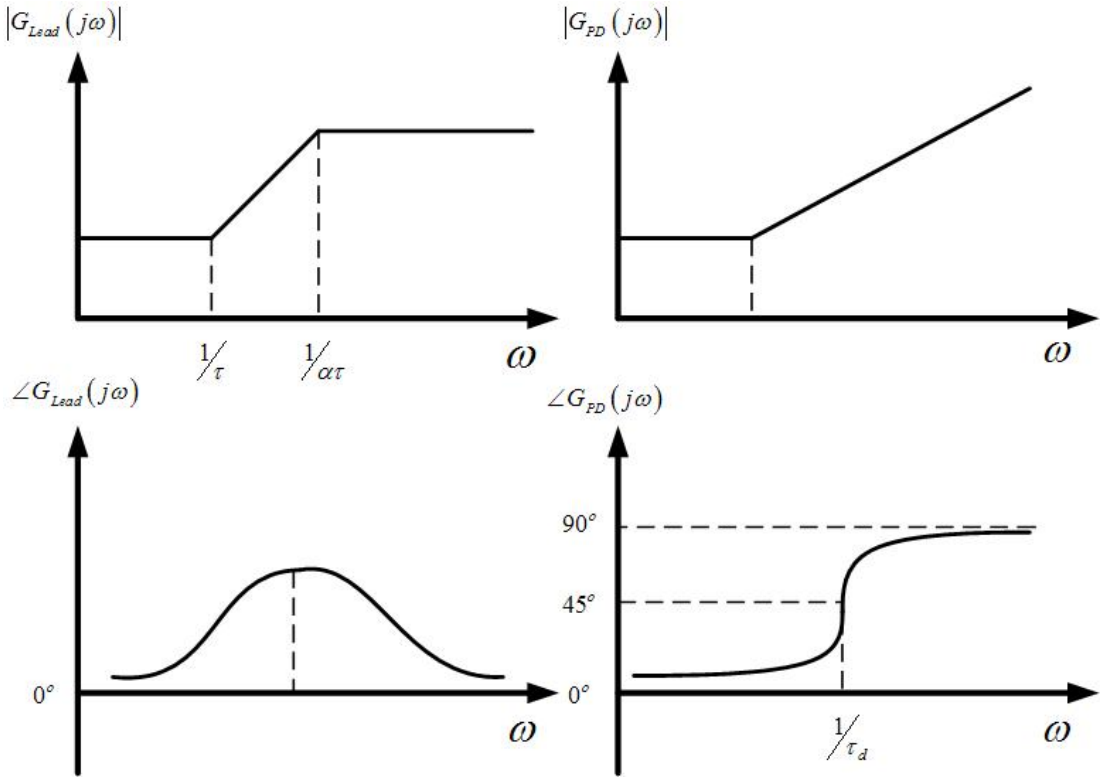

Figure 2.7 : Bode plots of phase lead compensator and PD controller.

Similar design method mentioned above can be used to design PD controllers. In Appendix A.2, the mathematical inference about analytical design procedure is extensively given.

2.3 Lag Compensation

Phase lag compensators are utilized to increase the steady-state accuracy without adversely affecting the overall dynamic response. Once satisfactory dynamic response has been obtained, perhaps by the use of lead compensation, the designer may want to increase the value of the relevant error constant (like K_v). For this reason, a pole close to the origin is introduced to approximate integration (recall that PI control or I control alone reduces the steady state error due to the high loop gain at low frequencies). A zero close to this pole is also introduced so that the pole-zero pair near the origin does not significantly interfere with the overall system dynamic response. This is the basis for the phase lag compensator (usually called lag compensator).

2.3.1 Characteristics of lag compensators

The transfer function of a general lag compensator is given by

$$G_{lag}(s) = K_C \beta \frac{Ts+1}{\beta Ts+1} G_C(s) = K_C \frac{s+\frac{1}{T}}{s+\frac{1}{\beta T}} \quad (\beta > 1) \qquad \textbf{(2.11)}$$

where β is an important factor for the lag compensator. In the complex plane, a lag compensator has a zero at s=-1/T and a pole at s=-1/(βT). The pole is always located to the right of the zero due to β>1. Figure 2.8 demonstrates a polar plot of the lag compensator. Figure 2.9 shows a Bode diagram of the compensator, where K_C=1 and β=10. The corner frequencies of the lag compensator are at ω=1/T and ω=1/(βT). According to Figure 2.9, where values of K_C and β are set equal to 1 and 10, respectively, the magnitude of the lag compensator becomes 20 dB at low frequencies and 0 dB at high frequencies. Furthermore, it can be said that the lag compensator is basically a kind of low-pass filter.

It is wanted to have close to unity gain at high frequencies ($K_C \cong 1$) so that the overall frequency response will not be affected at high frequencies. The phase lag (maximum one) is an undiserable property and the designer likes to work at frequencies where there is very small phase lag. This is in contrast to the lead compensator design procedure where the designer is the most intereseted at the frequency where the maximum phase lead occurs.

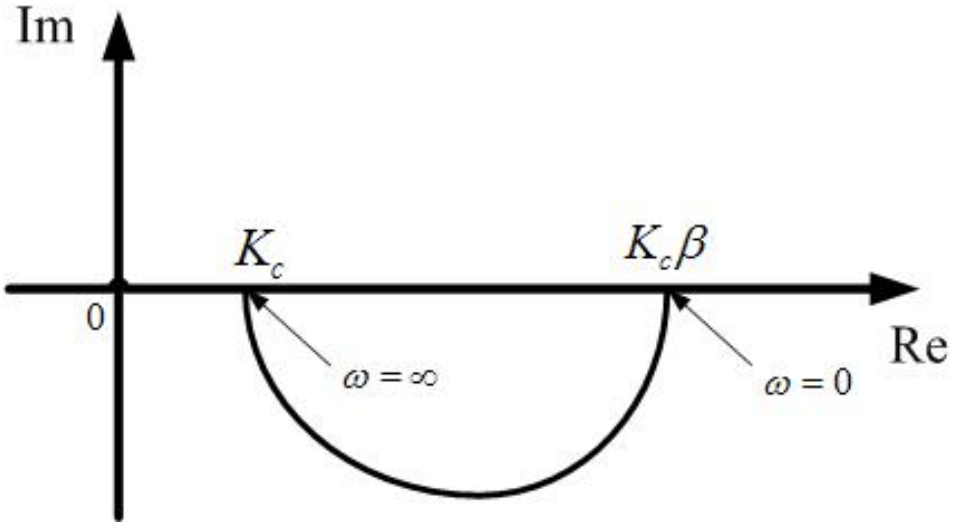

Figure 2.8 : Polar plot of a lag compensator.

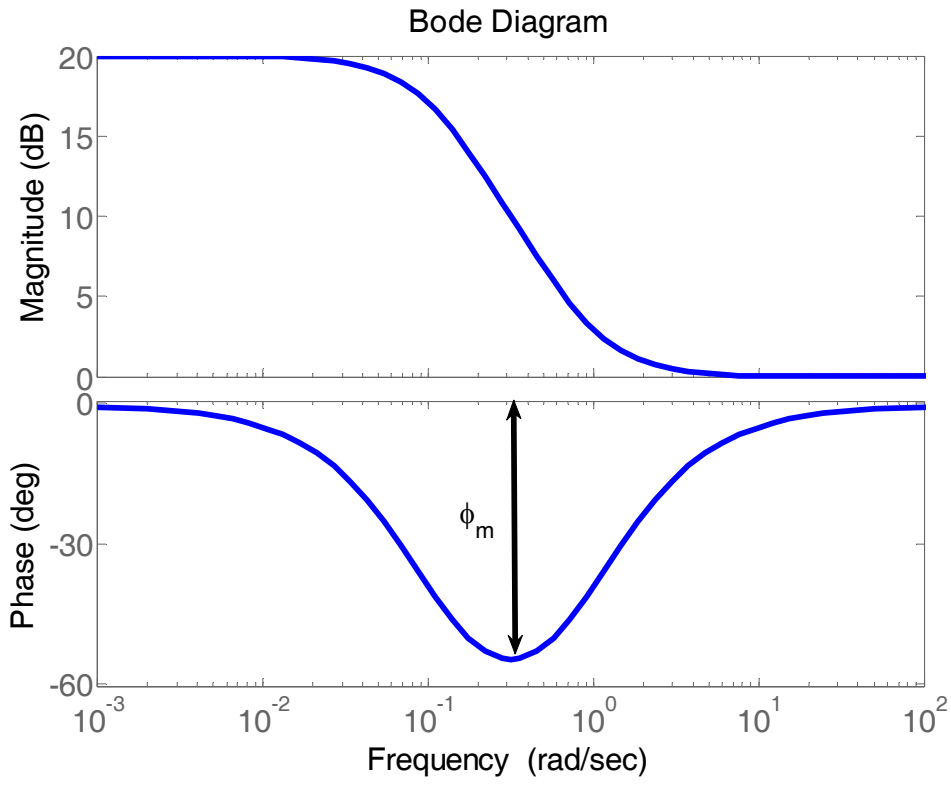

Figrue 2.9 : Bode diagram of a phase-lead compensator (for K_C=1, β=10 and T=1).

When we have a system (open-loop transfer function) with sufficieant phase margin and we desire to increase steady-state accuracy, the root-locus based design method described above can be used. This method introduces a lag filter at very low frequencies to increase the value of the relevant error constant (or the loop gain at low frequencie) while not affecting the rest of the system's dynamic response so that the PM will stay about the sense. In the example given earlier, a lag compensator was designed for the lead compensated plant $G(s)$ so that the desired phase margin was generated first by the lead compensator and the desired static accuracy was achieved by the in corporation of a lag compensator which did not affect the phase margin in any significant manner. The resulting control system was a lag-lead compensator, called lag-lead because the lag is at lower frequencies than the lead, and the procedure used was one method that can be used to design a lag-lead compensator.

It is also possible to use a lag compensator to obtain a desired phase margin for an uncompensated plant. Note that this could equally well have been done using a lead compensator which would also result in a higher bandwidth for the closed-loop system. However, one has to use a lag compensator whenever a desired phase margin is required along with a significant increase in steady-state accuracy. This is achived at the expense of lower bandwidth though.

Another motivation for the use of lag compensation is to achieve lower loop gains at higher frequencies where the attenuation of noise effects (noise imunity) is desired. Low loop gains at higher frequencies are also needed for improved stability robustness in the face of high frequency modeling errors.

2.3.2 Analytical lag compensator design in frequency domain

Note that the trial and error procedure involved in the lag compensator design method using the frequency response approach can be eliminated because an analytical solution is possible. The formulas derived for the analytical solution to lead compensator design in the frequency domain apply here as well. The constraints are different though. The trial and error approach introduced first since it is more initiative and helps the student in getting a feel for the design process rather than blind use of formulas. The analytical solution procedure explained above is outlined below.

Step 1: Evaluate the compensator gain $K_C\beta$ so that the desired velocity error constant K_v is obtained. Then, the compensator transfer function is rewritten as

$$C(s) = K_c\beta\frac{\tau s+1}{\beta\tau s+1} = K_c\beta C_p(s) \quad \textbf{(2.12)}$$

$$C_p(s) = \frac{\tau s+1}{\beta\tau s+1} \quad \textbf{(2.13)}$$

The rest of the procedure involves designing G_p for the desired phase margin. The designed $C_p(s)$ should result

$$\left|C_p\left(j\omega_{gc1}\right)\left[K_c\beta G_p\left(j\omega_{gc1}\right)H\left(j\omega_{gc1}\right)\right]\right| = 1 \quad \textbf{(2.14)}$$

$$\theta = \angle\left(C_p\left(j\omega_{gc1}\right)\right) = \pi + \phi_m + \tau_d\omega - \angle\left(G_p\left(j\omega_{gc1}\right)H\left(j\omega_{gc1}\right)\right) \quad \textbf{(2.15)}$$

where ϕ_m is the desired phase margin and ω_{gc} is the gain crossover frequency. The gain margin obtained should be checked at the end of the design procedure. The equation above can be written as two equations involving phase angles and magnitudes, respectively. When the desired phase margin ϕ_m and the desired gain crossover frequency ω_{gc} are selected only two unknowns remain in two equations above. It is possible to solve for these two unknowns which are τ and β in the expression for $C_p(s)$ (or $C_p(j\omega)$).

$$\frac{1}{\beta\tau} = \frac{\sin\theta}{\cos\theta - K_c\beta\left|G_p\left(j\omega_{gc1}\right)H\left(j\omega_{gc1}\right)\right|}\omega_{gc1} \quad \textbf{(2.16)}$$

$$\frac{1}{\tau} = \frac{\sin\theta}{\dfrac{1}{K_c\beta\left|G_p\left(j\omega_{gc1}\right)H\left(j\omega_{gc1}\right)\right|} - \cos\theta}\omega_{gc1} \quad \textbf{(2.17)}$$

The derivation of these two equations is skipped in this part because it is tedious. However, its derivation can be found in Appendix A.3. Their correctness might be verified by back substitution. By the way, some constraints must be satisfied for us to be able to use them, though.

Step 2: Generate the Bode diagram of open loop control system ($K_C\beta G(s)H(s)$) and locate the gain crossover frequency ω_{gc}. Choose the new gain crossover frequency ω_{gc} subject to $K_C\beta G(s)H(s)|_{s=j\omega}$ has magnitude lower than 0dB.

Step 3: Evaluate the angle θ using the equation seen below

$$\theta = \pi + \phi_m + \tau_d \omega - \angle\left(G_p\left(j\omega_{gc1}\right)H\left(j\omega_{gc1}\right)\right) \qquad \textbf{(2.18)}$$

Step 4: Evaluate $1/\tau$ and $1/(\beta\tau)$ using the equations

Step 5: Draw Bode diagram of compensated system $C(s)G(s)H(s)$. Evaluate phase margin and gain margin.

Constraints: (for the phase lead compensation)

i. $\theta < 0^o$

Need for negative phase shift.

ii. $\left|\dfrac{G_p\left(j\omega_{gc1}\right)}{K_c\beta}\right| < 1$

To be able to change the gain crossover frequency

iii. $\cos\theta < K_c\beta\left|G_p\left(j\omega_{gc1}\right)H\left(j\omega_{gc1}\right)\right|$

Need for $1/\beta\tau$ to be positive

An Example from the Literature: The same system used in the previous example is investigated here. The open-loop transfer function is given by

$$G(s) = \frac{1}{s(1+0.2s)(1+0.45s)} \qquad \textbf{(2.19)}$$

It is desired to design a compensator for the system so that the static velocity error constant K_v is 4 sec^{-1}, the phase margin is at least 55° and gain crossover frequency is 0.85 rad/sec. As it is mentioned in the example of Lead Compensation Section, the Conventional Controller Design part of COMES toolbox is utilized in order to design a lag compensator. Firstly, the static velocity error is entered to GUI. Then, the desired phase margin is entered to GUI. Finally, the gain crossover frequency is entered to GUI and it is pressed to "Calculation" to generate a controller.

In Figure 2.10, the transfer function of phase lag compensator calculated by COMES toolbox can be seen. Moreover, its transfer function can be generated in the MATLAB's workspace by pressing "Generate tf" button.

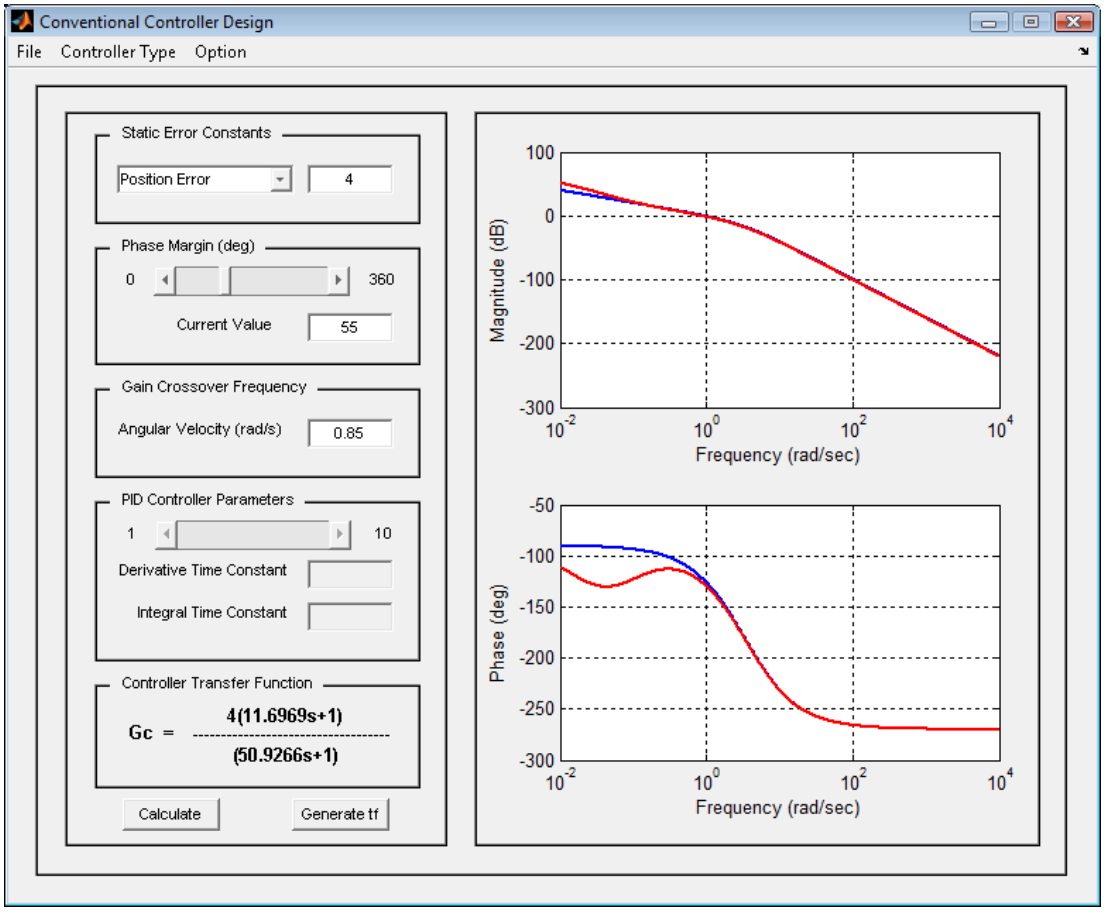

Figure 2.10 : Lag compensator design with the classical control part of COMES toolbox.

Lag compensators reduce the closed-loop control system's bandwidth resulting in a slower system as observed here. The speed of response could be increased by reducing β and meaning the lag compensator's pole closer to the origin. A lead compensator will need to be added in this case to achieve the desired PM margin. The Bode plots (with and without compensation) and the unit-step response of this phase lead compensated system are displayed on the following pages.

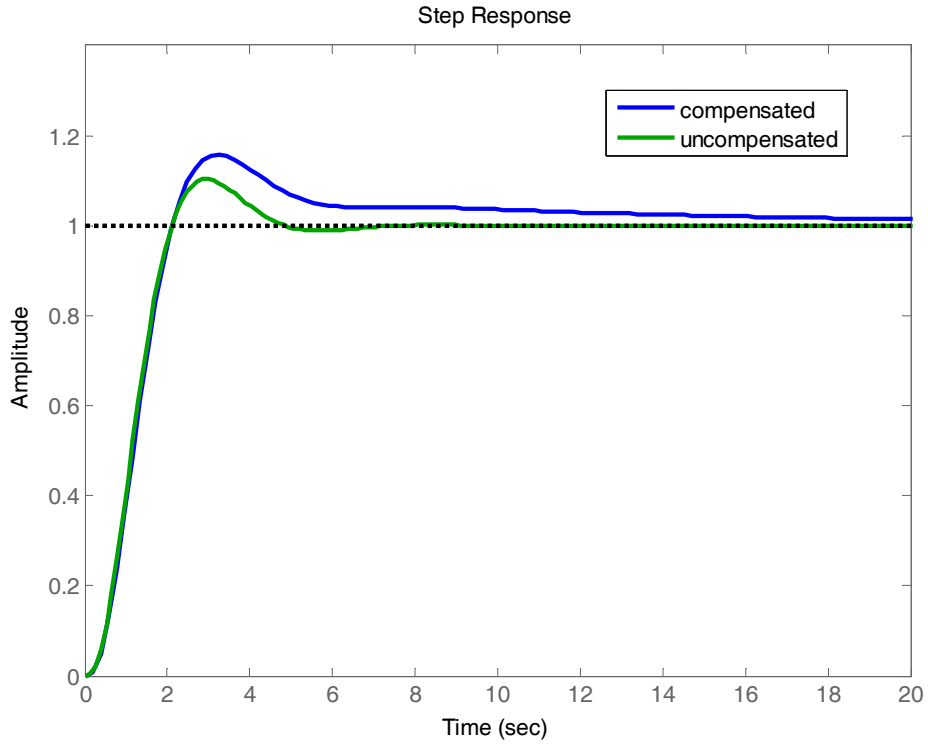

Figure 2.11 : Unit-step response of compensated and uncompensated systems.

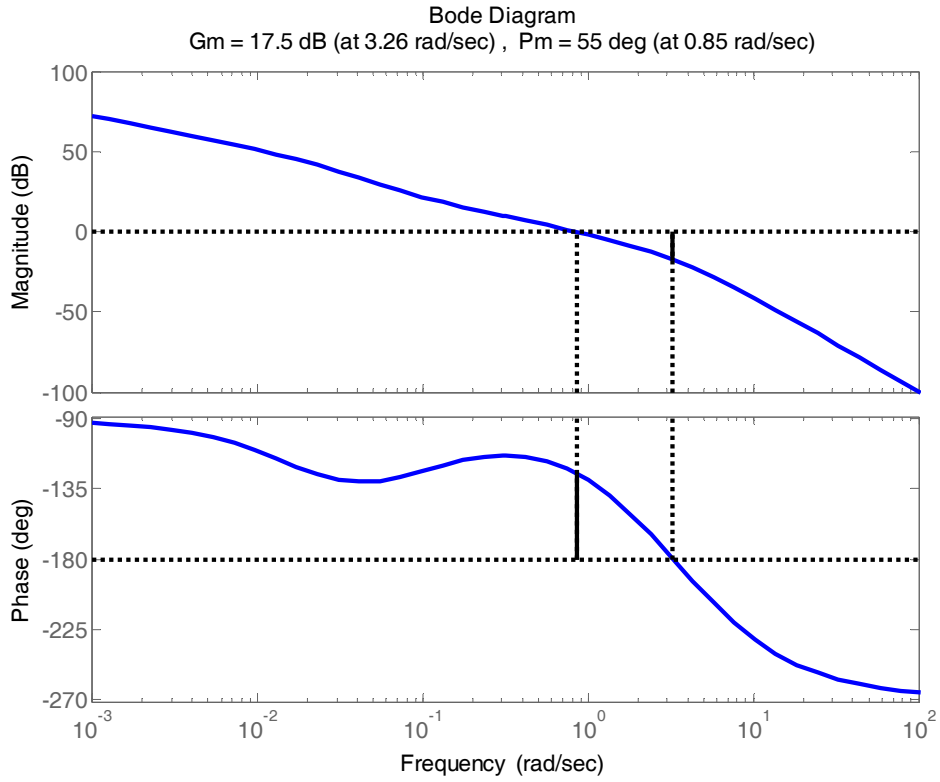

Figrue 2.12 : Bode plots of open-loop control system with design specifications like GM, PM and gain crossover frequency.

2.3.3 Special case: PI control

Note that PI control is just a special case of lag control with the compensator pole placed at the origin.

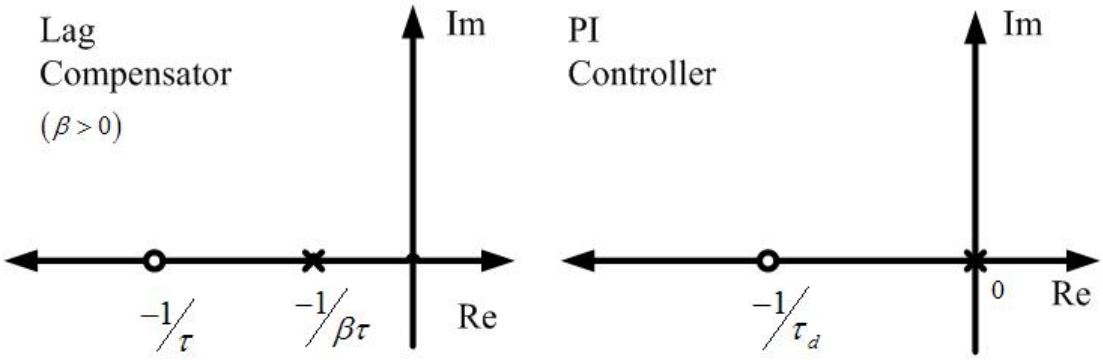

Figure 2.13 : The pole-zero location of phase lag compensator and PI controller.

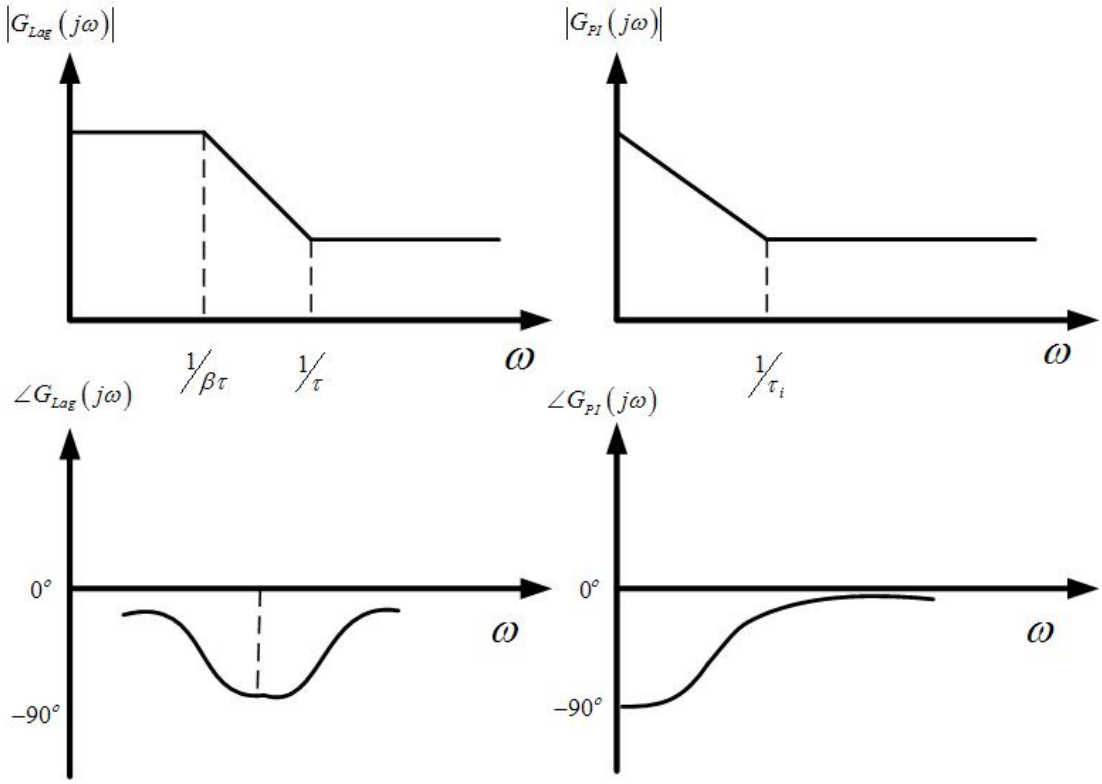

Figure 2.14 : Bode plots of phase lag compensator and PI controller.

The general comments on lag control also apply to PI control and similar design methods can be used for designing PI controllers. In Appendix A.4, the mathematical background of analytical design procedure for PI controller is explained, in detail.

2.4 Lag-Lead Compensation

The basic lag-lead compensator consists of a gain, two zeros and two poles. The form of transfer function is the combination of lag and lead network. The transfer function of the lag-lead compensator is given by

$$G_{lag-lead}(s) = K_C \alpha\beta \left(\frac{\tau_1 s + 1}{\alpha\tau_1 s + 1} \right) \left(\frac{\tau_2 s + 1}{\beta\tau_2 s + 1} \right) \quad \textbf{(2.20)}$$

where $\alpha<1$ and $\beta>1$. The term

$$\left(\frac{s + \frac{1}{\tau_1}}{s + \frac{1}{\alpha\tau_1}} \right) \quad (\alpha < 1) \quad \textbf{(2.21)}$$

produces the effect of the lead network, and the term

$$\left(\frac{s + \frac{1}{\tau_2}}{s + \frac{1}{\beta\tau_2}} \right) \quad (\beta > 1) \quad \textbf{(2.22)}$$

produces the effect of the lag network.

The phase lead portion of lag-lead compensator (the portion involving τ_1) alters the frequency response curve by adding phase lead angle and increasing the phase margin at the gain crossover frequency. The phase lag portion (the portion involving τ_2) provides attenuation near and above the gain crossover frequency and thereby allows an increase of gain at the low frequency range to improve the steady state performance.

Due to the higher crossover frequency, the system will respond more rapidly in the time-domain. The faster response may be an advantage in many applications, but a disadvantage of a wider bandwidth is that more noise and other high frequency signals (often unwanted) will be passed by the system. A smaller bandwidth also provides more stability robustness when the system has unmodeled high frequency dynamics, such as the bending modes in aircraft and spacecraft. Thus, there is a trade-off between having the ability to track rapidly varying reference signals and being able to reject high-frequency disturbances.

Notice that Proportional-Integral-Derivative (PID) control is a special case of lag-lead control with two compensator poles placed at the origin and at infinity. The all mathematical interferences about PID controller are given in Appendix A.5.

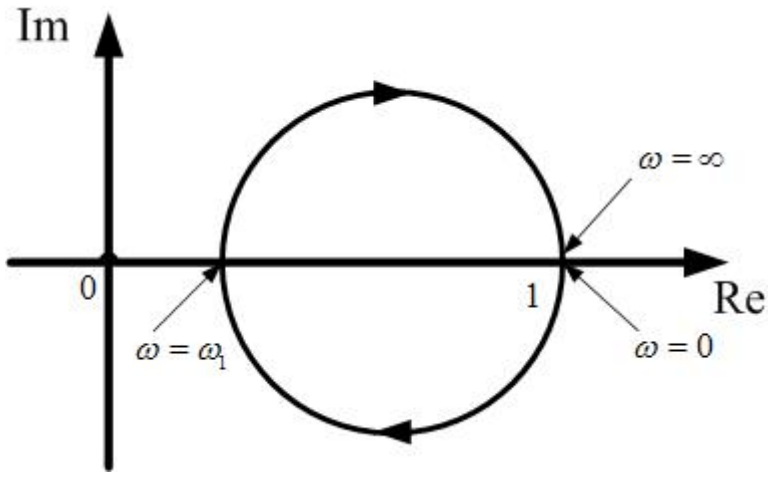

Figure 2.15 : Polar plot of a lag-lead compensator.

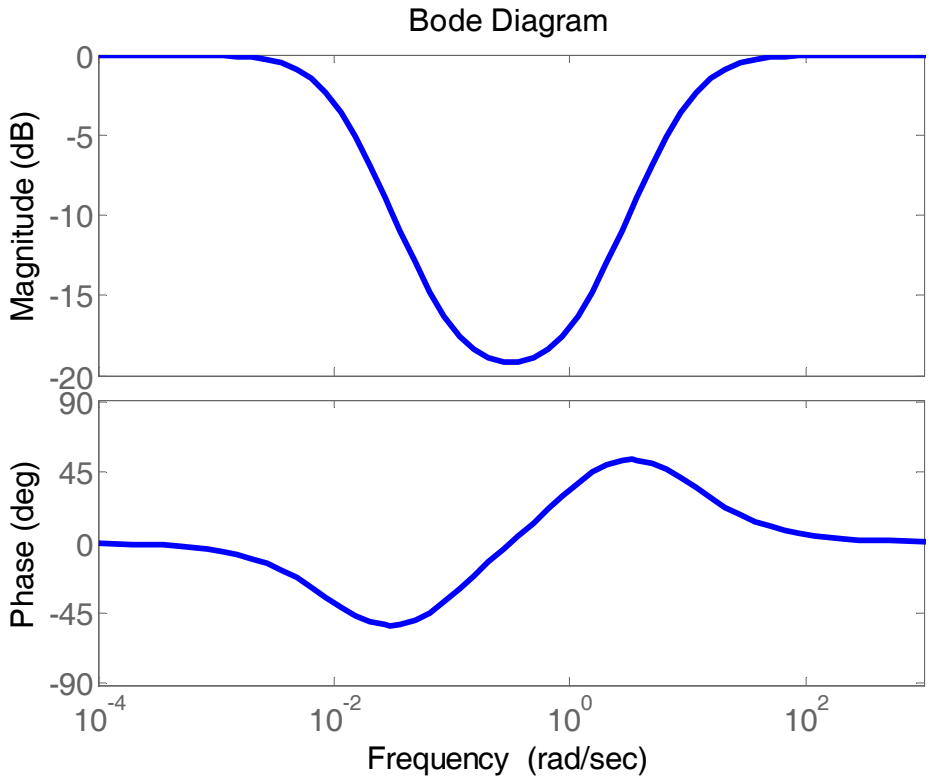

Figure 2.16 : Bode diagram of a phase lag-lead compensator (for K_C=1, α=0.1, β=10, τ_1=1, and τ_2=10).

2.5 COMES Toolbox: Classical Control System Design

Current version of COMES toolbox includes "Classical Control System Design" section. "Classical Control System Design" section has got only one window:

- Main Window

  has some edit fields for design specifications in frequency-domain and controller parameters.

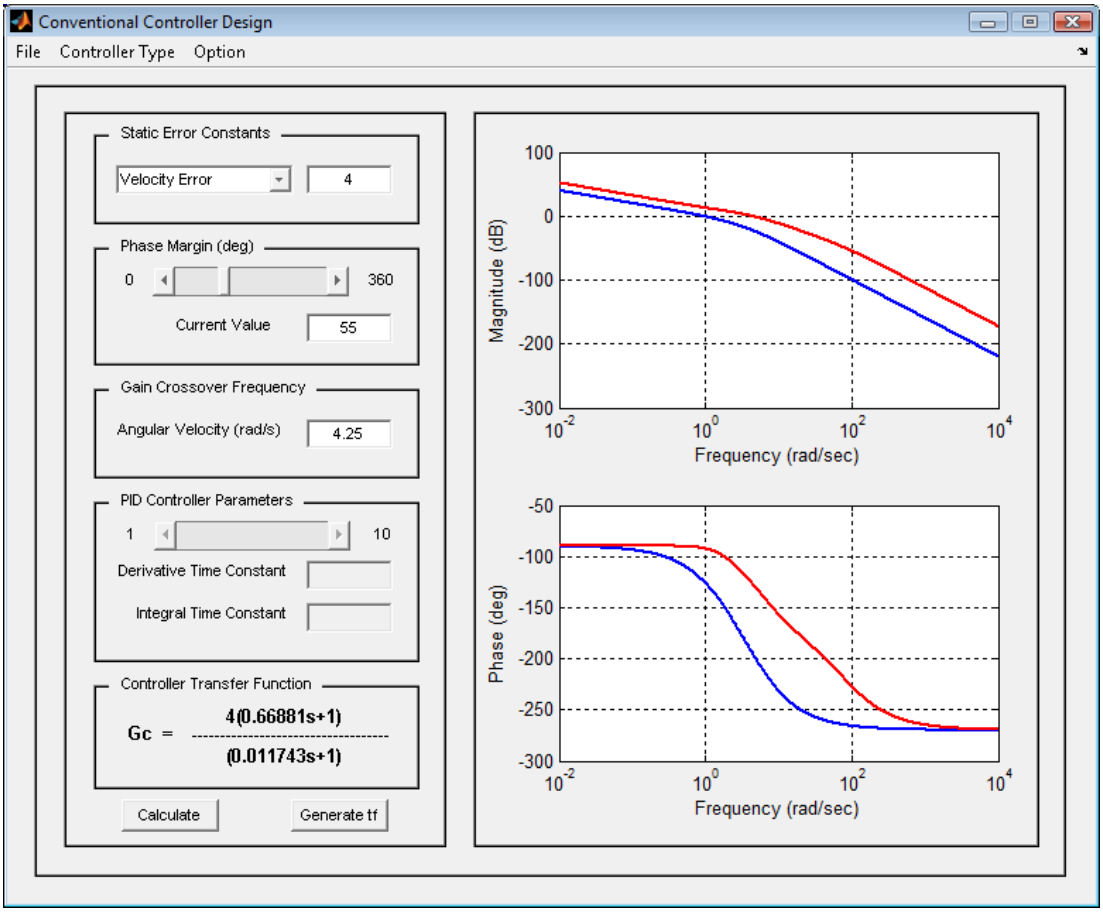

Figure 2.17 : A screenshot of classical control part of COMES toolbox.

It shows Bode magnitude and phase plots (for uncompensated and compensated plants) to help users to design controllers. Users change design specifications (i.e. static error constant, phase margin and gain crossover frequency) and controller parameters (i.e. derivative and integral time constants) to manipulate the transient response of control system. Then, they can observe the effect of changing design specifications and parameters on Bode diagram. Moreover, users are able to select a

controller among many different kinds of classical control systems (i.e. lead, lag, lead-lag, PI, PD or PID) by using "Controller Type" menu.

When pressing "Calculate" button, the corresponding algorithm working background of GUI calculates the parameters of chosen classical controller. Then, it demonstrates the chosen controller on the GUI.

2.6 Chapter Summary and Concluding Comments

We derived an analytical method in order to easily calculate the parameters of classical control systems in this chapter. Here, the trial and error procedure was compared with the analytical method. Analytical method has some advantages and disadvantages. The trial and error approach was introduced first as it is more initiative and easier to understand. In addition, it helps the student in getting a feel for the design process rather than blind use of formulas. However, somebody can decrease the design time which he/she spent and easily calculate the desired parameters. We also developed a MATLAB-based toolbox including this analytical method to analytically determine the parameters of classic controller. In next chapter, robust control based on parameter space approach will be explained in detail.

3. PARAMETRIC ROBUST CONTROL

3.1 Introduction to Parametric Robust Control

The method presented in this chapter is relied on mapping Hurwitz stability, *D*-stability and frequency domain constraints on the closed-loop transfer functions like nominal performance, robust stability and robust performance and gain/phase margin bounds to the parameter space of the chosen controller parameters by utilizing fixed controller structure. Several researchers have worked on the parameter space approach to robust control. Some of them presented a lot of papers about parameter space methods like Hurwitz stability and *D*-stability. The reader can get lots of information on these subjects in parameter space methods from the reference [24]. The other researchers have been dealing with mapping of various frequencies domain criteria into parameter space. The earlier papers in the literature which have generally focused on mapping the frequency domain specifications can be found in the references [25-33].

Outline of the Chapter: The organization of the rest of Chapter 3 is as follows. Section 3.2 presents the theoretical and mathematical background of Hurwitz stability, *D*-stability, robust performance frequency domain specifications and phase margin design. To illustrate the effectiveness of multi-objective approach, automated path following problem is utilized in section 3.3. Then, COMES toolbox being an interactive MATLAB-based design program is demonstrated in section 3.4. Finally, the methodology presented in this chapter is summarized.

3.2 Methodology

3.2.1 Hurwitz stability

The family of polynomials $P(s,Q)$ is robustly stable, if and only if,

i. there exists a stable polynomial $p(s,q) \in P(s,Q)$.

ii. $j\omega \notin Roots[P(s,Q)]$ for $\forall \omega \geq 0$.

If one plots the curves to the parameter plane that $j\omega \in Roots[P(s,Q)]$ holds, it is obviously understood that the parameters have to cross this boundary, for the roots of the characteristic polynomial to cross the imaginary axis. If all the roots of the polynomial were on the left half plane then basically this cross would destabilize the system. Hence, this boundary can be called as the stability boundary. However, the second condition will be used in a different manner while synthesizing controller. Notice that if the value of the polynomial has zero value for $\exists\omega \geq 0$ then it is basically has a root on the imaginary axis exactly at that frequency. If,

$$p(j\omega,q) = 0 \qquad \textbf{(3.1)}$$

holds for some $q \in Q$ then this polynomial family is on the stability margin. The task in the controller design is to plot the q values on the parameter space such that **(3.1)** holds. In this manner the stability boundaries can be observed upon variations of $q \in Q$.

Choosing two parameters to be varying and evaluating **(3.1)** would yield,

$$\begin{aligned} &p(j\omega,q) = (a_0(q) - a_2(q)\omega^2 + a_4(q)\omega^4 - ....) \\ &+ j\omega(a_1(q) - a_3(q)\omega^2 + a_5(q)\omega^4 - ....) = 0 \end{aligned} \qquad \textbf{(3.2)}$$

Equation (2.2) can be broken up into two separate equations,

$$\begin{aligned} &a_0(q) - a_2(q)\omega^2 + a_4(q)\omega^4 - .... = 0 \\ &a_1(q) - a_3(q)\omega^2 + a_5(q)\omega^4 - .... = 0 \end{aligned} \qquad \textbf{(3.3)}$$

Now, let us fix all the uncertain parameters except two, which may be uncertain parameters of the plant or the controller,

$$a_0(q_1,q_2) - a_2(q_1,q_2)\omega^2 + a_4(q_1,q_2)\omega^4 - .... = 0 \qquad \textbf{(3.4)}$$

$$\omega(a_1(q_1,q_2) - a_3(q_1,q_2)\omega^2 + a_5(q_1,q_2)\omega^4 - ....) = 0 \qquad \textbf{(3.5)}$$

The first approach should be to eliminate ω from the above equations and then plot the solution into the q_1–q_2 plane. However, note that this would then plot the solutions for complex values of ω [24]. Instead of this elimination, it is chosen as a parameter and evaluated in the interval $0 \leq \omega \leq \infty$. After each evaluation the parameters q_1, q_2 are solved from the equation set **(3.4)**, and the result is plotted in the parameter space. If the grid over the frequency ω is dense enough, then the

resulting curve will be a candidate for the stability boundary. By leaving ω in the equations one can restrict its values to non-negative real values, avoiding some fictitious boundaries, that ω takes complex values.

Roots of the uncertain polynomial can be crossing the imaginary axis through $\omega = 0$, $\omega = \infty$ or $0 < \omega < \infty$. Note that for $\omega = 0$ equation **(3.5)** drops and the two parameters in consideration become dependent. Then the solution becomes single line in the parameter space. The equation of this line can be obtained from **(3.4)** explicitly. This line provides the boundary that a crossing occurs from the origin, and is called the "real root boundary" (RRB). This condition is equivalent to $a_0 = 0$. The crossing over from $\omega = \infty$ is possible when the polynomial drops degree, which can be given as $a_n = 0$. The equation is again explicit in terms of the uncertain parameters, and it forms a line in the two dimensional parameter space. This line is called the "infinite root boundary" (IRB). Finally the solution of **(3.4)** and **(3.5)** for $0 < \omega < \infty$ gives curves in the two dimensional parameter space and these curves are called the "complex root boundary" (CRB).

3.2.2 *D*-stability

The abovementioned Hurwitz stability parameter space region computation procedure can be extended to relative stability called *D*-stability. The roots of characteristic polynomial of closed-loop system should be located inside of the *D*-stability region in complex plane as shown in Figure 3.1 if this system is *D*-stable.

The *D*-stability boundary ($\partial\Gamma$) can be described mathematically by:

$$\partial\Gamma = \{s \mid s = \sigma(a) + j\omega(a), a \in [a^-, a^+]\} \qquad \textbf{(2.6)}$$

The *D*-stability boundary has to be mapped to the parameter space to obtain $Q_{\Gamma-stable}$. For this purpose, we need to express $\partial\Gamma$ in a more convenient way. For the *D*-stable region shown in Figure 3.1 the *D*-stability boundary can be expressed as

$$\partial\Gamma = \partial\Gamma_1 + \partial\Gamma_2 + \partial\Gamma_3 \qquad \textbf{(2.7)}$$

The boundary ∂_1 in Figure 3.1 can be mapped into the parameter space by substituting s-σ for s in **(3.2)** so as to shift the stability boundary to ∂_1 in the complex plane. After that, solving for the controller parameters in **(3.3)** and **(3.4)** in the same manner and plotting the result in the chosen controller parameter plane leads to the ∂_1

boundary in the parameter space. Notice that no infinite root boundary (IRB) is able to exist because s is never equal to infinity in the D-shaped region shown in Figure 3.1. In order to map the boundary ∂_2 to the chosen parameter plane, we will use $re^{j\theta}$ for s in equation **(3.2)** and parameterize r in $a_0 = 0$ to obtain the complex root boundary (CRB) of ∂_1 after solving for the chosen controller parameters. No singular solution exists because r is never equal to zero or infinity. In addition, mapping the boundary ∂_3 to the chosen parameter plane can be carried out by substituting s with $Re^{j\theta}$ where R is a constant and parameterizing over θ while solving **(3.2)**. The real root boundaries (RRB) ∂_1, ∂_3 and complex root boundaries (CRB) ∂_1, ∂_2, ∂_3 can be obtained symbolically in terms of chosen controller parameters.

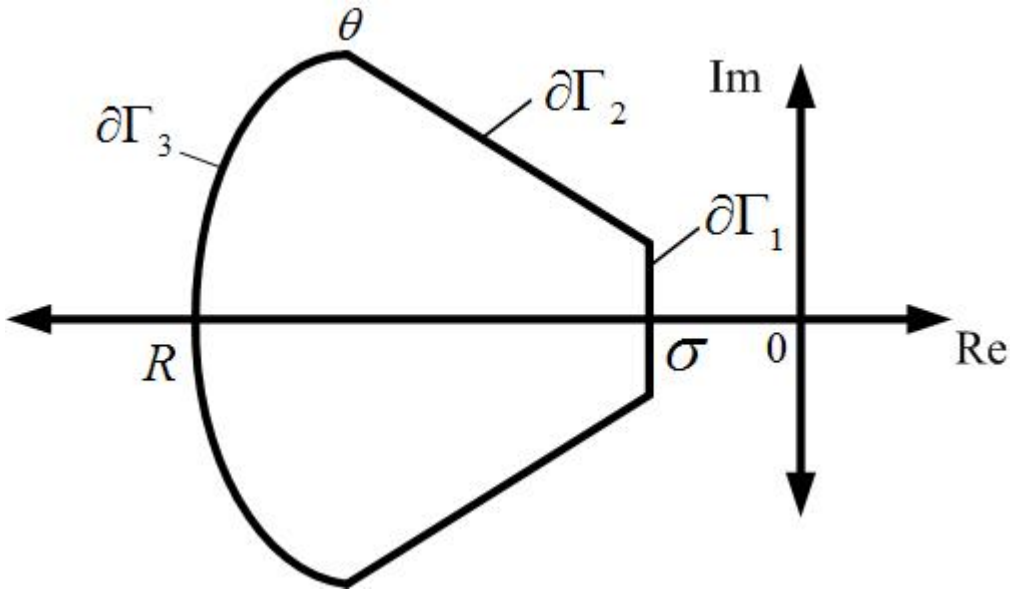

Figure 3.1: D-stability region.

3.2.3 Phase margin

The constant phase margin boundary can be plotted in a chosen controller parameter space. The constant phase margin boundary satisfies the following equation

$$L(j\omega) = e^{j(m_\phi - \pi)} \qquad \textbf{(3.8)}$$

where m_ϕ is the phase margin bound. Assume that the controller is given by

$$\begin{aligned} N_C(j\omega) &= N_{C,R}(j\omega) + jN_{C,I}(j\omega) \\ D_C(j\omega) &= D_{C,R}(j\omega) + jD_{C,I}(j\omega) \end{aligned} \qquad \textbf{(3.9)}$$

So, the plant is given by

$$N_C(j\omega) = N_{C,R}(j\omega) + jN_{C,I}(j\omega)$$
$$D_C(j\omega) = D_{C,R}(j\omega) + jD_{C,I}(j\omega) \quad \textbf{(3.10)}$$

The real and imaginary parts of $L(j\omega)$ can be expressed as

$$\mathrm{Re}\left[L(j\omega)\right] = \mathrm{Re}\left[\frac{N_{C,R}+jN_{C,I}}{D_{C,R}+jD_{C,I}}\frac{N_R+jN_I}{D_R+jD_I}\right] = -\cos(m_\phi)$$
$$\mathrm{Im}\left[L(j\omega)\right] = \mathrm{Im}\left[\frac{N_{C,R}+jN_{C,I}}{D_{C,R}+jD_{C,I}}\frac{N_R+jN_I}{D_R+jD_I}\right] = -\sin(m_\phi) \quad \textbf{(3.11)}$$

Benefiting from equations in **(3.11)**, the chosen controller parameters can be solved symbolically.

Notice that the symbolic solutions might be too long in size for higher order choices of these filters, necessitating a numerical solution. The constant gain margin region parameterization is also possible as it is obtained in a similar manner.

3.2.4 Design by mapping frequency domain bounds to parameter space

The aim of this section is to map the frequency domain criteria of robust control to parameter space. The mixed sensitivity problem will be considered in the analysis. Similar to the parameter space approach given in [34], the parameter space design is based on satisfying the mixed sensitivity requirement

$$\left\| |W_S S| + |W_T T| \right\|_\infty < 1 \quad \textbf{(3.12)}$$

or equivalently satisfying

$$|W_S S| + |W_T T| < 1 \text{ for } \forall\omega \quad \textbf{(3.13)}$$

where S and T are the sensitivity and complementary sensitivity transfer functions and W_S and W_T are the corresponding weights. Under the limit condition, this requirement can be presented as

$$|W_S| + |W_T L| = |1 + L| \text{ for } \forall\omega \quad \textbf{(3.14)}$$

which is called the point condition at each frequency. L in equation **(3.14)** is the loop gain. In order to obtain the region which satisfies expression **(3.13)** for all frequencies in the parameter space, equation **(3.14)** must be solved frequency at a time. The intersection of the regions for every calculated frequency leads to the

overall region searched for. The point condition is graphically illustrated in Figure 3.2.

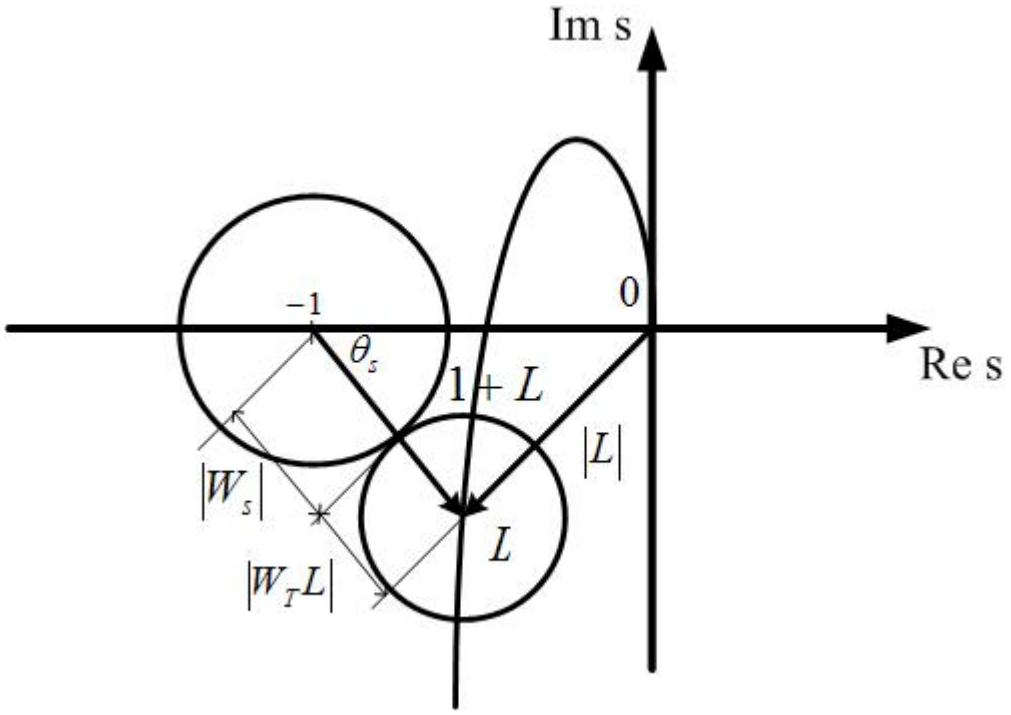

Figure 3.2: Point condition for the mixed sensitivity.

By applying the cosine rule to the shaded triangle in Figure 3.2, a graphical solution for $|L|$ results in,

$$\left|L(j\omega)\right| = \frac{\left(-\cos\theta_L + \left|W_S(\omega)\right|\left|W_T(\omega)\right|\right) \pm \sqrt{\Delta_M(\omega)}}{1-\left|W_T(\omega)\right|^2} \qquad \textbf{(3.15)}$$

where

$$\Delta = \cos^2\theta_L + \left|W_S\right|^2 + \left|W_T\right|^2 - 2\left|W_S\right|\left|W_T\right|\cos\theta_L - 1 \qquad \textbf{(3.16)}$$

When $L(j\omega)$, $W_S(j\omega)$ and $W_T(j\omega)$ are utilized in equations **(3.15)** and **(3.16)**, the solutions for L at the chosen frequency ω are obtained. The solution procedure is to sweep angle θ_L from *0* to 2π radians and to solve for $|L|$ at each value of θ_L for which a solution exists. Then, all possible values of $L = \left|L\right|e^{j\theta_L}$ at the chosen frequency ω are obtained. Each value of L satisfies

$$L = KG = \left(K_R + jK_I\right)G \qquad \textbf{(3.17)}$$

where K is the controller in an equivalent standard feedback architecture representation of the disturbance observer. The reader can be referred to [24] and [34] and the references therein for details of the general method of mapping frequency domain bounds to parameter space for standard feedback control architecture.

3.3 Case Study: Automated Path Following

In this part of the chapter, an automated path following problem that is described in the reference [35] is used as a numerical example to demonstrate the methodology of the multi-objective parameter space approach for linear system. The classical single track model is used in order to model the steering dynamics. It is obtained by lumping the two front wheels into one wheel in the centerline of the vehicle, the same is done with the two rear wheels.

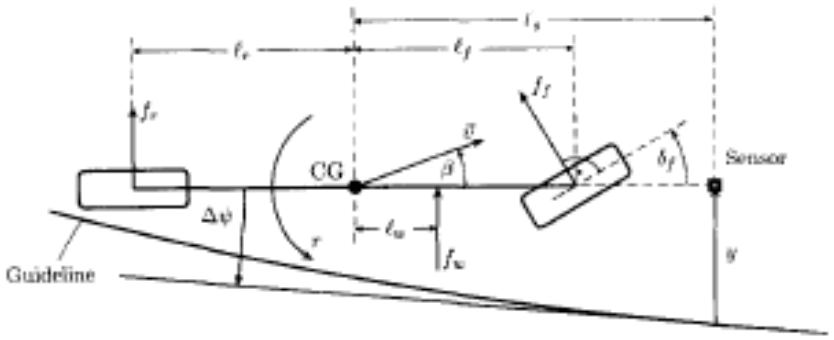

Figure 3.3 : Single track model for car steering, [35].

Together with the dynamics of the reference path and an actuator with integrating characteristics the vehicle dynamics is discribed by the fifth order model

$$\begin{pmatrix} \dot{\beta} \\ \dot{r} \\ \Delta\dot{\psi} \\ \dot{y} \\ \dot{\delta}_f \end{pmatrix} = \begin{pmatrix} a_{11} & a_{12} & 0 & 0 & b_{11} \\ a_{21} & a_{22} & 0 & 0 & b_{21} \\ 0 & 1 & 0 & 0 & 0 \\ v & l_s & v & 0 & 0 \\ 0 & -k_r & 0 & 0 & 0 \end{pmatrix} \begin{pmatrix} \beta \\ r \\ \Delta\psi \\ y \\ \delta_f \end{pmatrix} + \begin{pmatrix} 0 & 0 \\ 0 & 0 \\ 0 & -v \\ 0 & 0 \\ 1 & 0 \end{pmatrix} \begin{pmatrix} u_f \\ \rho_{ref} \end{pmatrix} \qquad \textbf{(3.18)}$$

where

$$a_{11} = -\left(c_r + c_f\right)/\tilde{m}v \qquad a_{12} = -1 + \left(c_r l_r - c_f l_f\right)/\tilde{m}v^2$$
$$a_{21} = \left(c_r l_r - c_f l_f\right)/\tilde{J} \qquad a_{22} = \left(c_r l_r^2 - c_f l_f^2\right)/\tilde{J}v$$

$b_{11} = c_f / \tilde{m}v$ $\qquad\qquad$ $b_{22} = c_f l_f / \tilde{J}$

The cornering stiffnesses are written as a product μc_f front axle and μc_r for rear axle, where μ is a common road adhesion factor with μ=1 for dry road and μ=0.5 for wet road. The vehicle mass m is normalized by μ, i.e., $\tilde{m} = m/\mu$ is a "virtual mass". Similarly, the moment of inertia J is normalized as $\tilde{J} = J/\mu$. The curvature $\rho_{ref}=1/R_{ref}$ of the guideline appears as a reference input to the system. It can be assumed that the reference path consists of circular arc i.e. the transition to new curvature corresponds to a step input in ρ_{ref}. The numerical values are taken from the product catalogue of Mercedes Sprinter and used in simulations for the minibuses operating on the metrobus line are $l_f = 2.725\,m$, $l_r = 1.60\,m$, $l_s = 4.125\,m$, $m = 8600\,kg$, $c_f = 100\,000\,N/rad$, $c_r = 235\,000\,N/rad$, $J = i^2 m$ (or $\tilde{J} = i^2\tilde{m}$) with $i^2 = 4.25\,m^2$.

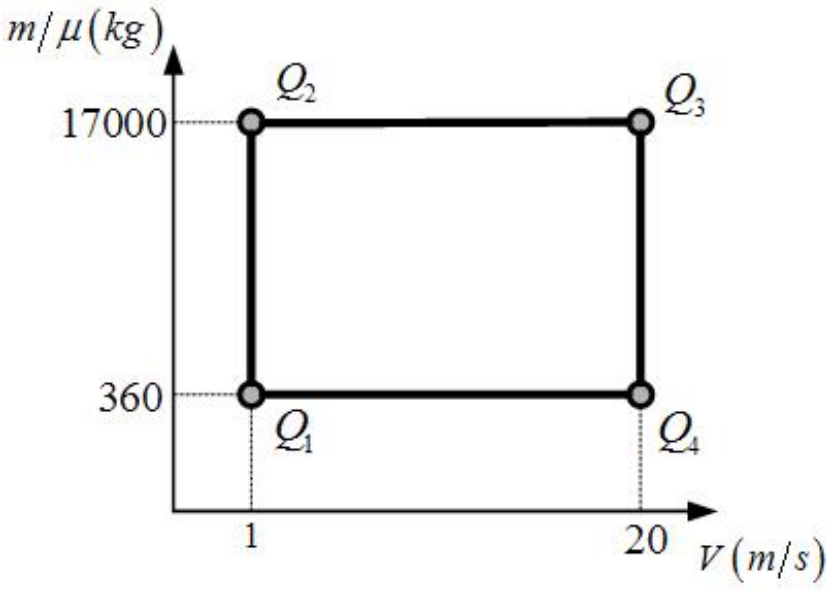

Figure 3.4 : Operating domain *Q* of Mercedes Sprinter.

The largest parametric variation occurs in the velocity v and virtual mass $\tilde{m}$ of the minibus during the operation. The corresponding operating ranges of v $v \in [1:20]\,m/s$ and $\tilde{m} \in [3600:17000]\,kg$ are illustrated in the uncertainty (or *Q*) box given in Figure 3.3 where the corners of the *Q*-box have been labeled as q_1 to q_4 and represent extreme points to be investigated in assessing robustness of performance.

In the automatic car steering problem, PID^2 controller can be utilized. It is proven the efficiency of controller in the previous works of Ackermann et al [35]. For this, PID^2 controller will be used in this work, as well.

$$G_C(s) = \omega_c^2 \frac{K_{dd}s^3 + K_d s^2 + K_p s + K_i}{s\left(s^2 + 2\varsigma\omega_c s + \omega_c^2\right)\left(s + \omega_c\right)} \qquad \textbf{(3.19)}$$

where third real compansator pole with the same bandwidth ω_c was chosen. By using the COntrol of MEchatronic Systems (COMES) Toolbox, the stability region of automated car steering system in the chose parameter space are figured out for each corner of *Q*-box. The Hurwitz stability regions calculated for each corner of *Q*-box are given in Figure 3.5. The intersection of Hurwitz stability regions is given with blue colour. The chosen compansator is

$$G_C(s) = 100^2 \frac{0.5s^3 + 10s^2 + 12.5s + 5}{s\left(s^2 + 120s + 100^2\right)\left(s + 100\right)} \qquad \textbf{(3.20)}$$

The chosen compensator (given above) should be robustly stable with respect to the parameter variations.

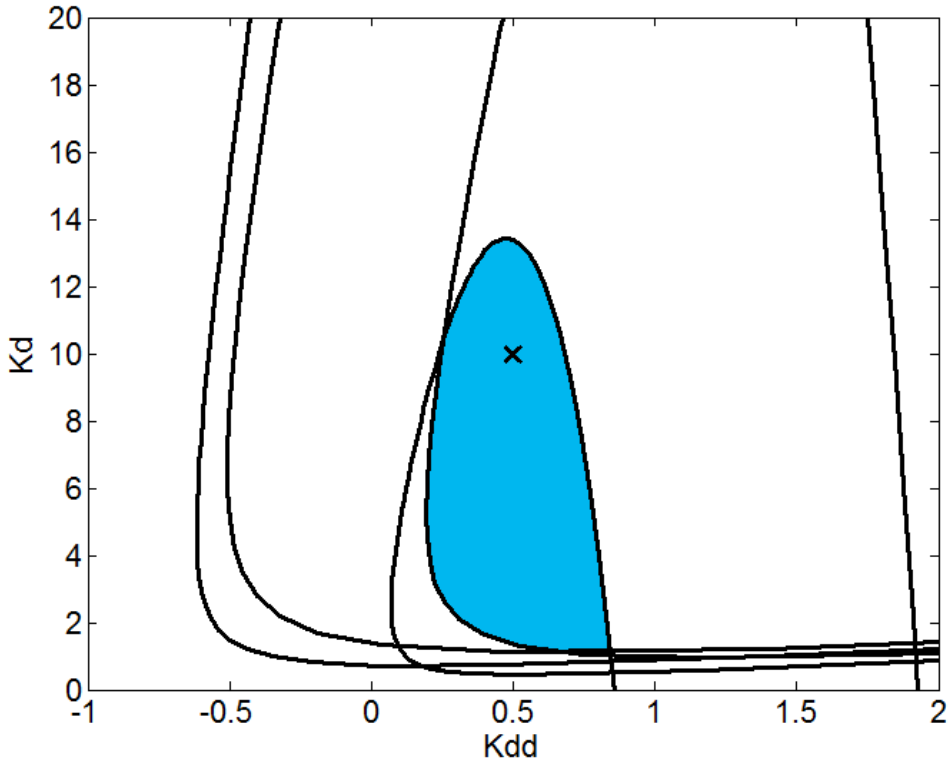

Figure 3.5 : Set of Γ-stabilizing controllers for ζ=0.6, ω=100, K_p=12.5 and K_i =5.

The curvature $\rho_{ref}=1/R_{ref}$ of the guideline is a measurable external disturbance. This external disturbance which is also the path to be followed comprises of circular arcs with the transition to a new curvature corresponding to a step input in ρ_{ref}.

In this part of our work, the simulations are made for two different type of road profile (Crows Landing and Richmond Field Station test tracks). When the minibus travels on these tracks, the external disturbances seen in Figure 3.6 are applied to it. The test tracks and simulation results can be seen in Figure 3.7 and 3.8. Additionally, the velocity of minibus will exponentially decrease to zero when it comes close to the bay less than 100 m. In order to obtain exponential decrease in seed, a PI controller is used as a cruise controller. The all simulation results are considered that the robust PID^2 controller is very appropriate for the automatic path following process. The lateral displacement is also less than 0.15 m being a specification given in an IFAC benchmark problem. In addition to lateral displacement, there do not exist any excessive yaw rates in the simulations for each test tracks.

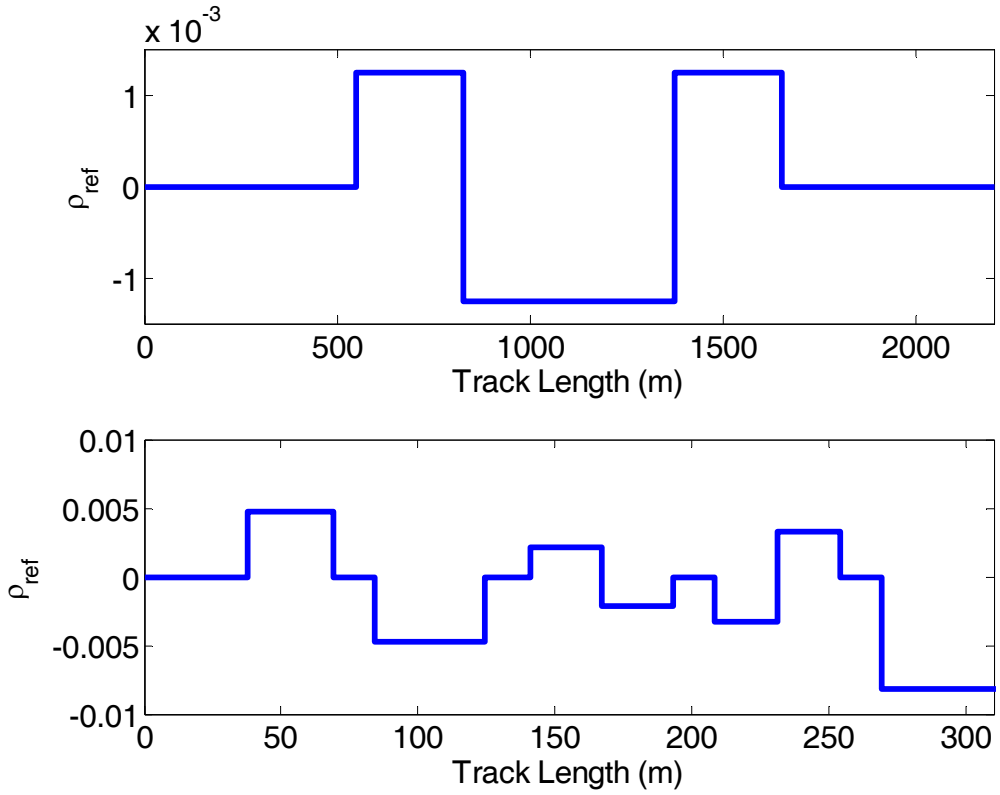

Figure 3.6 : External disturbance ρ_{ref} for two different test tracks.

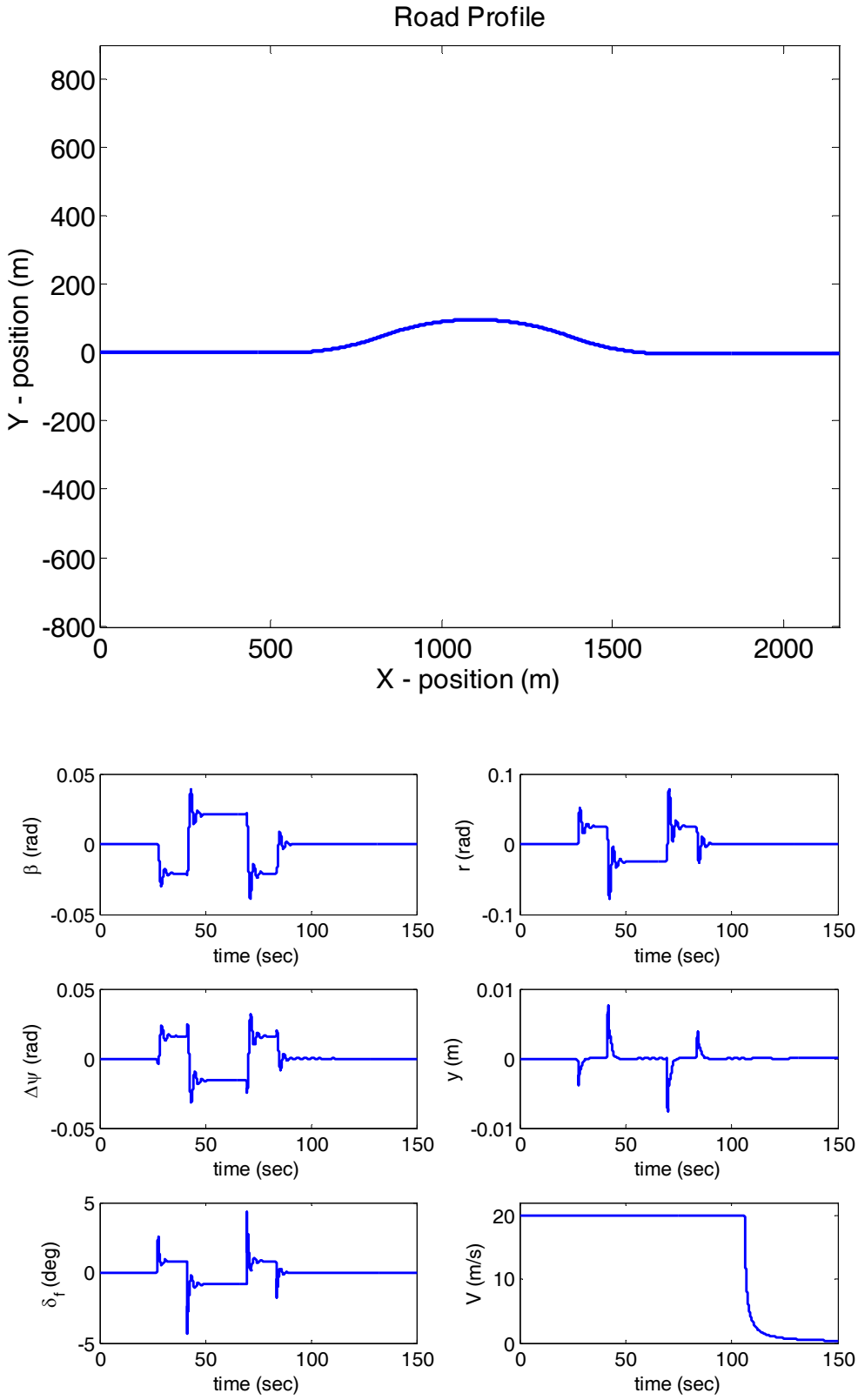

Figure 3.7 : Crows Landing test track.

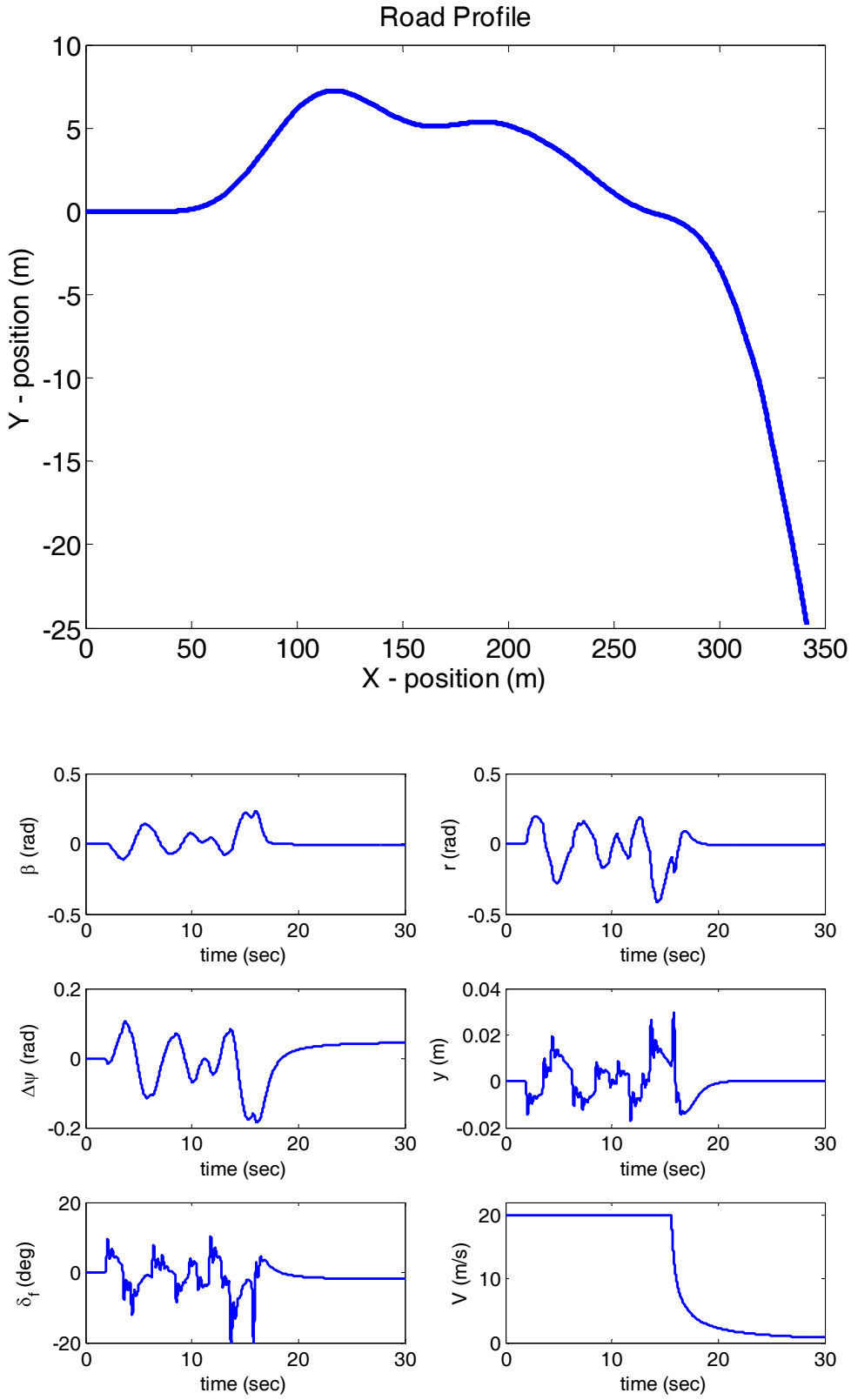

Figure 3.8 : Richmond Field Station test track.

3.4 COMES Toolbox: Parametric Robust Control System Design

Current version of COMES toolbox includes "Parametric Robust Control System Design" section. In this section three different has got four windows:

- Main Window

  has some buttons in order to open the other sub-windows like "D-Stability Analysis", "Gain Margin Design", "Phase Margin Design" and "Mapping Frequency Domain Specs". In addition, there is a button to enter symbolic controller and specify uncertain parameters. There also exist some checkboxes to draw the chosen parameter spaces on a figure.

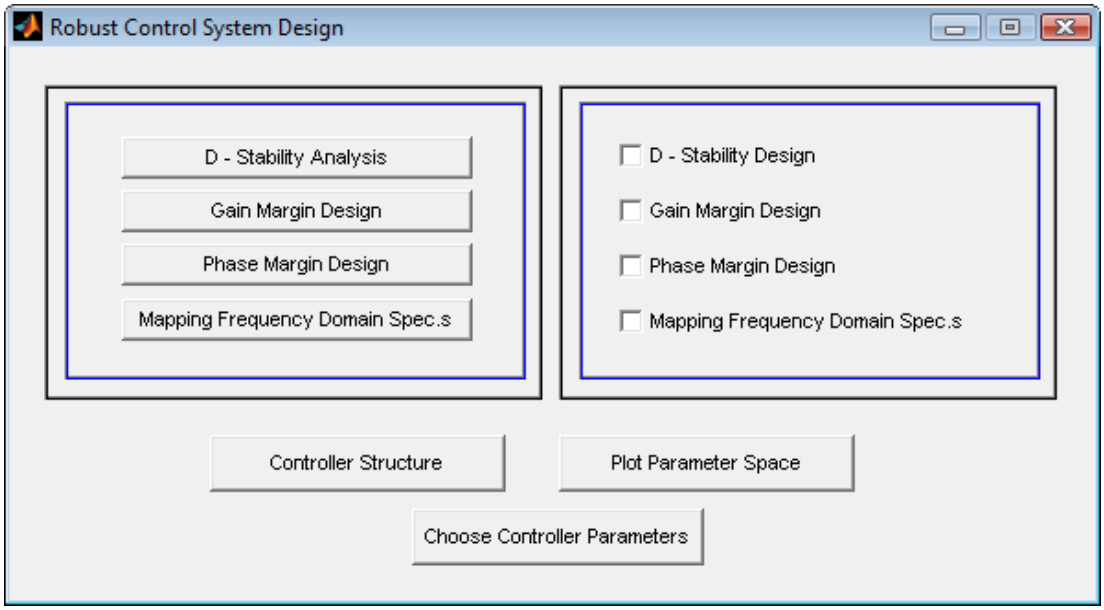

Figure 3.9 : Main window of robust control system design part of COMES toolbox.

- *D*-stability Analysis and Design Window

  This GUI includes two different plots. One of them is used for checking the location of poles in the *D*-stability region and the other one is used for the parameter space design. Moreover, there are some edit boxes to enter the contraints (such as settling time, damping and bandwidth). There are some buttons to calculate and plot the chosen repetitive controller parameter space. Moreover, the parameter space can be captured, zoomed on/off or plotted on a new figure whose number can be re-entered by the user by utilizing the buttons in the GUI.

- Phase Margin Design Window

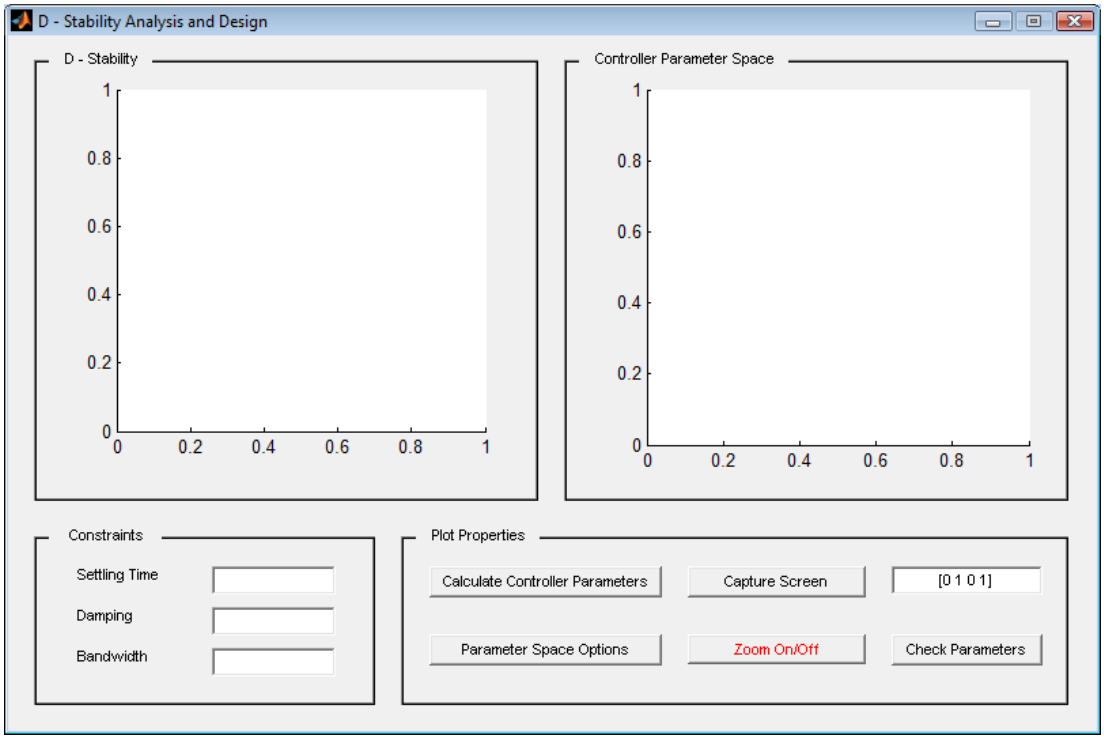

Figure 3.10 : *D*-stability analysis and design window.

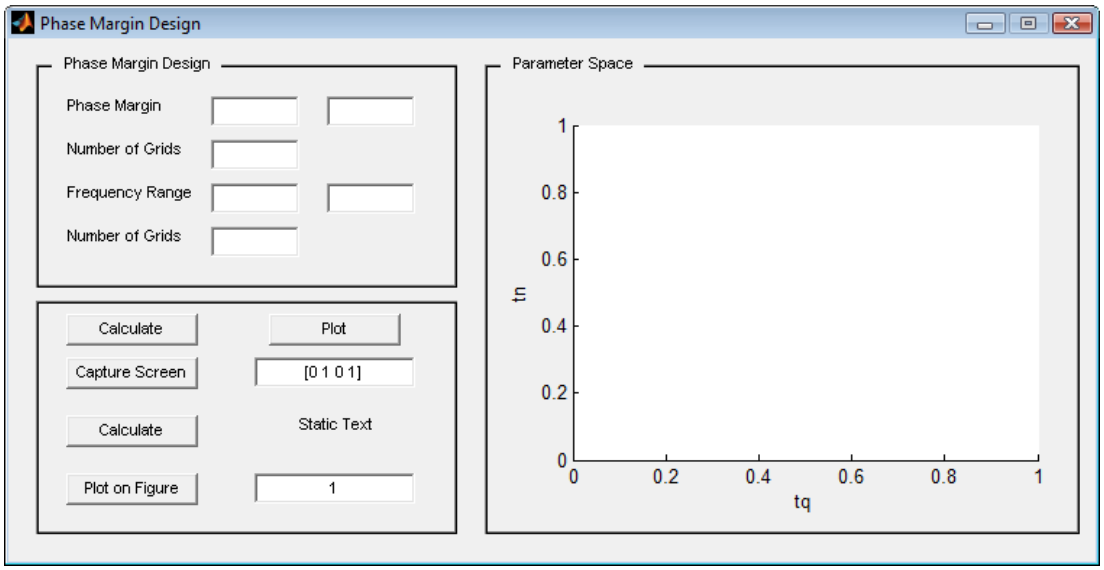

Figure 3.11 : Phase margin design window.

There are some edit boxes to enter the frequency range to determine the parameter space regions. Additionally, the user can check the numerical value of phase margin for chosen controller parameters by utilizing check button. There are some buttons to calculate and plot the chosen repetitive controller parameter space. Moreover, the parameter space can be captured, zoomed on/off or plotted on a new figure whose number can be re-entered by the user by utilizing the buttons in the GUI.

3.5 Chapter Summary and Concluding Comments

In this chapter, we presented a robust design based on mapping Hurwitz stability, *D*-stability and the frequency domain specifications of weighted sensitivity minimization and phase /gain margin bound to the chosen controller parameter plane. Additionally, we can achieve not only a single-objective controller synthesis but also multi-objective controller synthesis among the above specifications based on a parameter space approach. Moreover, a numerical example is used to demonstrate the effectiveness of abovementioned robust design. The robust control approach can be applied to all control systems given in this thesis instead of preview control.

4. PREVIEW CONTROL

4.1 Introduction to Preview Control

The goal of the reference feedforward tracking control is to obtain a low-pass filter of desired tracking bandwidth between the input and output to reduce tracking error below what is achievable with feedback alone. A two degree of freedom (2 DOF) controller architecture is utilized in order to achieve this purpose by cascading the closed-loop control system, already under feedback control, with its approximate inverse, as show in Figure 4.1. Seeking an exact inverse based on pole-zero cancellation to achieve perfect compensation of the plant or closed-loop system is the ideal goal. This is possible since nonminimum phase (NMP) zeros, if they exist, cannot be inverted directly. NMP zeros are common in models of process control systems with transport lag [13] and flexible structure [36]. Exact inversion is not a good idea because of the presence of model uncertainties at high frequencies even if the system consists of minimum phase zeros. Therefore, the approximate inverse should have low-pass filter characteristics between system's input and output.

There are several methods in literature in order to design approximate inverse filters for discrete-time systems with NMP zeros. The earliest method in literature is zero phase error tracking (ZPET) control of Tomizuka [37], where the phase error due to the NMP zeros is eliminated for achieving zero phase error trajectory tracking. However, ZPET filter cannot eliminate the gain error due to the NMP zeros. For this purpose, this gain error can be compensated by utilizing E-filter [38], precision tracking control (PTC) [39] or optimal precision tracking control (OPTC) [40]. Extended precision tracking control (EPTC) [41] is able to tackle discrete-time systems with complex NMP zeros as well as real ones. Furthermore, the designers have more freedom while using the EPTC method because both the desired tracking bandwidth and flat low frequency gain characteristics can be obtained in comparison to just one of them achieved in the PTC method. In truncated series approximation (TSA) method of Gross et al [42], polynomial long division is utilized to obtain a non-zero phase solution.

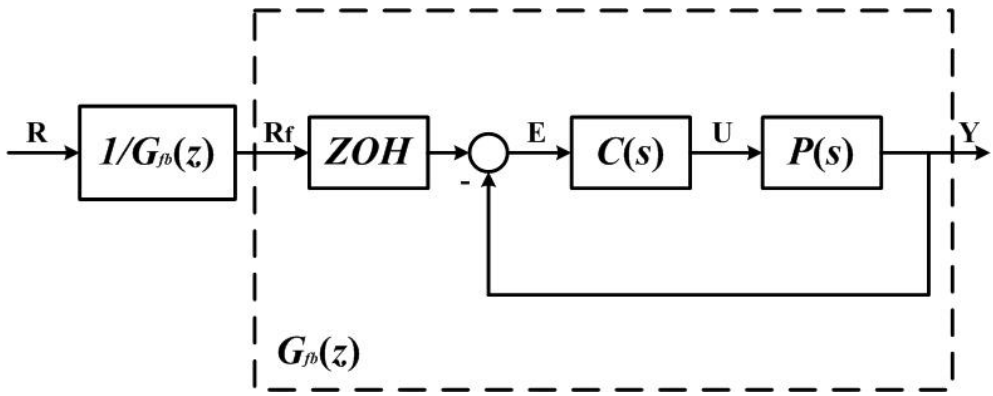

Figure 4.1 : Discrete time reference feedforward tracking control.

Outline of the Chapter: The organization of the rest of Chapter 4 is as follows. In Section 4.2, some basic information on non-minimum phase (NMP) zeros are given, in detail. The ZPET, PTC and OPTC methods of reference feedforward controller design are discussed briefly in Section 4.3. Then, in Section4.4, a numerical example of control of tool positioning in noncircular machining is used in order to demonstrate the ease of synthesizing input shaping filters by utilizing COMES toolbox. Section 4.5 demonstrates the Preview Control System Design part of COMES toolbox and gives some valuable information how to use this toolbox. Moreover, its use is explained with an example from the literature. Chapter ends with its summary and conclusions in Section 4.6.

4.2 Discrete Time Non-minimum Phase (NMP) Zeros

The condition under which complex NMP zeros occur is investigated in [43], in detail. In addition, the condition is extensively explained in the following part of this chapter. Furthermore, a characterization of complex NMP zeros will be made with respect to their gain plots. Let us consider the zero-order-hold (ZOH) discretized version $G(z)$ of the continuous time plant $P(s)$ illustrated in Figure 4.1. $G(z)$ has n poles and n-1 zeros, some of which may be at infinity, for $P(s)$ with n poles and m zeros. Even though poles p_i of $P(s)$ are transformed simply into poles $e^{p_i T_s}$ of $G(z)$, the transformation of the zeros is much more complicated. In the limiting case of small sampling time T_S, the location of the zeros of $G(z)$ are governed by the following theorem.

Theorem 4.1 (Aström et al, [43]): Let be the rational function

$$P(s) = K\frac{(s-z_1)(s-z_2)...(s-z_m)}{(s-p_1)(s-p_2)...(s-p_m)} \quad (m<n) \tag{4.1}$$

and $G(z)$ the corresponding pulse transfer function. Then, as $T_S \rightarrow 0$, m zeros of $G(z)$ go to 1 as $e^{z_i T_s}$ and the remaining n-m-1 zeros of $G(z)$ go to zeros of the polynomial $B_{n-m}(z)$. The polynomials $B_{n-m}(z)$ are given in Aström et al [43] and have both MP and NMP real zeros for n-m>2 and no complex zeros. Therefore, G(z) corresponding to P(s) with relative degree greater than or equal to 2 (n-m>2) will necessarily have real NMP zeros coming from $B_{n-m}(z)$ for small sampling time. Complex NMP zeros, if they exist, occur in complex conjugate pairs since $G(z)$ is real rational. Complex NMP zeros occur for small sampling time can be determined using Theorem 4.1 and is summarized by the following corollaries which are taken from the reference [44].

Corollary 4.1: For small sampling rate T_S, the m_c ($2m_c<m$) complex conjugate zero pairs of $P(s)$, if any, in equation **(4.1)** result in m_c complex conjugate zero pairs of $G(z)$ which go to 1 as as $T_S \rightarrow 0$.

Remark 4.1: For small sampling rate T_S, complex zeros of $G(z)$ are only possible for $H(s)$ with $m \geq 2$.

Remark 4.2: For small sampling rate T_S, $G(z)$ will have complex NMP zeros if and only if $H(s)$ has complex NMP zeros.

The location of zeros of $G(z)$ in the limiting case of large sampling time is characterized by the following theorem.

Theorem 4.2 (Aström et al, [43]): Let $P(s)$ be a strictly proper, stable and rational transfer function with $P(0)\neq 0$. Then, all zeros of $G(z)$ go to 0 as $T_S \rightarrow \infty$.

Note that for large sampling time, complex zeros of $P(s)$ might become real zeros of $G(z)$. Moreover, it is not possible for $G(z)$ to have NMP zeros for large enough sampling time if $P(s)$ satisfies the conditions of Theorem 4.2. A conservative approach to guarantee minimum phase $G(z)$ is given in Aström et al [43]. Less conservative conditions can be found in Fu and Dumont [45] and Ishitobi [46].

The condition under which NMP zeros are able to occur for large sampling time can be determined by utilizing Theorem 4.2 and also summarized by the following corollary.

Corollary 4.2: For large sampling time T_S, $G(z)$ can have NMP zeros if and only if $P(s)$ does not satisfy one of the conditions of Theorem 4.2 (for instance, $P(s)$ is unstable, biproper or $P(0)=0$).

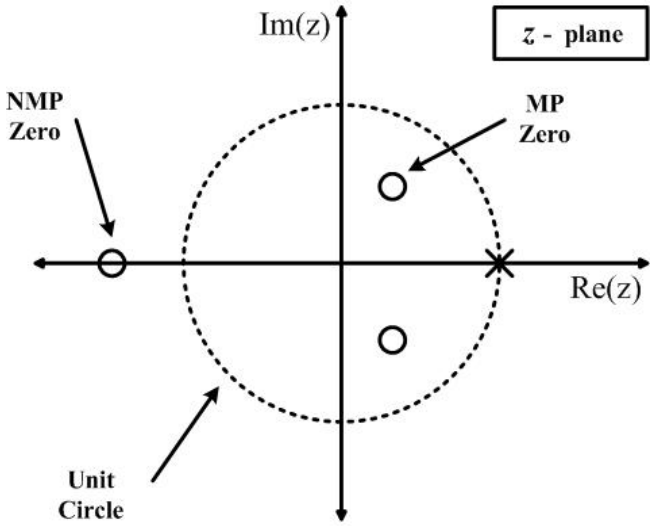

Figure 4.2 : Pole-zero map of a discrete control system.

Real NMP zeros have been categorized as type I and type II zeros. Type I zeros lie to the left of the unit circle and type II lie to the right of the unit circle. Type I and type II zeros have decreasing and increasing gain characteristics, respectively. Hence, the gain error of type I zeros can be compensated by using type II zeros and vice versa when applying PTC method of feedforward compensation.

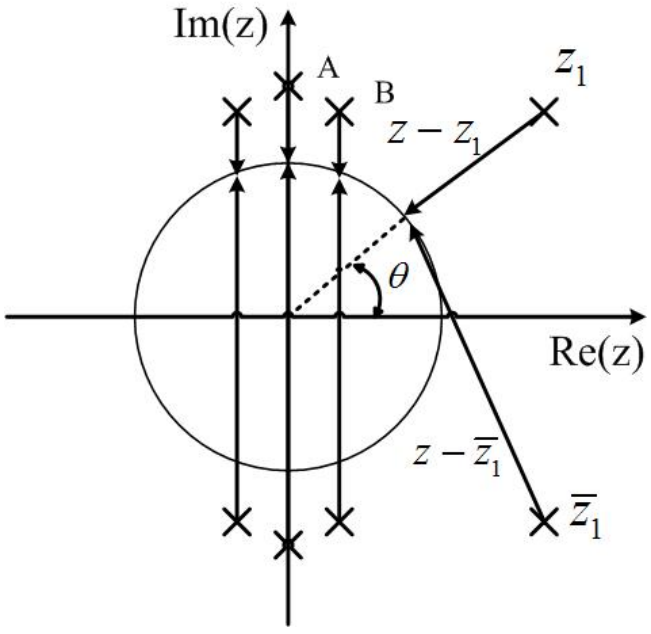

Figure 4.3 : Illustration of discrete time magnitude frequency response calculation for equation 4.1.

The magnitudes of $(z\text{-}z_1)$ and its complex conjugate are multiplied and recorded in a sweep of the point $z=e^{j\theta}$ with $\theta=\omega T_S$ from 0 to the Nyquist frequency of π radians in order to obtain the magnitude frequency response. According to Figure 4.3, purely imaginary NMP zeros will have a valley at $\theta=\pi/2$ in their magnitude frequency response which will get deeper as the zero approaches the unit circle.

4.3 Different Feedforward Controller Designs

There are several methods which can be utilized to design non-causal approximate inverse filters for discrete-time systems with NMP zeros. Some of these techniques are demonstrated in the following part of this chapter.

4.3.1 Zero phase error tracking (ZPET) control

The earliest method of designing preview control system based on reference feedforward controllers is the ZPET scheme of Tomizuka et al [37], where the phase error due to the NMP zeros can be eliminated in order to achieve zero phase error trajectory tracking. Let us consider how to design ZPET feedforward controller. It is expressed below, in detail.

The nominal transfer function of closed-loop control system within the dashed box in Figure 4.1 can be expressed as

$$G_{fb}(z)=\frac{n_{mp}(z)\,n_{nmp}(z)}{d(z)} \qquad \textbf{(4.1)}$$

where $n_{mp}(z)$ and $n_{nmp}(z)$ are the minimum and non-minimum phase parts, respectively, of the numerator. The non-minimum phase part of the numerator can be factored into

$$n_{nmp}(z)=\prod_{k=1}^{m}(z-z_k) \qquad \textbf{(4.2)}$$
$$z_k \in C,\ \ |z_k| \geq 1$$

where C denotes complex numbers, z_k are the m non-minimum phase zeros of the feedback system. Note that complex conjugation of factors of the form $z\text{-}z_k$ ($z_k \in C$) over the unit circle amounts to

$$\overline{(z-z_k)}\Big|_{z=e^{j\theta}}=\left(z^{-1}-\overline{z}_k\right)\Big|_{z=e^{j\theta}} \qquad \textbf{(4.3)}$$

The ZPET approximate inverse of $G_{fb}(z)$ is given by

$$\tilde{G}_{ZPET}^{-1}(z) = \frac{d(z)}{n_{mp}(z)} \prod_{k=1}^{m} \frac{\left(z^{-1} - \overline{z}_k\right)}{\left(1 - z_k\right)\left(1 - \overline{z}_k\right)} \qquad \textbf{(4.4)}$$

The first part of equation **(4.4)** is invertible part of $G_{fb}(z)$. The remaining part of equation **(4.4)** has been expressed so that the compensated system $\tilde{G}_{ZPET}^{-1}(z) G_{fb}(z)$ has zero phase angles at all frequencies. Whatever can be inverted in $G_{fb}(z)$ has been inverted and the remaining nonminimum phase part has been multiplied by its complex conjugate in the frequency domain. The $(1\text{-}z_k)$ type terms in the denominator of equation **(4.4)** are introduced to make the d.c. gain of the feedforward compensated system equal to unity. The transfer function of the ZPET feedforward compensated system becomes

$$\tilde{G}_{ZPET}^{-1}(z) G_{fb}(z) = \prod_{k=1}^{m} \frac{\left(z - z_k\right)\left(z^{-1} - \overline{z}_k\right)}{\left(1 - z_k\right)\left(1 - \overline{z}_k\right)} \qquad \textbf{(4.5)}$$

4.3.2 Precision tracking (PTC) control

The ZPET approach might increase the gain errors while the phase errors are cancelled. Therefore, the desired tracking control characteristics can be obtained only within a relatively small bandwidth. For this reason, it should combine the zero phase error of the ZPET method with a gain error compensation method. To achieve this purpose, the PTC (Precision Tracking Control) method adds gain error compensating zeros while preserving zero phase error characteristics.

In the PTC method, terms involving real nonminimum phase zeros are separated into two different categories as type I and type II relied on whether their amplitude Bode plots rise or fall with respect to frequency. Gain error due to type I NMP zeros can be compensated by adding appropriate type II NMP zeros to the feedforward compensator and vice versa. The PTC feedforward compensator is given by

$$\tilde{G}_{PTC}^{-1}(z) = \frac{d(z)}{n_{mp}(z)} \prod_{k=1}^{m} \frac{\left(z^{-1} - \overline{z}_k\right)}{\left(1 - z_k\right)\left(1 - \overline{z}_k\right)} \frac{\left(z - z_k^*\right)\left(z^{-1} - \overline{z}_k^*\right)}{\left(1 - z_k^*\right)\left(1 - \overline{z}_k^*\right)} \qquad \textbf{(4.6)}$$

where $z_k^* \in C$ indicates the gain compensating zero corresponding to the NMP zero z_k. The PTC feedforward compensator given in equation **(4.6)** adds gain compensating zero expression in order to use for zero phase on top of the ZPET controller of

equation **(4.5)**. The transfer function of the feedforward compensated system becomes

$$\tilde{G}_{PTC}^{-1}(z)G_{fb}(z)=\prod_{k=1}^{m}\frac{(z-z_k)(z^{-1}-\overline{z}_k)}{(1-z_k)(1-\overline{z}_k)}\frac{(z-z_k^*)(z^{-1}-\overline{z}_k^*)}{(1-z_k^*)(1-\overline{z}_k^*)} \qquad \textbf{(4.7)}$$

The gain compensating zeros are determined using

$$\left|\tilde{G}_{PTC}^{-1}(e^{j\theta})G_{fb}(e^{j\theta})\right|_{\theta=\theta^*}=1 \qquad \textbf{(4.8)}$$

By utilizing the PTC method, the system tracking bandwidth can be assigned arbitrarily according to the tracking signal and the tracking accuracy can be totally improved. However, it should be kept in mind that it is not an optimal method and there are situations where the desired bandwidth is not achieved even if the PTC design method usually leads to satisfactory results.

4.3.3 Optimum precision tracking (OPTC) control

In this section, the nonminimum phase part of the numerator can be factored into

$$n_{nmp}(z)=\prod_{k=1}^{m_r}(z-z_k)\prod_{l=1}^{mc}(z-z_l)(z-\overline{z}_l) \qquad \textbf{(4.9)}$$

and has m_r real and m_c complex conjugate pairs of NMP zeros. Hence, $n_{nmp}(z)$ in expression **(4.9)** has a total of m_r+2m_c NMP zeros. Note that complex conjugation of factors in equation **(4.1)** for z on the unit circle amounts to the equation given in **(4.3)**.

The OPTC feedforward compensator is given by

$$\begin{aligned}\tilde{G}_{OPTC}^{-1}(z)=&\left[\frac{d(z)}{n_{mp}(z)}\right]\left[\prod_{k=1}^{m_{r1}}\frac{(z^{-1}-\overline{z}_k)}{(1-z_k)^2}\prod_{l=1}^{m_{c1}}\frac{(z^{-1}-z_l)(z^{-1}-\overline{z}_l)}{(1-z_k^*)(1-\overline{z}_k^*)}\right]\\&\left[\prod_{r=1}^{m_{r2}}\frac{(z-z_r)(z^{-1}-z_r)}{(1-z_r)^2}\right]\left[\prod_{c=1}^{m_{c2}}\frac{(z-z_c)(z^{-1}-\overline{z}_c)}{(1-z_c)^2}\frac{(z-\overline{z}_c)(z^{-1}-z_c)}{(1-\overline{z}_c)^2}\right]\end{aligned} \qquad \textbf{(4.10)}$$

where $z_r \in \mathbb{R}$ and $z_c \in \mathbb{C}$. The first expression of equation **(4.10)** is invertible part of $G(z)$ in equation **(4.1)**. The second expression of equation **(4.10)** is zero phase of $n_{nmp}(z)$ after compensation. The last two expressions are used for gain error compensation with m_r real and m_c complex conjugate pairs of gain compensation

zeros. The compensated system $\tilde{G}_{ZPET}^{-1}(z)G_{fb}(z)$ has by construction zero phase at all frequencies and the gain compensation zeros are determined optimally by solving

$$\min_{\substack{z_r\in R;\, r=1,2,\ldots,m_{r2}\\ z_c\in C;\, c=1,2,\ldots,m_{c2}}} \int_0^{\pi} \left| W(\theta)\left(1-\tilde{G}_{PTC}^{-1}\left(e^{j\theta}\right)G_{fb}\left(e^{j\theta}\right)\right)\right|^2 d\theta \qquad \textbf{(4.11)}$$

$W(\theta)$ in expression **(4.11)** is a weighting function that is usually chosen as

$$W(\theta)=\begin{cases}1, & \theta\le\theta^*\\ 0, & \theta>\theta^*\end{cases} \qquad \textbf{(4.12)}$$

where is desired bandwidth of feedforward compensation. Moreover, the weight can be alternatively chosen in order to minimize the tracking error for an input signal if the desired input trajectory is known in advance. The formulation give in equation **(4.11)** works well for both real and complex conjugate NMP zeros. However, there could be some problems when the complex conjugate NMP zeros are close to the imaginary axis or unit circle.

4.4 Case Study: Control of Tool Positioning in Noncircular Machining

The closed-loop position control system of a hydraulic linear actuating system which is used for tool positioning in noncircular machining in [47] is chosen for the simulation study since its model includes a complex conjugate NMP zero pair. The discrete time, reduced order model of closed-loop system is given by

$$G(z)=\frac{0.06z^2+0.034z+0.071}{z^7-0.606z^6-0.747z^5+0.519z^4} \qquad \textbf{(4.13)}$$

The complex NMP zeros are $z_1,\overline{z}_1=-0.2833\pm j1.0503$. This pair of complex conjugate NMP zero is close to the imaginary axis and the unit circle. For this reason, it is hard to compensate. In addition, the gain plot has a valley close to $\theta=\pi/2$ rad and then it rises to about unity at $\theta=\pi$ rad. To compensate for this gain characteristics, the compensating zeros must be added for introducing sufficient gain attenuation at high frequencies. However, the optimization formulation given in **(4.11)** might create some problems for this kind of hard to compensate complex conjugate NMP zero pairs. For this purpose, the weighting function $W(\theta)$ is selected to have large gain at high frequencies above θ^* and is chosen in this case study as $3.61/|e^{j\theta}+0.9|^2$ to provide large weight at high frequencies.

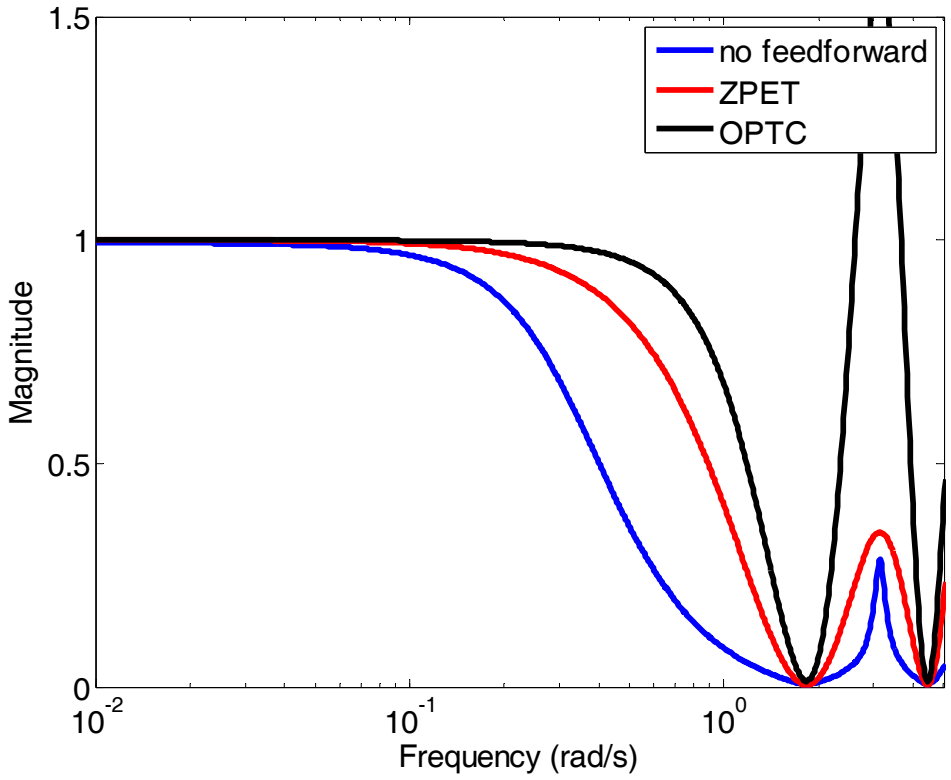

Figure 4.4 : Magnitude frequency responses of OPTC and ZPET compensated systems.

The OPTC calculations, successively, with one real, two real and one complex conjugate gain compensating zero pair leaded to the best result which is obtained by the two real zeros case (m_{r2}=2 and m_{c2}=0). The two real gain compensating zeros are z_1=0.0867 and z_2=0.2874. The magnitude frequency response plots seen in Figure 4.4 show the comparison between the gain compensation ability of two input shaping filters: ZPET and OPTC.

4.5 COMES Toolbox: Preview Control System Design

Current version of COMES toolbox includes "Preview Control System Design" section. "Preview Control System Design" section has got only one window:

- Main Window

  has some edit fields for adding discrete plant, adding weighting function, specifications on optimization routine and controller parameters.

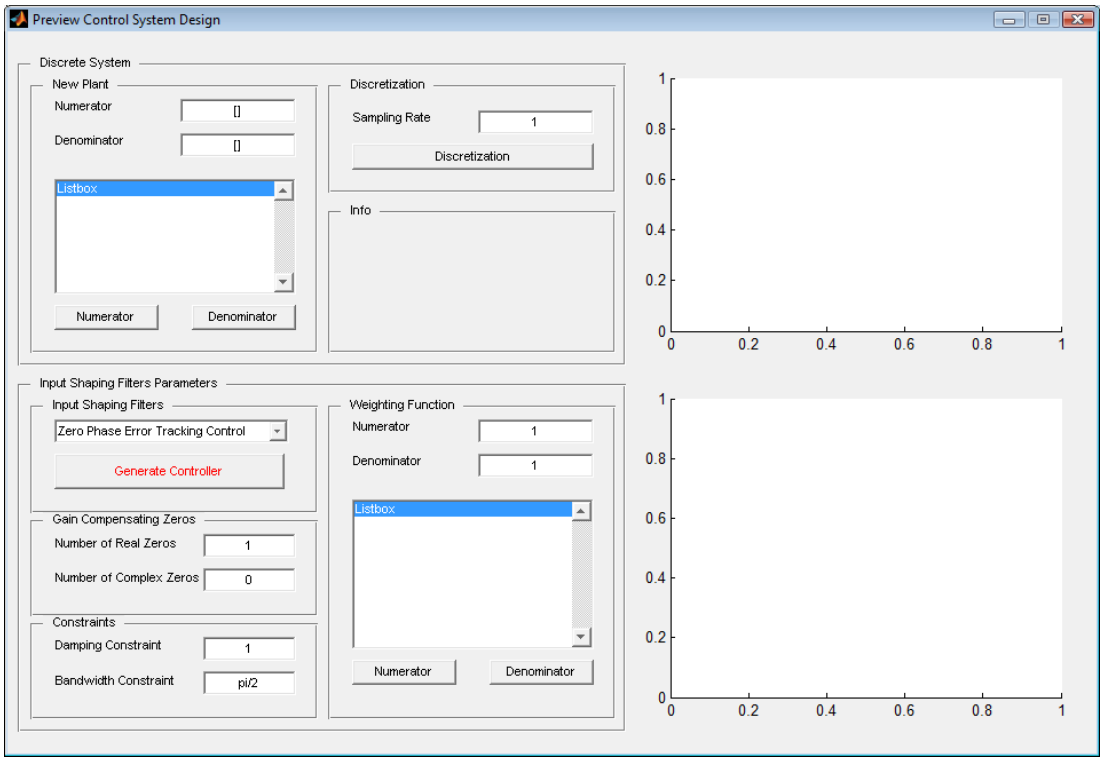

Figure 4.5 : Main window of preview control system design part of COMES toolbox.

It shows a Bode magnitude plot (for closed-loop control system with/without input shaping filter) and a pole-zero map. By benefiting from pole-zero map, the location of gain compensating zeros can be seen. Utilizing Bode magnitude plot, several systems with input shaping filter can be compared with each other and best one can be selected. Furthermore, users can change specifications to manipulate the frequency response of the closed-loop control system with input shaping filter.

In the current version of this toolbox, two different type of controller can be designed. First one is zero phase error tracking (ZPET) controller and the other one is optimal precision tracking controller (OPTC). The designation of ZPET controller is very easy because users cannot enter any parameters or design specifications. In order to calculate controller parameters, they just push "Generate Controller" button. However, users should choose a weighting function and number of real (or complex pair of) gain compensating zeros if they would like to design an OPTC. When designing OPTC, the Big-Bang Big-Crunch (BB-BC) optimization method is utilized so as to determine the real (or complex pair of) gain compensating zeros. Meanwhile, some constraints can be specified when BB-BC method searches the chosen

parameter space. For instance, the damping (or bandwidth) constraint can be specified.

4.6 Chapter Summary and Concluding Comments

In this chapter, the effect of discrete-time real NMP zeros and complex conjugate NMP zero pairs to system performance was given in detail. The gain error associated with these NMP zeros was characterized based on their location in the complex plane. Notice that the locations closer to the imaginary axis and the unit circle leads to gain characteristics being difficult to compensate for preview based feedforward control. In order to perfect tracking of a reference signal, we investigated several types of non-causal approximate inverse filters for discrete-time:

- ZPETC (Zero Phase Error Tracking Controller)
- PTC (Precision Tracking Controller)
- OPTC (Optimal Precision Tracking Controller)

After comparing theses three input shaping filters with each others, it was shown that the best result belongs to OPTC when dealing with the system which contains NMP zeros. ZPET can cancel the phase error but not cancel the all gain error. However, PTC and especially OPTC can eliminate both phase error and gain error. Moreover, the MATLAB-based toolbox is used to design preview control system. In the next chapter, model regulator control architecture and its robust design based on mapping frequency domain specifications like nominal performance, robust stability and robust performance to chosen parameter space will be presented. The all calculation will be done using COMES toolbox.

5. MODEL REGULATOR CONTROL

5.1 Introduction to Model Regulator Control

The model regulator (disturbance observer) is a particular method of designing a two degree-of-freedom (2 DOF) control architecture in order to achieve insensitivity against modelling errors due to model order reduction, linearization and the presence of parameter uncertainties and also good sensor noise attenuation as well as disturbance rejection [48-49]. It has been successfully applied to many application areas: motion control applications including high speed direct drive positioning [50], friction compensation [51] and vehicle steering control [52-53]. The augmentation of a plant with the model regulator (disturbance observer) forces it to behave just like its nominal (or desired) model within the bandwidth of model regulator (disturbance observer), called the bandwidth of the model regulation. The model regulation can be achieved by means of comparing the actual input to the plant with the input that should have been applied to obtain the measured output relied on the nominal (or desired) knowledge of the plant and then by passing the difference through a positive feedback loop. Unlike its name, disturbance rejection is not the only feature of a disturbance observer. Its model regulation capability allows specification and achievement of desired system dynamics which was applied to the vehicle yaw stability control problem in [54-55].

In addition to desirable model regulation and disturbance rejection effects, the disturbance observer introduces stability and stability robustness problems due to the use of positive feedback. Use of unstructured model uncertainty and low-pass filtration of the disturbance observer output is very practical manner to avoid stability robustness problem at high frequencies due to the presence of unmolded dynamics. Many problems like [52] and [53] involve well-defined real parametric uncertainty in a known plant. The conventional stability robustness analysis based on unstructured uncertainty becomes more conservative for some cases. In Chapter 5, structured singular value (SSV) analysis is proposed and used to investigate the effect of mixed parametric/complex uncertainty on stability and performance

robustness of disturbance observer compensated systems. Furthermore, an interactive MATLAB program with a graphical user interface (GUI) was prepared by the author in order to determine parameter space regions corresponding to chosen frequency-domain criteria.

Outline of the Chapter: The organization of the rest of the Chapter 5 is as follows. Section 5.2 introduces the model regulator (disturbance observer) and its general architecture. The technique of mapping robust performance frequency domain specifications into model regulator parameter space is investigated in Section 5.3. Then, a numerical design example and simulation study of four wheel vehicle steering control for yaw stabilization is utilized an illustrated example in Section 5.4. In Section 5.5, the "Model Regulator Control System Design" section of COMES toolbox is demonstrated and its specialities are explained, in detail. The chapter ends with conclusions given in the last section.

5.2 Model Regulator Architecture

The idea of model regulator (disturbance observer) was created by Ohnishi in the late 1980's, which has been successfully applied in design of servo-control systems. The fundamental principle of model regulator control is the comparison between the output error of the real system and the nominal target to estimate the equivalent disturbance in the control signal, and to introduce the same amount of compensation to eliminate the impact of disturbance. This method is able to effectively inhibit the adverse impact of nonlinearities in the system, and also linearize the system. Therefore, model regulator can inhibit various external disturbance and parameter changes in the small scope.

A schematic block diagram of a closed-loop control system with disturbance observer can be seen in Figure 5.1, where r is the reference input, y is the measured output signal, n is the sensor noise, d is the disturbance input. Additionally, G_n represents the nominal model of the nominal plant to be controlled, Δ_m represents its normalized unstructured multiplicative model uncertainty. Let us consider now the mathematical background of model regulation. For this purpose, some expressions and comments are given below.

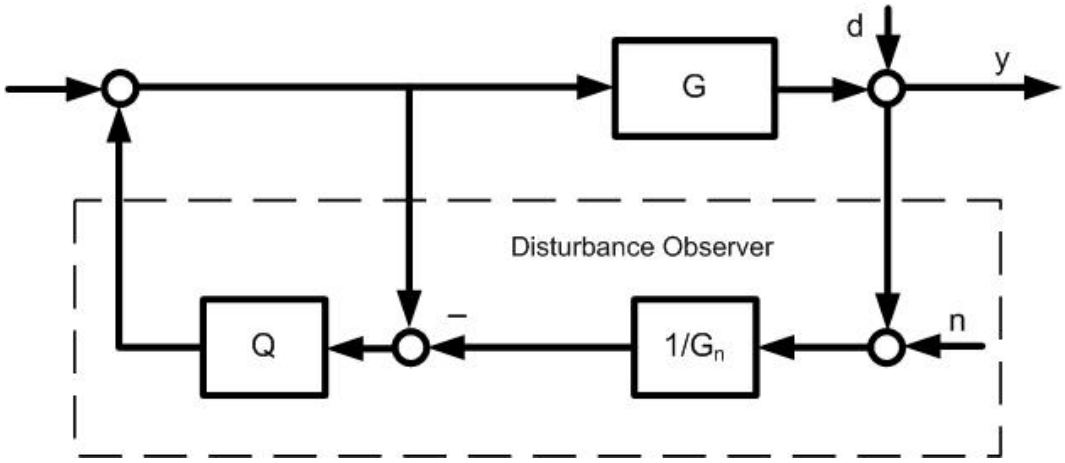

Figure 5.1: Closed-loop structure with disturbance observer.

The loop gain of the disturbance observer compensated plant is given by

$$L = \frac{GQ}{G_n(1-Q)} \tag{5.1}$$

with the model regulation, disturbance rejection, and sensor noise rejection transfer functions given by:

$$\frac{y}{r} = \frac{G_n G}{G_n(1-Q)+GQ} \tag{5.2}$$

$$\frac{y}{d} = \frac{G_d}{1+L} \equiv G_d S = \frac{G_n(1-Q)G_d}{G_n(1-Q)+GQ} \tag{5.3}$$

$$\frac{y}{n} = \frac{-L}{1+L} \equiv -T = \frac{-GQ}{G_n(1-Q)+GQ} \tag{5.4}$$

In (5.3) and (5.4), S and T are the sensitivity and complementary sensitivity, functions, respectively. Q must be a low pass filter with unity d.c. gain. This choice of Q results in $y/r \rightarrow G_n$ which is the desired steering dynamics, $y/d \rightarrow 0$ (disturbance rejection) at low frequencies where $Q \rightarrow 1$. At higher frequencies where there may be considerable sensor noise, $y/n \rightarrow 0$ (sensor noise rejection) will be achieved as $Q \rightarrow 0$. This choice of $Q \rightarrow 0$ at higher frequencies is also necessitated by the robustness of stability. Then the input-output behaviour of the controlled system including its steady-state behaviour will be the same as those of the nominal (or desired) model G_n up to the bandwidth of the low pass filter Q (control system regulation along with good disturbance rejection).

5.3 Mapping Robust Performance Frequency Domain Specifications into Model Regulator Parameter Space

Similar to the parameter space approach given in [24], the parameter space design is based on satisfying the mixed sensitivity requirement

$$\left\| |W_S S| + |W_T T| \right\|_\infty < 1 \qquad \textbf{(5.5)}$$

or equivalently satisfying

$$|W_S S| + |W_T T| < 1 \text{ for } \forall \omega \qquad \textbf{(5.6)}$$

where S and T are the sensitivity and complementary sensitivity transfer functions and W_S and W_T are the corresponding weights. Under the limit condition, this requirement can be presented as

$$|W_S| + |W_T L| = |1 + L| \text{ for } \forall \omega \qquad \textbf{(5.7)}$$

which is called the point condition at each frequency. L in equation **(5.7)** is the loop gain. In order to obtain the region which satisfies expression **(5.6)** for all frequencies in the parameter space, equation **(5.7)** must be solved frequency at a time. The intersection of the regions for every calculated frequency leads to the overall region searched for. The point condition is graphically illustrated in Figure 5.2.

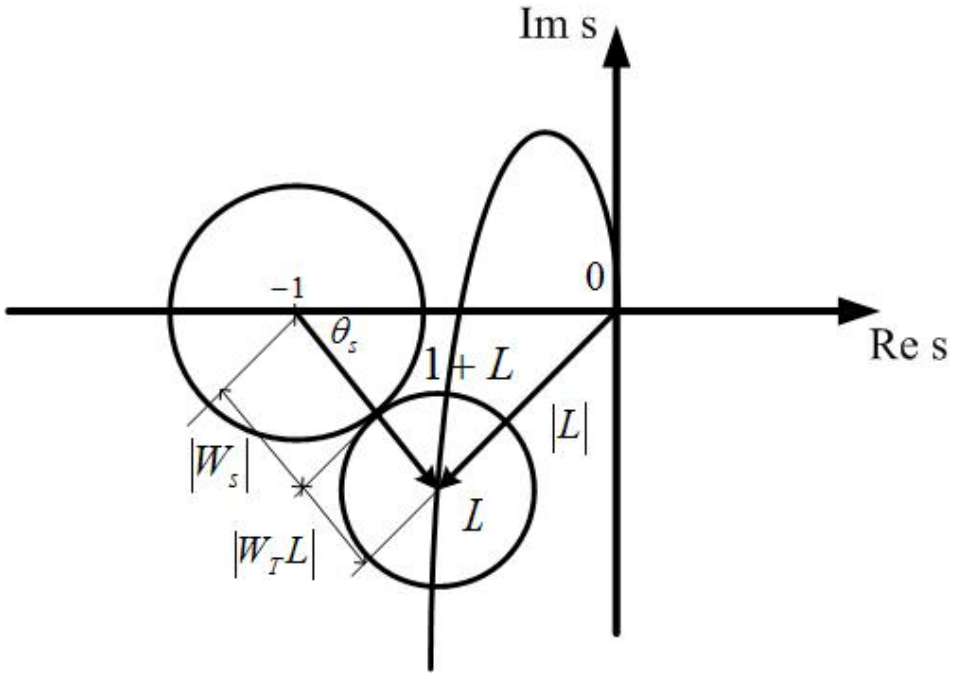

Figure 5.2: Point condition for the mixed sensitivity.

By applying the cosine rule to the shaded triangle in Figure 5.2, a graphical solution for $|L|$ results in,

$$\left|L(j\omega)\right| = \frac{\left(-\cos\theta_L + \left|W_S(\omega)\right|\left|W_T(\omega)\right|\right) \pm \sqrt{\Delta_M(\omega)}}{1-\left|W_T(\omega)\right|^2} \tag{5.8}$$

where

$$\Delta = \cos^2\theta_L + \left|W_S\right|^2 + \left|W_T\right|^2 - 2\left|W_S\right|\left|W_T\right|\cos\theta_L - 1 \tag{5.9}$$

When $L(j\omega)$, $W_S(j\omega)$ and $W_T(j\omega)$ are utilized in equations **(5.8)** and **(5.9)**, the solutions for L at the chosen frequency ω are obtained. The solution procedure is to sweep angle θ_L from *0* to 2π radians and to solve for $|L|$ at each value of θ_L for which a solution exists. Then, all possible values of $L = \left|L\right|e^{j\theta_L}$ at the chosen frequency ω are obtained. Each value of L satisfies

$$L = KG = \left(K_R + jK_I\right)G \tag{5.10}$$

where K is the controller in an equivalent standard feedback architecture representation of the disturbance observer. The reader can be referred to [24] and [34] and the references therein for details of the general method of mapping frequency domain bounds to parameter space for standard feedback control architecture. For the case of a SISO system with disturbance observer, the loop gain can be determined from Figure 5.1 as

$$L = \frac{GG_aQ}{G_n\left(1-G_aQ\right)} \tag{5.11}$$

Then, the disturbance observer parameters can be solved for frequency at a time and mapped into the parameter space for robust design of SISO systems with disturbance observer. For a specific structure defined as,

$$\begin{aligned} G_n &= \frac{K_n}{\tau_n s + 1} \\ Q &= \frac{1}{\tau_Q s + 1} \end{aligned} \tag{5.12}$$

where K_n is the desired static gain of the disturbance observer controlled system, the solution can be obtained by solving for τ_Q and τ_n form

$$K_R + jK_I = \frac{L}{G} = \frac{G_a Q}{G_n\left(1 - G_a Q\right)} \tag{5.13}$$

$$K_R + jK_I = \frac{G_a\left(j\omega\right)\left[\tau_n j\omega + 1\right]}{K_n\left[\tau_Q j\omega + 1 - G_a\left(j\omega\right)\right]} \tag{5.14}$$

for τ_Q and τn while assuming G_a=1 leads to

$$\tau_Q = -\frac{1}{K_n K_I \omega} \tag{5.15}$$

$$\tau_n = -\frac{K_R}{K_I \omega} \tag{5.16}$$

In order for more complicated and predefined structures of Q and G_n, a solution for τ_Q and τ_n exists and can also be found by either searching for a symbolic solution of equation **(5.9)** or by solving it numerically. The final result is a region in a chosen controller parameter plane where the mixed sensitivity limit condition **(5.6)** is satisfied for the chosen frequency. The overall solution region, where the robust performance frequency domain bounds is satisfied, can be obtained by means of repetition of the abovementioned procedure for a sweep of sufficiently many frequencies and the superposition of their results by graphical intersection in chosen parameter space. The τ_Q – τ_n controller parameter space is utilized for the selection of disturbance observer filters **(5.15)** and **(5.16)**.

The point condition **(5.7)** solution procedure is outlined below.

S1. Choose a specific ω value. $\left|W_S\left(\omega\right)\right|$, $\left|W_T\left(\omega\right)\right|$ and $G\left(j\omega\right)$ at frequency ω are known at this point.

S2. Let $\theta_L \in \left[0, 2\pi\right]$. Evaluate Δ_M by using equation **(5.9)** and select the active range of θ_L where $\Delta_M \geq 0$ is satisfied. For all values of θ_L in the active range:

S2a. Evaluate $\left|L\right|$ by using equation **(5.8)**. Keep only the positive solutions.

S2b. Evaluate $L = \left|L\right| e^{j\theta_L}$.

S2c. Solve for the corresponding model regulator controller real and imaginary parts K_R and K_I in equation **(5.9)**.

S2d. Substitute for K_R and K_I into right-hand sides of equations **(5.11)** and **(5.12)**, and solve for τ_Q and τ_n .

S3. Plot the closed curve obtained in the chosen controller parameter space. Either the inside or outside of this curve is a solution of equation **(5.3)** at chosen frequency. The region obtained is the point condition solution in the chosen controller parameter space at the frequency chosen in step S1.

S4. Go back to step S1 and repeat the procedure at a different frequency.

S5. Plot the intersection of all point condition solutions for all frequencies considered. This is the overall solution region for the mixed sensitivity requirement.

5.4 Case Study: Robust Yaw Stability Controller Design

The front wheel steering-based vehicle yaw stability control problem is utilized here as a numerical example in order to illustrate the design method developed in the previous section. Based on the linear single track model, the yaw stability controller is designed in this example. The transfer function from the front wheel steering angle δ_f to the yaw rate r is given by

$$G_{r\delta_f}(s,v)=\frac{r(s)}{\delta_f(s)}=\frac{b_1(v)s+b_0(v)}{a_2(v)s^2+a_1(v)s+a_0(v)} \qquad \textbf{(5.17)}$$

with

$$\begin{aligned} b_0 &= c_f c_r (l_f + l_r)v \\ b_1 &= c_f l_f m v^2 \\ a_0 &= c_f c_r (l_f + l_r)^2 + (c_r l_r - c_f l_f)mv^2 \\ a_1 &= (c_f (I_z + l_f^2 m) + c_r (I_z + l_r^2 m))v \\ a_2 &= I_z m v^2 \end{aligned} \qquad \textbf{(5.18)}$$

The design variables and their numerical values, which are used in the design and simulation, are given as follows: F_f (lateral force at front wheel), F_r (lateral force at rear wheel), M_{zd} (yaw disturbance moment), r (yaw rate), a_{fl} (lateral acceleration at front wheel), β (chassis side slip angle at vehicle centre of gravity), v (magnitude of vehicle velocity at centre of gravity, will be chosen from Figure 5.3), l_f (distance from front axle to centre of gravity, 1.25 m), l_r (distance from rear axle to centre of gravity, 1.32 m), δ_f (front wheel steering angle), δ_r (rear wheel steering angle), m

(vehicle mass, 1296 kg), I_z (moment of inertia w.r.t. vertical axis at centre of gravity, 1750 kgm^2), c_f (rear wheel cornering stiffness, 84000 N/rad), c_r (rear wheel cornering stiffness, 96000 N/rad), μ (road-tire lateral friction coefficient, will be chosen from Figure 5.3). The numerical values presented corresponding to a mid-size passenger car. In addition, the new variables $\tilde{m} = m/\mu$ and $\tilde{J} = J/\mu$ called virtual mass and virtual moment of inertia are defined and also used in the equation give above. Furthermore, some detailed information on nonlinear single track model is given in Appendix B.

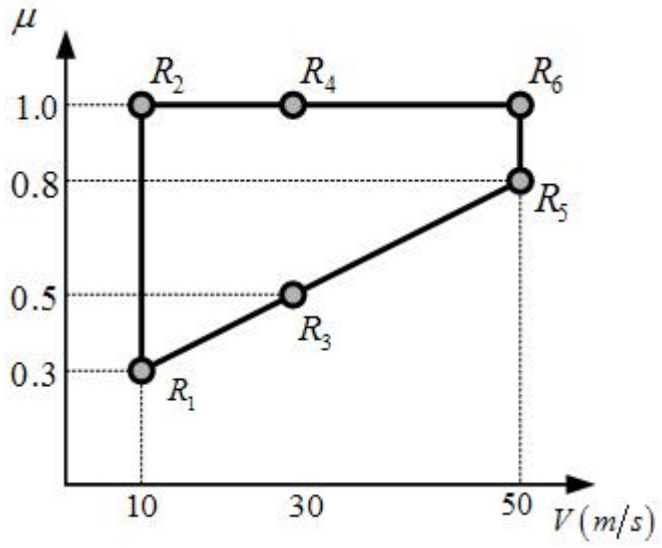

Figure 5.3: Uncertainty specifications.

The inverse of the sensitivity function weight is chosen as

$$W_S^{-1}(s) = h_S \frac{s + \omega_S l_S}{s + \omega_S h_S} \qquad \textbf{(5.19)}$$

with l_S=0.2 (i.e. less than 20% steady state error) being the low frequency sensitivity bound, h_S=4 being the high frequency sensitivity bound, and ω_S=15 rad/s being the approximate bandwidth of the model regulation.

The complementary sensitivity weighting function is chosen as

$$W_T(s) = h_T \frac{s + \omega_S l_T}{s + \omega_T h_T} \qquad \textbf{(5.20)}$$

where the low frequency gain is l_T = 0.5, the high frequency gain is h_T=1.5 (corresponds to uncertainty of up to 150% at high frequencies), and the frequencies

of transition to significant model uncertainty is ω_T =120 rad/s. Check the reference [24] for additional information on how to choose these weighting functions.

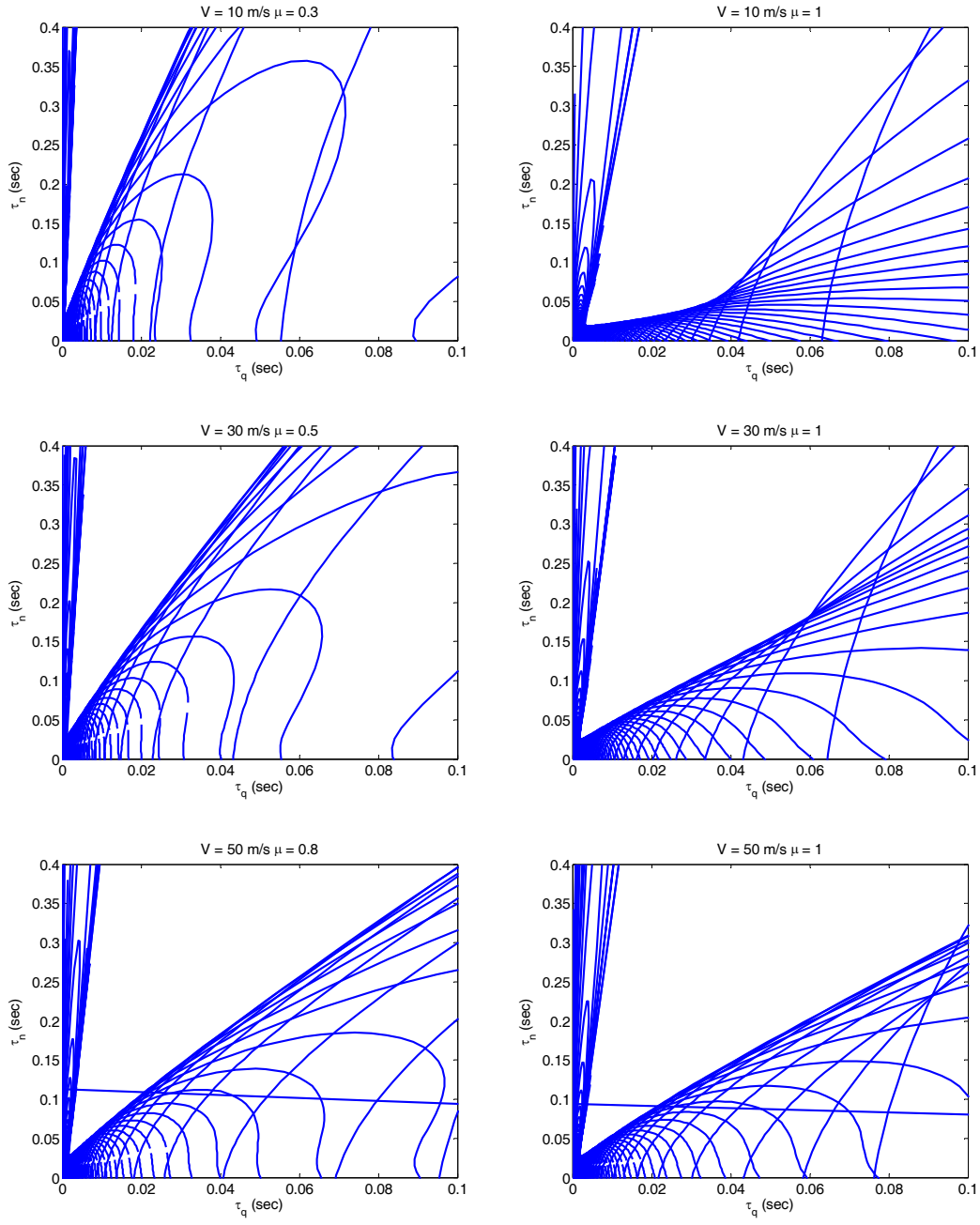

Figure 5.4: Solution region in the parameter space for each of operating points.

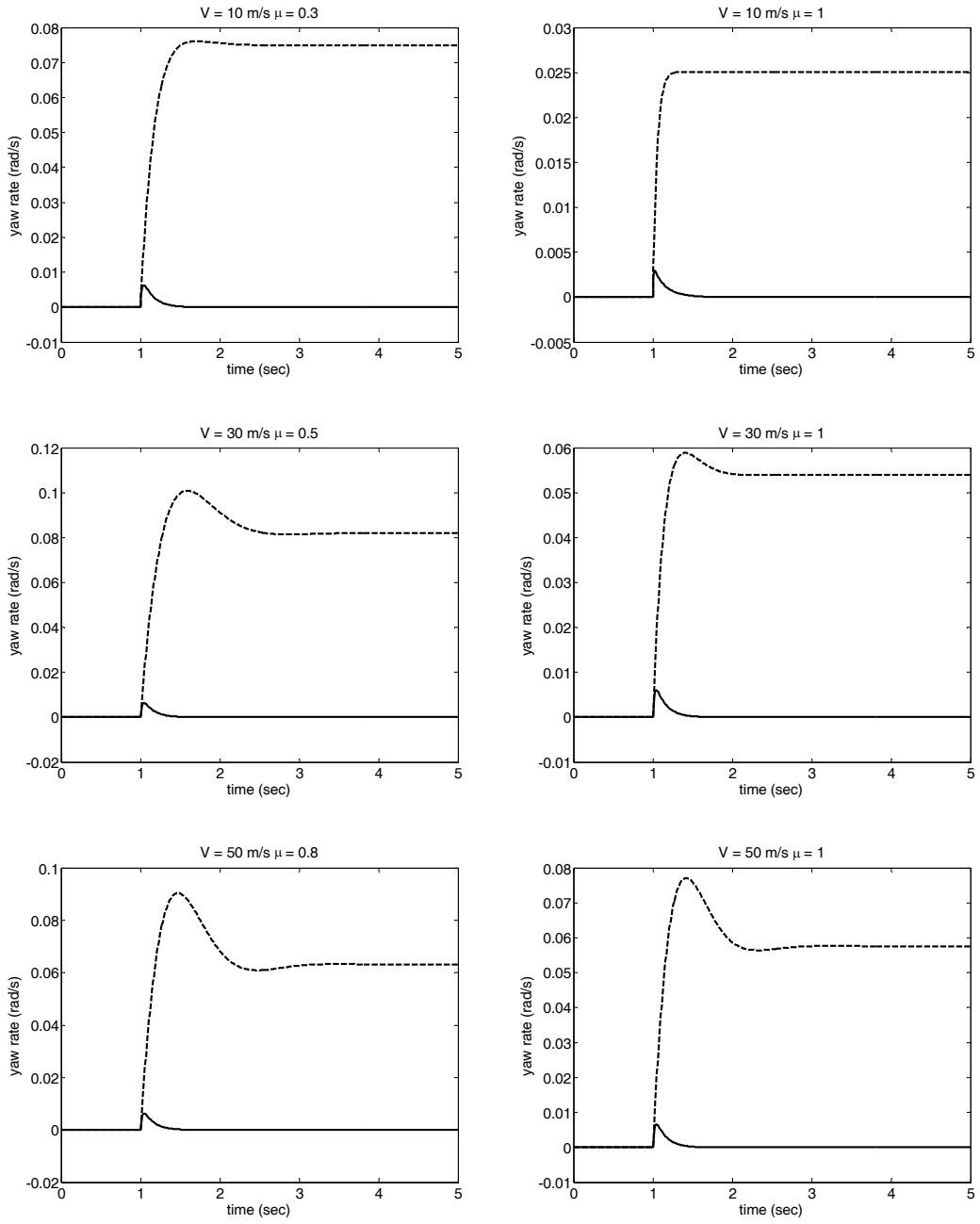

Figure 5.5: Simulation results for yaw moment disturbance input. (Dashed line) Uncontrolled. (Solid line) Controlled.

By utilizing the "Model Regulator Control System Design" section of COMES toolbox, the controller parameter space plots seen in Figure 5.4 are obtained for each of the six operating conditions in Figure 5.3. The controller parameters are chosen as τ_n=0.15 sec and τ_Q=0.02 sec and corresponds to a point within the solution regions for all six operating points. These controller parameters were used in each simulation presented in this chapter. The simulations of the yaw stability control system are

carried out for yaw moment disturbance. The simulations are repeated for each operating conditions given in Figure 5.3. The results can be seen in Figure 5.5.

5.5 COMES Toolbox: Model Regulator Control System Design

Current version of COMES toolbox includes "Model Regulator Control System Design" section. "Model Regulator Control System Design" section has got four windows:

- Main Window

  has some buttons in order to open the other sub-windows like "General Specifications", Sensitivity Specifications" and "Controller & Actuator". There also exist some buttons to calculate and plot the chosen parameter space. Moreover, the parameter space can be captured, zoomed on/off or plotted on a new figure whose number can be re-entered by the user by utilizing the buttons in the GUI.

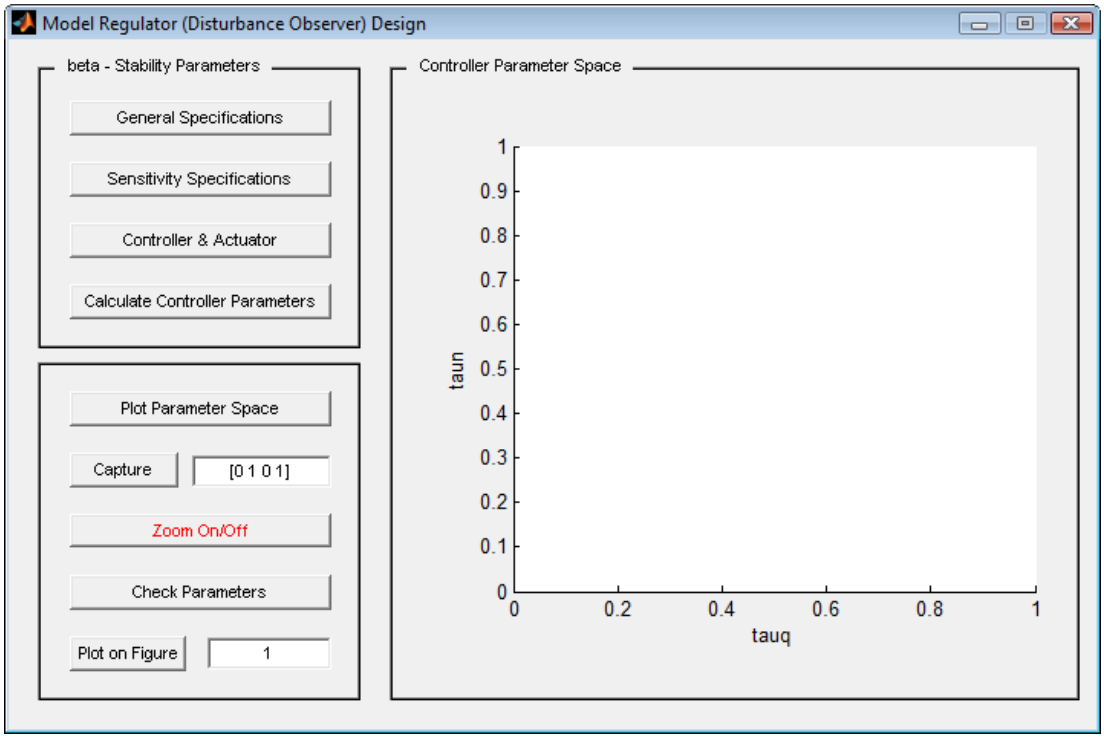

Figure 5.6: Main window.

- General Specifications Window (see Figure 5.7)

  has some edit fields to enter frequency range and sweep angle range between [0,2π). In addition, it has got some buttons for getting vectors from MATLAB workspace and verifying the chosen numeric values.

- Sensitivity Specifications Window (see Figure 5.8)

  has some edit fields to enter the numerator and denominator of the sensitivity and complementary sensitivity functions. In addition, these numerators and denominators can be gotten from MATLAB workspace. By using the buttons, the frequency magnitude response of two functions can be calculated and also plotted on the figure of GUI.

- Controller & Actuator Window (see Figure 5.9)

  has some edit fields to enter the numerator and denominator of the actuator transfer function if it exits. Additionally, these numerators and denominators can be gotten from MATLAB workspace. In this GUI, the order of model regulator filter can be selected. The desired order of model regulator filters can enter to the edit fields in the GUI. For each order of filters, only two variables can be selected to plot the controller parameter space.

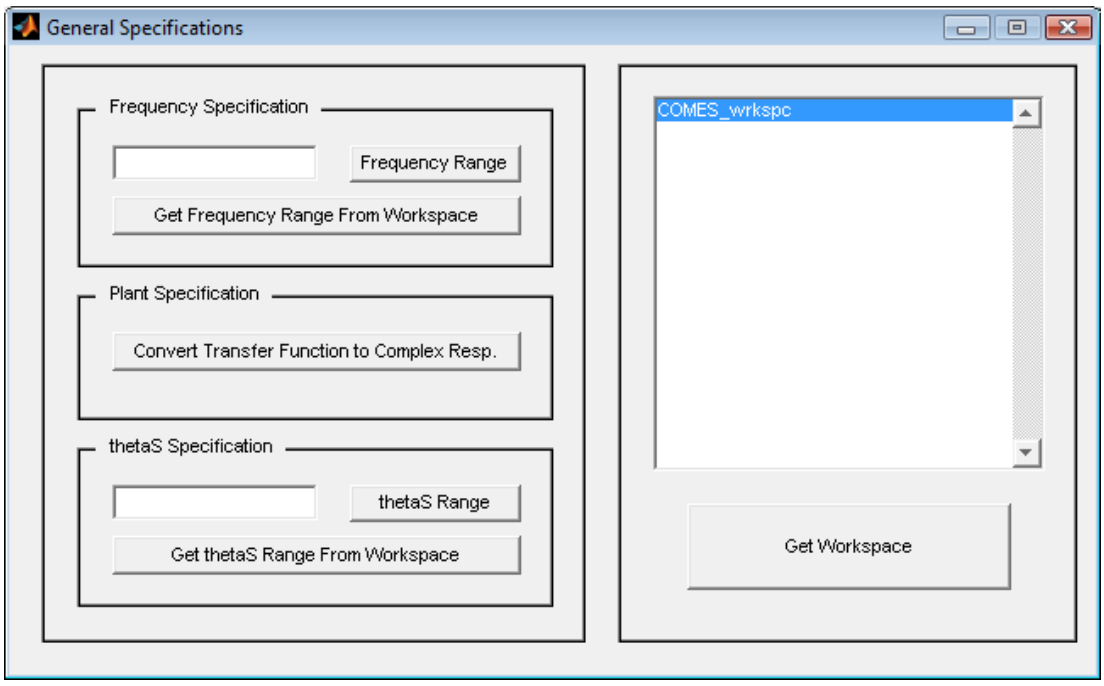

Figure 5.7: General specifications window.

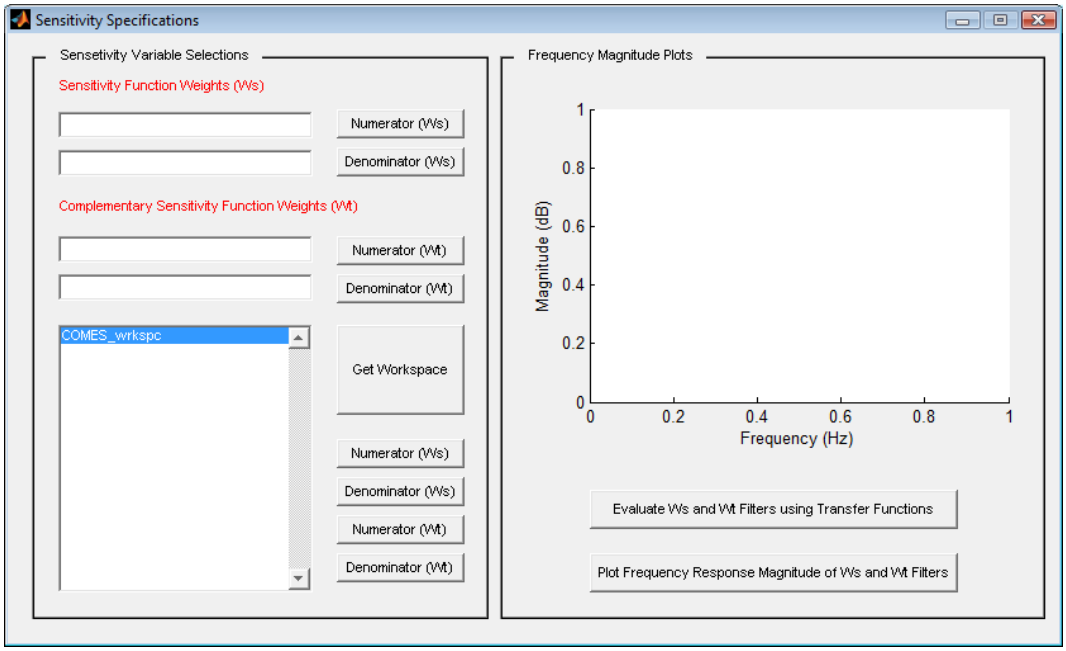

Figure 5.8: Sensitivity specifications window.

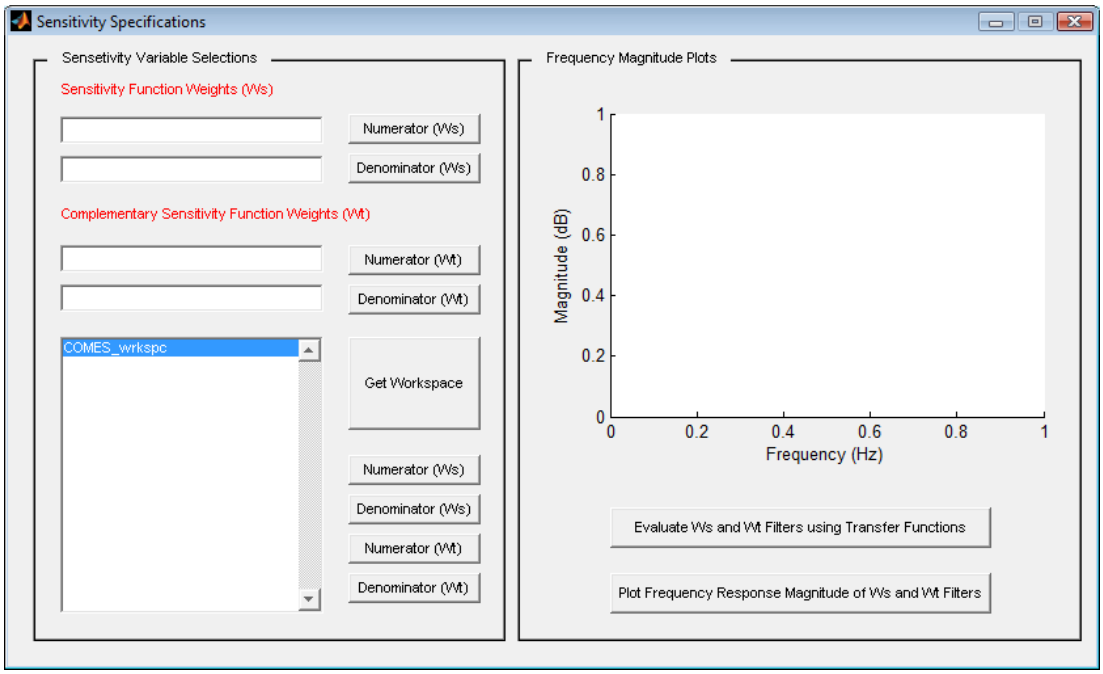

Figure 5.9: Controller & Actuator Window.

5.6 Chapter Summary and Concluding Comments

In this chapter, we proposed a different type of control system called model regulator (disturbance observer). Thanks to model regulator, the effect of disturbance can be

eliminated and also some kind of systems can be decoupled. Robust design based on mapping frequency-domain specifications to chosen controller parameter plane was presented next. Then, the interactive MATLAB-based program with a graphical user interface was utilized in order to determine the parameter space regions. In the next chapter, repetitive control being an effective way to track a periodic reference or reject a periodic disturbance will presented.

6. REPETITIVE CONTROL

6.1 Introduction to Repetitive Control

Repetitive controllers are used to accurately track a periodic reference signal or to reject a periodic disturbance with a known period by introducing a highly frequency selective gain through a positive feedback loop which contains a time delay element as this is a generator of periodic signals. The delay time is equal to the known period of the repetitive reference (or disturbance) signal. Repetitive control system is a special type of servo-system but its basic structure is based on the Internal Model Principle of Francis and Wonham [56]. Significant improvements in the tracking accuracy or disturbance rejection characteristics of systems subject to periodic exogenous signals can be achieved using repetitive control. The idea of repetitive control was first created by Inoue et al [57] to replace conventional motion control techniques in the control of a proton synchrotron magnet power supply. Until recently, it has been widely utilized in many application areas including control of hard disc drives [58], control of optical disc drives [59], control of noncircular tuning [47], trajectory control of industrial robot arms [60, 61], motor speed control [62], high precision rotational control [63], control of material testing machine [64], control of cold rolling process [65], suppression of torque vibration in motors [66], reduction of waveform distortion in PWM inverter or UPS [67-69] and accurate position control of piezoelectric actuators [70, 71].

The earlier papers in the literature have generally focused on the stability analysis in both continuous time [72, 73] and discrete time systems [74]. Tsao and Tomizuka [47] have analyzed the robust stability of repetitive control systems applied to plants with unstructured modelling error. In order to achieve a specified level of nominal performance, Srinivasan et al [75] have utilized the Nevanlinna-Pick interpolation method to modify repetitive controller design by means of optimizing a measure of stability robustness. Peery and Özbay have modified H_∞ optimal design approach presented in [76] and then applied the extension of this methodology based on Youla parameterization to repetitive control systems in [77]. Moon et al [59] have

developed a robust design methodology for parametric uncertainty in interval plants under repetitive control. Similarly, Roh and Chung [78] have created a new synthesis method based on Kharitonov's theorem for repetitive control systems with uncertain parameters. Weiss et al [79-81] have made a stability and robustness analysis for MIMO repetitive control systems based on H_∞ control theory. Doh et al [82] reformulated the repetitive control filters design problem as an optimization problem with Linear Matrix Inequality (LMI) constraint of the chosen parameters. μ analysis has been used for assessing stability and performance robustness of SISO continuous time repetitive control systems by Güvenç [83]. μ synthesis has been applied to sampled data repetitive controller design by Li and Tsao [84].

The repetitive controller design approach presented in this chapter of the thesis is a continuation of the work presented in Aksun Güvenç and Güvenç [85] on repetitive controller design based on mapping the nominal performance and robust stability frequency domain constraints to controller parameter space where a servo-hydraulic material testing machine application was used. This work, in contrast, treats the robust performance constraint. Additionally, the efficiency of methodology is illustrated by using a high speed AFM scanner application. Moreover, the repetitive controller design approach presented in this work is significantly different from those of the abovementioned references including the application of H_∞ methods. The significant advantages of the approach here in comparison with H_∞ methods are: (i) the ease of visualization due to the graphical representation of the solution in the parameter space approach and the capability and ease of doing multi-objective optimization by simply intersecting solution regions for different objectives, (ii) the determination of a solution region rather than one specific solution for the control system satisfying a frequency domain constraints (this makes it easier to design non-fragile controllers as changes in controller parameters will not violate the chosen objectives so long as the parameters are within the solution region), (iii) the determination of controller parameters that guarantee robust performance, (iv) being able to treat plants with time delay and poles on the imaginary axis, (v) not having to use rational, continuous weights in the robust performance specifications, and (vi) obtaining fixed structure low order repetitive controller filters that are easily implementable. There are also some shortcomings of the proposed design method in comparison to the methods that exist in the literature including H_∞ methods such as:

i) the method can simultaneously accommodate the design of only two controller parameters due to its graphical display of the solution region, ii) the method does not result in a single analytical solution and the methods used do not look mathematically elegant as a constructive frequency-by-frequency design approach is used.

It is difficult to apply standard robust control methods like H_∞ control to repetitive controller design for robust performance as the repetitive control system is infinite dimensional due to the presence of the inherent time delay in the controller. Robust control methods such as H_∞ optimal control have been extended to infinite dimensional systems and applied to repetitive control (see [75] and [77] for example). However, very high order weighting functions need to be used in the robust controller synthesis. Consequently, the resulting repetitive controller filters also have high order. Model order reduction techniques are used to reduce the order of the repetitive controller filters in an actual implementation. Some of the most powerful characteristics of the proposed method are that the weights used in the design do not need to be continuous functions of frequency and that plants can have time delay and/or poles on the imaginary axis because the computations are naturally carried out only at the frequencies of interest. Secondly, the choice of the frequency grid used is not a problematic issue for the repetitive control design procedure presented here as the main design frequencies are exactly known and are the fundamental frequency of the periodic exogenous signal (reference or disturbance) with the period τ_d and its harmonics. The largest harmonic frequency considered is chosen to be close to the bandwidth of the repetitive control system which is limited by the bandwidth of the actuator used in the implementation. The method presented here is for SISO systems; however, it can be used to design controllers for MIMO systems where one loop at a time design is possible.

The organization of the rest of Chapter 6 is as follows. In Section 6.2, some analysis techniques on the stability of repetitive control system are pointed out. Section 6.3 gives some basic information on design principle of robust repetitive control systems. In Section 6.4, the technique of mapping mixed sensitivity frequency domain specifications into repetitive controller parameter space is explained, in detail. In Section 6.5, the repetitive control system part of COMES toolbox is demonstrated. Then, a numerical example of high speed AFM scanner position

control application is utilized in order to demonstrate the effectiveness of the proposed method presented in Section 6.6. The paper ends with conclusions in Section 6.7.

6.2 Stability Analysis of Repetitive Control System

Stability analysis is one of the most important steps of the control system design procedure. For this purpose, many researchers pay more attention and consume much more time to check the system stability while designing any kind of control systems. For instance, Nyquist theorem or root-locus plot can be used to check the stability of systems while designing a continuous-time SISO, linear time-invariant (LTI) control systems including conventional controller. Similarly, the parameter space approach which is partially relied on the stability analysis of robust control systems like Hurwitz stability and *D*-stability condition can be quietly used to guarantee the stability of control system for conventional control systems (see Chapter 2 for the details).

In contrast to the stability checking of conventional (classical) control systems, stability analysis of repetitive control systems is very tough issue due to the presence of the controller time delay. This kind of systems is called infinite dimension systems and also they have got infinitely many poles. Therefore, the controller design and synthesis is very difficult for this kind of control systems. Let me give you a brief history on the stability analysis of repetitive control systems from the literature. In the earlier papers, Inoue et al [57] was used the BIBO stability criterion to protect the system's stability. Analysis given in [86] exposed that the stability might be guaranteed only if the plant were proper but not strictly proper. From this analysis, it can be well understood that there is an important limitation because of controller parameterization [87] as well as unrealistic demand for perfect tracking of arbitrary periodic signals which include high frequency components.

In order to overcome the abovementioned problem, Inoue et al [57] modified the repetitive controllers by adding the low-pass filter $q(s)$ in front of the controller time delay. As a consequence, the stability robustness of repetitive control systems was improved; however, the tracking performance was dramatically reduced at high frequencies. Indeed, this one is an expected situation because the low-pass filter $q(s)$ adding in front of the time delay causes the sensitivity of control system to equal to

any value different from infinity. Therefore, the tracking performance absolutely decreases. Hara et al [88] extended the modified repetitive controller to MIMO systems presented the corresponding exponential stability. For SISO continuous repetitive control systems, Hara et al indicated that any low-pass filter $q(s)$ satisfying $\|q(s)\|_\infty<1$ can be utilized in minimum phase systems [86]. However, there are bandwidth limitations on $q(s)$ for non-minimum phase systems [89].

There are lots of different design and synthesis methods in the literature for the modified repetitive control systems. The design problem is essentially based upon choosing and optimizing the low-pass filter $q(s)$ and dynamic compensator $b(s)$ for the plug-in repetitive control system seen in Figure 6.1. The selection of repetitive controller parameters involves a trade-off between steady state accuracy and stability robustness. $G(s)$ is the compensated or uncompensated plant, $G_{cl}(s) = G(s)/(1+G(s))$. In order to satisfy the stability, the low-pass filter $q(s)$ and dynamic compensator $b(s)$ must be chosen such that $\|q(s)\ (1+b(s)G_{cl}(s))\|_\infty<1$.

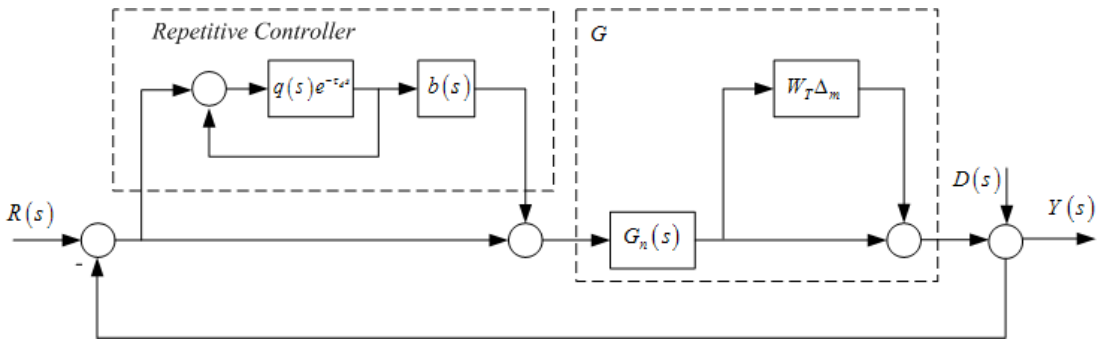

Figure 6.1 : Repetitive control structure.

The frequency domain analysis is the main approach for repetitive control system design because the use of the pole assignment approach for repetitive control systems is very difficult due to presence of the controller time delay. Indeed, there are some pole assignment methodologies based on parameter space approach in the literature to design controller for continuous time, linear-time invariant, time-delayed systems (see [90]). However, these methods are not well-suited for repetitive control systems. For this reasons, shaping the regeneration spectrum is the most effective way to improve the relative stability and transition response of system. In the following part of this chapter, the regeneration spectrum analysis will be given in detail, and also its use in repetitive control systems will be extensively explained.

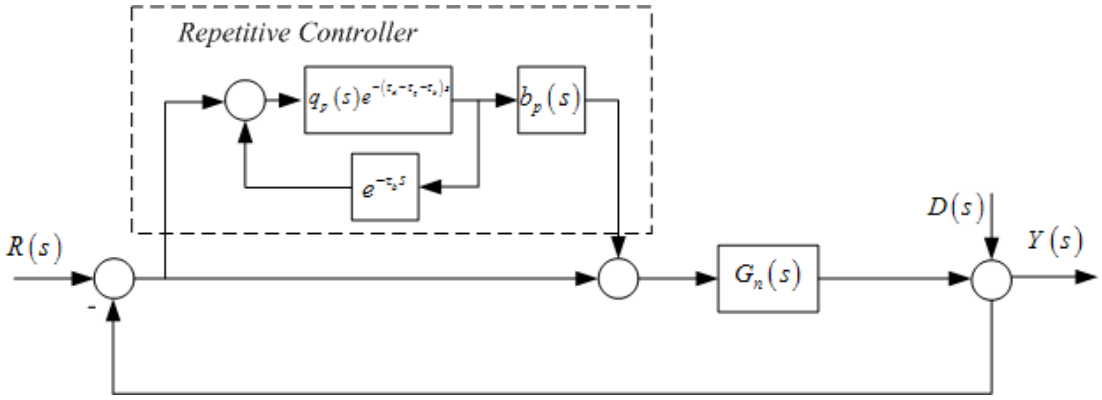

Figure 6.2 : Modified repetitive control structure.

6.2.1 Regeneration spectrum analysis

The characteristic equation of a continuous-time, linear time-invariant, time-delayed system with single time delay τ_d is given by

$$P(s)+Q(s)e^{-\tau_d s}=0 \qquad \textbf{(6.1)}$$

where $P(s)$ and $Q(s)$ are polynomials whose independent variables are Laplace variables s. *The regeneration spectrum* for such a system is defined as a plot of $R(\omega)$ versus the frequency ω. The stability of time-delayed control system can be analyzed by using the regeneration spectrum function.

$$R(\omega)=\left|\frac{Q(j\omega)}{P(j\omega)}\right| \qquad \textbf{(6.2)}$$

A relationship between the regeneration spectrum and absolute stability can be established by using the amplitude-phase method of stability analysis [91], which is basically based on an application of the Nyquist criterion for time-delayed systems. If the polynomial $P(j\omega)$ has no zeros in the right hand side of s-domain (so, if the system is asymptotically stable) and also if

$$R(\omega)<1 \quad \text{for } \forall\omega \qquad \textbf{(6.3)}$$

the closed loop system **(6.1)** is stable for all values of time delay. Hence, the condition **(6.3)** is a sufficient condition for the control system stability. The system is independent of controller time delay τ_d. In addition, it can be easily evaluated.

The usefulness of the regeneration spectrum for stability analysis and controller synthesis for time-delayed system depends not so much on the absolute stability result mentioned above but on its relationship to the degree of stability of such

systems, for large values of time delay. The time delay τ_d is considered to be large if it satisfies

$$\tau_d >> \frac{1}{|\alpha_{\max}|} \tag{6.4}$$

where α_{max} is the real part of zero of the polynomial $P(s)$ which is closest to the imaginary axis. The requirement **(6.4)** for a large time delay was arbitrarily simplified by Sirinivasan and Nachtigal [92] just like the statement seen below,

$$\tau_d \geq \frac{5}{|\alpha_{\max}|} \tag{6.5}$$

For the systems with a large time delay, Srinivasan and Nachtigal [92] shows that the regeneration spectrum bore a simple relationship to the dominant characteristic roots of the equation **(6.1)** if the time delay τ_d was large enough.

$$\alpha_{i,-i} \cong \frac{\ln\left(R(\omega)\right)}{\tau_d} \tag{6.6}$$

where $\alpha_{i,-i}$ are the real part of complex conjugate roots with their imaginary parts equal to ω_i in magnitude. Since ω_i are not known beforehand, the practical implication of equation **(6.6)** is that the continuum of complex numbers $\ln(R(\omega))/\tau_d \pm j\omega$ for ω varying from 0 to ∞ includes the characteristic root locations of the system **(6.1)** closest to the imaginary axis. The transcendental characteristic equation **(6.1)** has infinitely many roots, therefore; it needs considerable computational effort for the numerical solution of this equation. The regeneration spectrum suggests an alternative way to estimate the significant features of the system dynamic response. While designing a controller for time-delayed system, shaping of the regeneration spectrum by selecting appropriate compensator could be a successful method in order to change the characteristic root distribution of the system and also its transient response.

The equation **(6.6)** is solely an approximate version of the characteristic equation **(6.1)** given by

$$\alpha_{i,-i} = \frac{\ln\left|\frac{Q(\alpha_i + j\omega_i)}{P(\alpha_i + j\omega_i)}\right|}{\tau_d} \tag{6.7}$$

The requirement **(6.4)** for a large time delay leads to one category of roots of the equation **(6.1)** being close to the imaginary axis. If the system is stable, the all roots would be located in the left half of the complex plane. The roots, which are close to the imaginary axis, have played an important role in the system stability. Bartalucci and Lisini [93] have termed these roots as the regenerative effects of poles due to their critical dependence on the time delay τ_d. Setting α_i to zero on the right hand side of equation **(6.7)** yields the equation **(6.6)** for these roots. For better approximation of equation **(6.7)** by equation **(6.6)**, Srinivasan [73] has described a generalization of the regeneration spectrum involving an iterative solution of equation **(6.7)**. It requires knowledge of the time delay τ_d and scarifies the ease of computation to improve the accuracy of approximation.

6.2.2 Regeneration spectrum analysis to repetitive control

As it is mentioned above, the basic repetitive control system must be improved by using a low-pass filter $q(s)$ in front of the time delay located in the periodic signal generator. Hence, the system stability can be guaranteed at the high frequencies. However, the tracking performance at high frequencies is sacrificed by adding a low-pass filter $q(s)$. Figure 6.1 shows the block diagram of a modified continuous-time SISO repetitive control system. $G_p(s)$ is the uncompensated or compensated plant transfer function, $q(s)$ is a low-pass filter that is needed to guarantee the system stability, and $b(s)$ is a dynamic compensator transfer function. τ_d is the period of reference (or disturbance) signal. The continuous-time SISO repetitive control system model given in Figure 6.1 is very similar to the control system configuration proposed by Hara et al [86]. However, only difference between two control system configurations is the use of $b(s)$ dynamic compensator whose effect on the system stability is obviously illustrated below. The characteristic equation of the closed-loop system is given by

$$1+G_p(s)+q(s)\left[b(s)G_p(s)-G_p(s)-1\right]e^{-\tau_d s}=0 \qquad \textbf{(6.8)}$$

In Appendix C, the subtraction of characteristic equation for the closed-loop repetitive control system is given in detail. From characteristic equation, the regeneration spectrum is obtained as

$$R(\omega)=\left|q(j\omega)\left[1-b(j\omega)\frac{G(j\omega)}{1+G(j\omega)}\right]\right| \qquad \textbf{(6.9)}$$

The expression for the regeneration spectrum demonstrates the effect of the different aspects of controller design on the stability of the repetitive control systems. If the equation

$$1+G_p(s)=0 \qquad \textbf{(6.10)}$$

has no roots in the right half of the complex s-plane and also if the regeneration spectrum **(6.9)** is less than one in magnitude at all frequencies, the repetitive control system is stable. Consequently, the first condition proposes that the control system must be stable when the repetitive controller is omitted from the closed-loop control system. The other condition indicates clearly the need of a low-pass filter $q(s)$. The expression within parentheses in equation **(6.9)** is approximately equal to unity as $\omega\rightarrow\infty$ since $G_p(j\omega)\rightarrow 0$ at high frequencies for the physical systems. By this way, $q(j\omega)$ must be lower than one at high frequencies in order to confirm system stability. The stability condition is a sufficient one and is valid for all values of time delay τ_d. The effect of the dynamic compensator $b(s)$ on the system stability can be clearly seen from equation **(6.9)**. The selection of $b(j\omega)$ which compensates the amplitude and phase of the frequency response of $G_p(j\omega)/(1+G_p(j\omega))$ would keep the magnitude of the term within the parenthesis in equation **(6.9)** close to zero for a wider frequency range. Thus, the stability of closed-loop system can be improved.

For the large value of time delay τ_d in the sense of equation **(6.9)**, the sufficient stability condition tends to become a necessary and sufficient one. Moreover, the regeneration spectrum **(6.9)** can be utilized to approximately determine the dominant roots of characteristic equation **(6.8)** with very good degree of accuracy by using equation **(6.6)**.

If the time delay τ_d is assumed to be equal to a large value, the equation **(6.4)** or **(6.5)** should be checked for each specific application of interest. Nevertheless, the assumption of a large time delay can be effectively utilized for many repetitive control applications [73]. The right hand side of expression **(6.4)** is the dominant or slowest time constant of the system when the repetitive controller is omitted. Hence, the condition **(6.4)** solely expresses that the time delay τ_d should be much larger than the time constant of the system when the repetitive controller is omitted. Under all

circumstances, the compensated plant transfer function $G_p(s)$ can be chosen in order to satisfy the condition **(6.4)** throughout the first stage of the repetitive controller design procedure described later. The absolutely stability results which are relied on the regeneration spectrum would carry on being valid even if the condition **(6.4)** is violated.

More conventional relative stability measures such as gain and phase margins can be determined by applying the Nyquist criterion to characteristic equation **(6.8)** which is restated as

$$1+\frac{1+q(s)\left(b(s)-1\right)e^{-\tau_d s}}{1-q(s)e^{-\tau_d s}}G_p(s)=0 \qquad \textbf{(6.11)}$$

Hence, the gain and phase margin would demonstrate the amount of gain increase and the additional phase lag due to the uncompensated or compensated plant $G_p(s)$. However, the usefulness of these design measures in controller design is limited because the effect of changing the design parameters of the low-pass filter $q(s)$ and dynamic compensator $b(s)$ on these measures is not easy to understand. Nevertheless, equation **(6.9)** demonstrates very clearly the effect of changing the low-pass filter $q(s)$ on system stability. In order to improve the degree of system stability, $q(j\omega)$ needs to have lower magnitude. The effect of changing the dynamic compensator $b(s)$ on regeneration spectrum is slightly more difficult.

6.3 Repetitive Controller Basics

The basic working principle and elements of repetitive control system seen in Figure 6.1 and 6.2 are investigated, in detail, here.

6.3.1 Internal model principle

The internal model principle presented by Francis and Wonham [56] can be especially used in the servo-system design. The general structure of internal model system extensively used in control of servo-systems can be seen in Figure 6.3. The internal model principle is explained below in detail with its mathematical theory and proof.

Theorem 6.1 (Francis and Wonham, [56]): *Internal Model Principle (IMP)* means that a controlled output is able to track a class of reference signal without steady-

state error if the generator of this reference signal is included in a stable closed-loop control system. For instance, no steady state error occurs for step reference signal in a type 1 stable feedback system which has a free integrator 1/s (i.e. the generator of step function) in this loop.

Proof: The unity feedback closed loop system error transfer function is given by

$$\frac{E(s)}{R(s)} = \frac{1}{1+G(s)} \tag{6.12}$$

The n[th] type system transfer function is

$$G(s) = \frac{N(s)}{s^k D(s)} \tag{6.13}$$

The class of reference input signal in time domain and frequency domain can be seen below.

$$r(t) = \sum_{n=0}^{N} a_n t^n \tag{6.14}$$

$$R(s) = \sum_{n=0}^{N} a_n \frac{1}{s^{n+1}} \tag{6.15}$$

System error transfer function is shown as

$$E(s) = \frac{1}{1+\dfrac{N(s)}{s^k D(s)}} \sum_{n=0}^{N} a_n \frac{1}{s^{n+1}} \tag{6.16}$$

where n, N and k are integers and also a_n is a set of constant coefficients. It is supposed that the plant transfer function $G(s)$ is proper and stable and also $N(s)$ and $D(s)$ are coprime. By using the final value theorem, the steady state error can be calculated just like the statement seen below.

$$e_{ss} = \lim_{s\to 0} sE(s) = \lim_{s\to 0} \frac{1}{1+\dfrac{N(s)}{s^k D(s)}} \sum_{n=0}^{N} a_n \frac{1}{s^n} \tag{6.17}$$

$$e_{ss} = \begin{cases} 0 & N < k \\ k_e & N = k \\ \infty & N > k \end{cases} \tag{6.18}$$

Equation **(6.17)** and **(6.18)** demonstrates that a feedback control system with the type of k can track a polynomial type of reference input with degree of k-1 without steady-state error. If k is equal to N+1, the steady-state error is a limited constant. This expresses the Internal Model Principle (IMP) and it denotes that the controlled output can track to a class of reference inputs without steady-state error if the signal generator for the reference (or disturbance) is included in the stable closed-loop system.

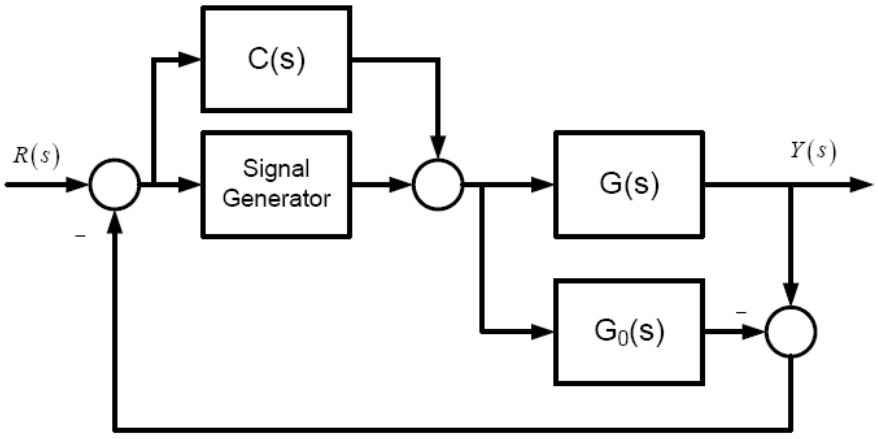

Figure 6.3 : Internal model control system structure.

For periodic signals this means to achieve asymptotic tracking of a reference input (or rejection of a disturbance), the controller needs to contain poles at the frequency of the periodic signal and its entire non-zero harmonics. This can be easily achieved by inclusion of the so called periodic signal generator, which is discussed next.

6.3.2 Periodic signal generator

A periodic signal with a known period can be generated by the periodic signal generator shown in Figure 6.4 with an appropriate initial function. Based on the Internal Model Principle (IMP) which is extensively expressed with its mathematical background above, it is well known that the controlled output can track a periodic reference commands without a steady-state error if the closed-loop control system includes this periodic signal generator. The periodic signal generator includes a time delay element under a positive feedback loop. The time delay is equal to the period of the repetitive reference input (or disturbance). Moreover, the transfer function of signal generator from e to z is given by

$$\frac{Z(s)}{E(s)} = \frac{e^{-\tau_d s}}{1 - e^{-\tau_d s}} \qquad \textbf{(6.20)}$$

The system **(6.20)** has infinitely many poles on the imaginary axis: $jk\omega$: k=0,±1,±2,… where $\omega=2\pi/\tau_d$ (see Figure 6.5). According to the IMP, the asymptotic tracking performance for exogenous periodic inputs can be achieved by implementing the model $e^{-\tau s}/(1-e^{-\tau s})$ into the closed-loop system.

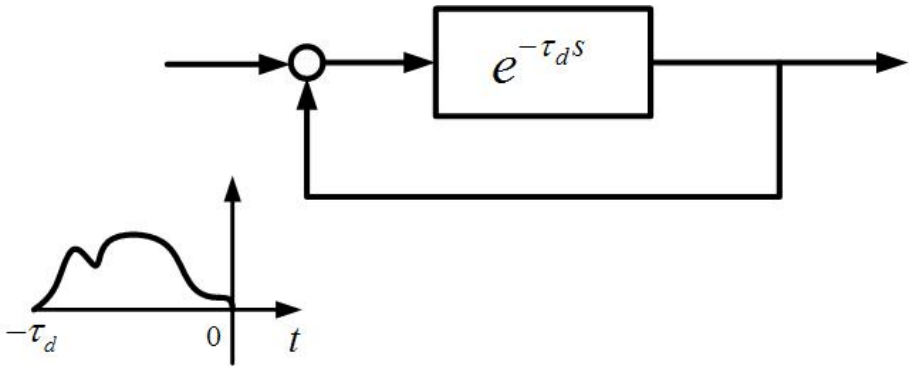

Figure 6.4 : Periodic signal generator with an appropriate initial function.

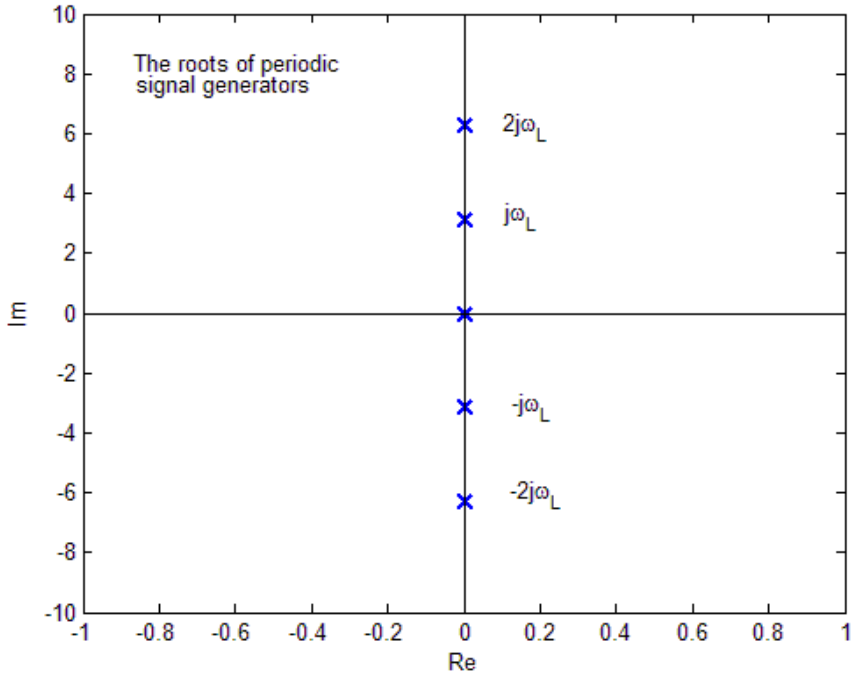

Figure 6.5 : The root loci of generator of the periodic signals.

The positive feedback loop in the repetitive control system generates the periodic signal needed at the plant input in order to asymptotically track the periodic reference signal accurately or reject the periodic disturbance effectively. Let us consider

obtaining the mathematical proof of zero steady state error while using repetitive control system. For this purpose, the transfer function of the closed-loop repetitive control system (seen in Figure 6.1) is obtained as

$$G(s)=\frac{\left(1+(b-1)qe^{-\tau_d s}\right)G}{(1+G)\left(1-q\left(1-b\frac{G}{1+G}\right)e^{-\tau_d s}\right)} \qquad \textbf{(6.21)}$$

From equation **(6.21)**, the error transfer function is obtain as

$$\frac{E(s)}{R(s)}=\frac{1-qe^{-\tau_d s}}{(1+G)\left(1-q\left(1-b\frac{G}{1+G}\right)e^{-\tau_d s}\right)} \qquad \textbf{(6.22)}$$

Then, if the final value theorem is applied to equation **(6.22)**, the expression seen below can be determined.

$$\lim_{s\to 0} s\frac{E(s)}{R(s)}=\lim_{s\to 0}\frac{s(1-q)}{(1+G)\left(1-q\left(1-b\frac{G}{1+G}\right)\right)}R(s) \qquad \textbf{(6.23)}$$

If $q(s)$ is chosen as unity, the steady state error is equal to zero in theoretical. However, this causes stability problems at high frequencies in practise. Therefore, $q(s)$ is a low-pass filter with a gain of 1 at low frequencies that determines the frequency band of the reference command to be tracked. For this, there is a trade-off between stability robustness and steady state accuracy because of the determination of the low-pass filter $q(s)$ bandwidth.

In comparison to time domain analysis, the closed-loop repetitive control system has infinite loop gain, for this reason; the closed-loop sensitivity of repetitive system has zero. This shows that at this frequency and its harmonics the system track perfectly the reference signal. However, the infinity loop gain can cause instability at high frequencies. In order to prevent this, a low-pass filter $q(s)$ should be added to the periodic signal generator. This will explain in the next sections.

6.3.3 Time advance

Cancellation of the phase shift of the plant $G(s)$ and of the phase shifts due to the low-pass filter $q(s)$ and the dynamic compensator $b(s)$ within the repetitive control loop is required to verify efficient operation of the repetitive control system. Without

this phase cancellation, the improvement in tracking performance is reduced. Moreover, the system stability might be reduced if the closed-loop plant phase shift is not cancelled. For this reason, the phase lag mentioned above should be eliminated. The phase cancellation with a time advance is the one of the most effective way to eliminate the abovementioned phase lags. Time advance produces a phase shift which is linearly proportional to the frequency. The time advance can be presented for continuous-time systems as $e^{\tau s}$.

The key feature of the phase cancellation with time advance in repetitive control is that the phase shift within the repetitive control system should be completely cancelled up to the cut-off frequency of the low-pass filter. Beyond this frequency range, the ability of repetitive controller to reduce the periodic disturbances begins dramatically to decrease as long as the system stability is protected. The positive phase shift of the time advance has got no adverse effect on the system [94].

The relative stability of repetitive control system is independent from the phase shift of the low-pass filter $q(s)$ but the tracking performance of the system will be adversely affected if this phase is not cancelled. Nevertheless, the phase shift of the dynamic compensator $b(s)$ is directly linked to the relative stability of repetitive control system [94].

In order to protect the stability of repetitive control system under worst case condition, the regeneration spectrum condition ($\|R(\omega)\|_\infty<1$ at all frequencies) is not only sufficient but this condition should be also modified as $\angle R(\omega)\cong 0$ at all frequencies. It means that the phase shift of the regeneration spectrum should be approximately equal to zero. The best phase cancellation is the minimum excursion from 0° when the total phase $\angle R(\omega)$ is added to the phase due to the time advances τ_q and τ_b.

An Example from Literature: The satellite mirror servo-control system problem [94] is utilized here as a numerical example in order to demonstrate how to cancel the phase shift of a control system. For this purpose, the closed-loop transfer function of the plant (6.11) is given by

$$G(s)=\frac{439.8^2}{s^2+247.3s+439.8^2} \qquad \textbf{(6.24)}$$

In this example, the dynamic compensator $b(s)$ is chosen as the approximately inverse of the closed-loop system's plant $G(s)$. The transfer function of dynamic compensator $b(s)$ is given by

$$b(s) = \frac{s^2 + 247.3s + 439.8^2}{439.8^2\left[\left(s/400\right)^2 + s/400 + 1\right]} \qquad \textbf{(6.25)}$$

From the abovementioned information, the time advance of the dynamic compensator is calculated as 4 ms. The phase lag of the plant $b(s)G(s)$, the linear phase lead of the time advance and the multiplication of each others are demonstrated in Figure 6.6. For chosen bandwidth, time advance τ (linear phase lead) eliminates the phase lag of closed-loop system very well.

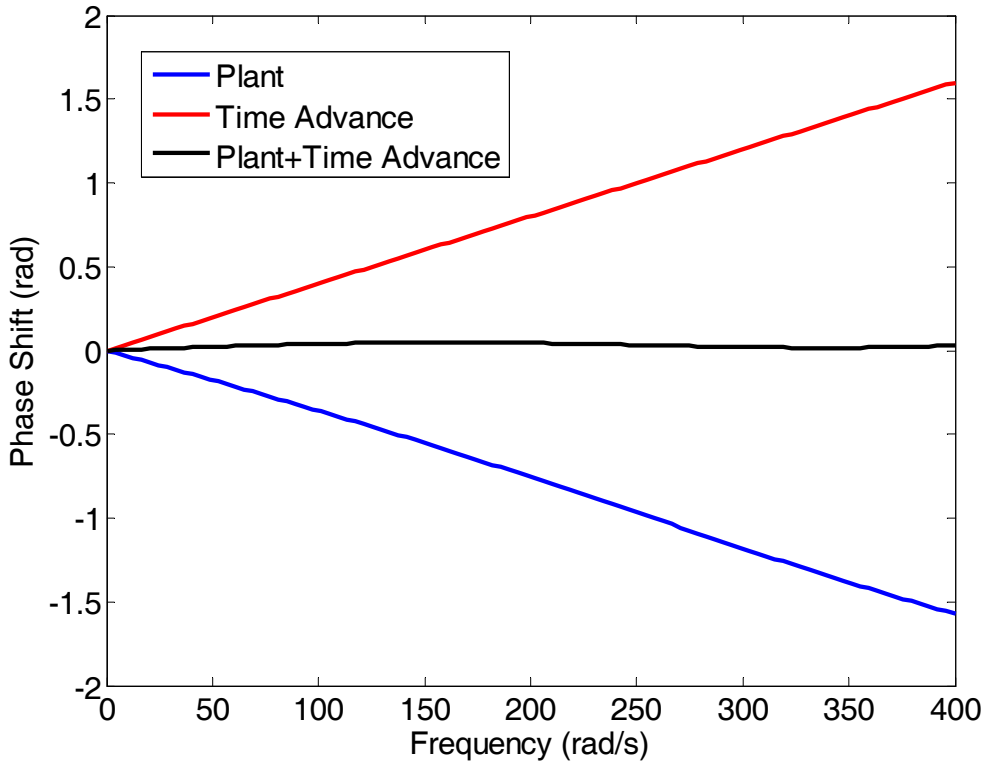

Figure 6.6 : Compensation of the phase lag by time advance.

6.3.4 Low-pass filter *q*(*s*) and dynamic compensator *b*(*s*)

Consider the repetitive control structure shown in Figure 6.1 where G_n is the nominal model of the plant, Δ_m is the normalized unstructured multiplicative model uncertainty, W_T is the multiplicative uncertainty weighting function and τ_d is the period of the periodic exogenous signal. $q(s)$ and $b(s)$ are filters used for tuning the

repetitive controller. Repetitive control systems can track periodic signals very accurately and can reject periodic disturbances very satisfactorily. This is due to the fact that the positive feedback loop in Figure 6.1 is a generator of periodic signals with period τ_d for $q(s)=1$. A low pass filter with unity d.c. gain is used for $q(s)$ for robustness of stability [72, 79].

The repetitive controller design involves the design of the two filters $q(s)$ and $b(s)$ seen in Figure 6.1. In the frequency domain, the ideal low-pass filter $q(j\omega)$ would be 1 in the frequency range of interest and zero at higher frequencies. This is not possible and $q(j\omega)$ will have negative phase angle which will make $q(j\omega)$ differ from 1, resulting in reduced accuracy. So as to improve the accuracy of the repetitive controller, a small time advance is customarily incorporated into $q(s)$ to cancel out the negative phase of its low-pass filter part within its bandwidth. This small time advance can easily be absorbed by the much larger time delay τ_d corresponding to the period of the exogenous input signal and does not constitute an implementation problem (see Figure 6.2).

The main objective of the usage of the dynamic compensator $b(s)$ is improving the relative stability, the transition response and the steady state accuracy in combination with the low-pass filter $q(s)$. Consider the function of frequency given by

$$R(\omega)=\left|q(j\omega)\left[1-b(j\omega)\frac{G(j\omega)}{1+G(j\omega)}\right]\right| \qquad \textbf{(6.26)}$$

which is called the regenerative spectrum in [73]. According to the same reference, $R(\omega)<1$ for $\forall\omega$ is a sufficient condition for stability. Moreover, $R(\omega)$ can be utilized to obtain a good approximation of the locus of the dominant characteristic roots of the repetitive control system for large time delay, thus resulting in a measure of relative stability, as well. Accordingly, the compensator $b(s)$ is designed to approximately invert $G/(1+G)$ within the bandwidth of $q(s)$ in an effort to minimize $R(\omega)$. The dynamic compensator $b(s)$ can be selected as only a small time advance or time advance multiplied by a low-pass filter in order to minimize $R(\omega)$. In order to make $R(\omega)<1$, the time advance in the filter $b(s)$ is chosen to cancel out the negative phase of $G/(1+G)$. This small time advance can easily be absorbed by the much larger time delay τ_d corresponding to the period of the exogenous input signal and does not constitute an implementation problem (see Figure 6.2).

The $q(s)$ and $b(s)$ filters are thus expressed as

$$q(s) = q_p(s)e^{\tau_q s} \tag{6.27}$$

$$b(s) = b_p(s)e^{\tau_b s} \tag{6.28}$$

The time advances τ_q and τ_b are firstly chosen to decrease the magnitude of $R(\omega)$ given in equation **(6.26)** Then, the design focuses on pairs of chosen parameters in $q_p(s)$ or $b_p(s)$ to satisfy a frequency domain bound on the mixed sensitivity performance criterion. If L denotes the loop gain of a control system, its sensitivity and complementary sensitivity transfer functions are

$$S := \frac{1}{1+L} \tag{6.29}$$

$$T := \frac{L}{1+L} \tag{6.30}$$

The parameter space design, presented in the following section, aims at satisfying the robust performance requirement

$$\left\| |W_S S| + |W_T T| \right\|_\infty < 1 \quad \text{or} \quad |W_S S| + |W_T T| < 1 \text{ for } \forall\omega \tag{6.31}$$

where W_S and W_T are the sensitivity and complementary sensitivity function weights.

The loop gain of the repetitive control system seen in Figures 6.1 and 6.2 are given by

$$L = G_n\left(1 + \frac{q_p}{1 - q_p e^{(-\tau_d+\tau_q)s}} b_p e^{(-\tau_d+\tau_q+\tau_b)s}\right) \tag{6.32}$$

The mixed sensitivity design requires

$$|W_S(\omega)S(j\omega)| + |W_T(\omega)T(j\omega)| = \left|\frac{W_S(\omega)}{1+L(j\omega)}\right| + \left|\frac{W_T(\omega)L(j\omega)}{1+L(j\omega)}\right| < 1 \text{ for } \forall\omega \tag{6.33}$$

or equivalently

$$|W_S(\omega)| + |W_T(\omega)L(j\omega)| < |1+L(j\omega)| \text{ for } \forall\omega \tag{6.33}$$

to be satisfied.

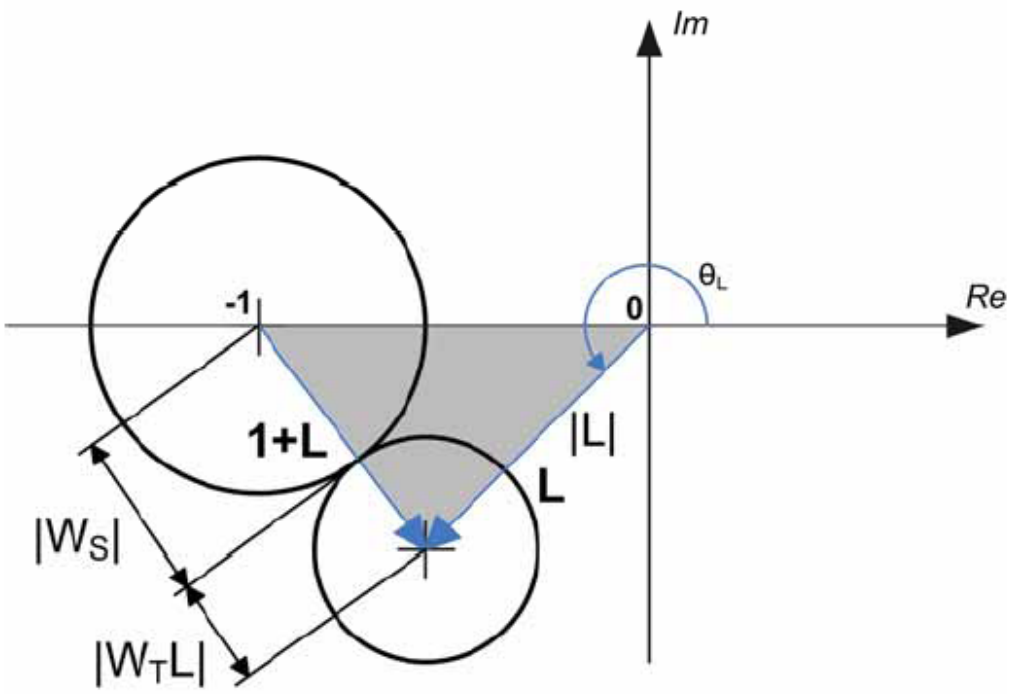

Figure 6.7 : Illustration of the point condition for the mixed sensitivity.

6.4 Parameter Space Approach to Repetitive Control

Conventional controller design methodologies such as pole placement and trial and error approach give unique controllers for each plant. No further robustness criteria can be incorporated in the design step [24]. The parameter space approach can be used in order to determine a set of coefficients for a given controller structure that simultaneously stabilizes a family of plants [24]. The parameter space approach allows determining the set of controller parameters, for which the characteristic polynomial is stable. The parameter vector might consist of uncertain plant parameters or it might consist of coefficients of a fixed structure controller. Additionally, the parameter space approach can provide information about effects of parameter variations on stability and it can provide information about the closeness to instability upon parameter variations. The resulting controllers are not fragile because they are chosen in the inner part of the parameter space.

6.4.1 Mapping robust performance frequency domain specifications into repetitive controller parameter space

In the present section, a repetitive controller design procedure based on mapping the mixed sensitivity frequency domain performance specification given in equation **(6.33)** with an equality sign into the chosen repetitive controller parameter plane at a chosen frequency is described.

Consider the mixed sensitivity problem given in Figure 6.7 illustrating equation **(6.33)** with an equality sign (called the mixed sensitivity point condition). Apply the cosine rule to the triangle with vertices at the origin, -1 and L in Figure 6.7 to obtain

$$\left(\left|W_S(\omega)\right|+\left|W_T(\omega)L(j\omega)\right|\right)^2=\left|L(j\omega)\right|^2+1^2+2\left|L(j\omega)\right|\cos\theta_L \qquad \textbf{(6.34)}$$

Equation **(6.34)** is a quadratic equation in $\left|L(j\omega)\right|$ and its solutions are

$$\left|L(j\omega)\right|=\frac{\left(-\cos\theta_L+\left|W_S(\omega)\right|\left|W_T(\omega)\right|\right)\pm\sqrt{\Delta_M(\omega)}}{1-\left|W_T(\omega)\right|^2} \qquad \textbf{(6.35)}$$

where

$$\Delta_M(\omega)=\cos^2\theta_L+\left|W_S(\omega)\right|^2+\left|W_T(\omega)\right|^2-2\left|W_S(\omega)\right|\left|W_T(\omega)\right|\cos\theta_L-1 \qquad \textbf{(6.36)}$$

Only, positive and real solutions for $\left|L\right|$ are allowed, i.e., $\Delta_M \geq 0$ in equation **(6.35)** must be satisfied. The point condition solution procedure is outlined below.

M1. Define the set of frequencies to be used as

$$\Omega := \left\{\omega_1,\omega_2,...,\omega_n;\omega_{n+1},\omega_{n+2},...,\omega_m;\omega_{m+1},\omega_{m+2},...,\omega_l\right\},\quad \omega_k=\frac{2\pi k}{\tau_d},k=1,2,3,...,n$$

where $\omega_1=2\pi/\tau_d$ is the frequency of the periodic exogenous input and $\omega_k=2\pi k/\tau_d$ is the chosen bandwidth of repetitive control (limited by the bandwidth of the actuator used). Frequencies ω_{m+1} to ω_l are high frequencies where significant model uncertainty exists $(\omega_{m+1}>10\omega_n)$ and the intermediate frequencies ω_{n+1} to ω_m.

M2. Choose a specific frequency value $\omega=\omega_i\in\Omega$, $i=1,2,...,l$ from set Ω in step M1 $\left|W_S(\omega)\right|$, $\left|W_T(\omega)\right|$ and $G(j\omega)$ at frequency ω are known at this point.

M3. Let $\theta_L \in [0, 2\pi]$. Evaluate Δ_M by using equation **(6.36)** and select the active range of θ_L where $\Delta_M \geq 0$ is satisfied. For all values of θ_L in the active range:

M3a. Evaluate $|L|$ by using equation **(6.35)**. Keep only the positive solutions.

M3b. Evaluate $L = |L| e^{j\theta_L}$.

M3c. Solve for the corresponding repetitive controller filters $q_p(j\omega)$ or $b_p(j\omega)$ at the chosen frequency ω by utilizing

$$q_p(j\omega) = \frac{L(j\omega) - G(j\omega)}{L(j\omega) - G(j\omega)\left[1 - b(j\omega)\right]} e^{(\tau_d - \tau_q) j\omega} \qquad \textbf{(6.37)}$$

$$b_p(j\omega) = \left[L(j\omega) - G(j\omega)\right]\left[\frac{1 - q(j\omega) e^{-\tau_d j\omega}}{q(j\omega) e^{-\tau_d j\omega}}\right] e^{-\tau_b j\omega} \qquad \textbf{(6.38)}$$

M3d. Using the specific structure of $q_p(j\omega)$ or $b_p(j\omega)$, back solve for the two chosen controller parameters within them. For example, $q_p(s)$ and $b_p(s)$ can be chosen as a multiplication of the second order controllers given by

$$q_p(s) = \prod_{i=1}^{n} \frac{q_{5i} s^2 + q_{4i} s + q_{3i}}{q_{2i} s^2 + q_{1i} s + q_{0i}}, \qquad b_p(s) = \prod_{i=1}^{n} \frac{b_{5i} s^2 + b_{4i} s + b_{3i}}{b_{2i} s^2 + b_{1i} s + b_{0i}} \qquad \textbf{(6.39)}$$

There are five tuneable parameters for n=1 in equation **(6.39)** which can be used to represent different types of controllers. These six tuneable parameters are q_{5i}, q_{4i}, q_{3i}, q_{2i}, q_{1i} and q_{0i} for $q_p(s)$. For n=1, the controller structure in **(6.39)** consists of some well-known controller types such as proportional-integral-derivative (PID), lead-lag controller, first or second order filters as illustrated in Table 6.1. By increasing n, larger order controllers can be easily synthesized. If the performance of the filters which are utilized in the repetitive controller for n=1 is unsatisfactory, n can be increased and new larger order filters can be synthesized. For the filter structure choice in equation **(6.39)**, the back solution procedure uses

$$\begin{aligned} \mathrm{Re}\left[q_p(j\omega)\right] &= \frac{\left(q_{3i} - q_{5i}\omega^2\right)\left(q_{0i} - q_{2i}\omega^2\right) + q_{1i} q_{4i} \omega^2}{\left(q_{0i} - q_{2i}\omega^2\right)^2 + \left(q_{1i}\omega\right)^2} \\ \mathrm{Im}\left[q_p(j\omega)\right] &= \frac{q_{4i}\omega\left(q_{0i} - q_{2i}\omega^2\right) - q_{1i}\omega\left(q_{3i} - q_{5i}\omega^2\right)}{\left(q_{0i} - q_{2i}\omega^2\right)^2 + \left(q_{1i}\omega\right)^2} \end{aligned} \qquad \textbf{(6.40)}$$

$$\mathrm{Re}\left[b_p(j\omega)\right] = \frac{\left(b_{3i} - b_{5i}\omega^2\right)\left(b_{0i} - q_{2i}\omega^2\right) + b_{1i}b_{4i}\omega^2}{\left(b_{0i} - b_{2i}\omega^2\right)^2 + \left(b_{1i}\omega\right)^2}$$
$$\mathrm{Im}\left[b_p(j\omega)\right] = \frac{b_{4i}\omega\left(b_{0i} - b_{2i}\omega^2\right) - b_{1i}\omega\left(b_{3i} - b_{5i}\omega^2\right)}{\left(b_{0i} - b_{2i}\omega^2\right)^2 + \left(b_{1i}\omega\right)^2} \qquad \textbf{(6.41)}$$

M4. The solution in step M3 above results in a closed curve which is plotted for solving two of the twelve parameters q_{0i} to q_{5i} and b_{0i} to b_{5i}. Plot the closed curve obtained in the chosen controller parameter space. Either the inside (drawn with a solid boundary) or outside (drawn with a dashed boundary) of this curve is a solution of equation **(6.33)** at the chosen frequency (see the ellipses in Figure 6.9, for example). The region obtained is the point condition solution in the chosen repetitive controller parameter plane at the frequency chosen in step M2.

M5. Go back to step M2 and repeat the procedure at a different frequency until all frequencies in set Ω are used.

M6. Plot the intersection of all point condition solutions for all frequencies in set Ω. This is the overall solution region for the mixed sensitivity requirement.

As the solution procedure only uses frequency response data and is numerical in nature, plants with time delay or poles on the imaginary axis and discontinues weights do not pose any problems. Note that solution regions for nominal performance $|W_S S|<1$ for $\forall\omega$ and for robust stability $|W_S S|<1$ for $\forall\omega$ can easily be obtained using the algorithm above with $W_S = 0$ and $W_T = 0$, respectively. It is then possible to concentrate on nominal performance at low frequencies, mixed sensitivity at intermediate frequencies and robust stability at high frequencies, obtaining three solution regions. The overall solution region in the controller parameter space is then determined by the intersection of all three regions for nominal performance, mixed sensitivity and robust stability. This procedure is easily programmable and quickly results in a controller parameter space representation of the solution. The controller parameter space presentation obtained offers the ease of visualization of parameter space methods (see Figure 6.9) when one accepts the shortcoming of treating only two controller parameters at a time. Multi-objective design can easily be formed in parameter space as it amounts simply to intersection of individual solution regions. It is also possible to determine the final design (or tuning point) by optimizing some other criteria, such as nominal time domain performance within the solution region

obtained. In contrast to H_∞ optimal control synthesis, there is no relationship between the order of repetitive control filters and the complexity of weights in this proposed method. The main strength of this method is that low-order, easily implementable repetitive control filters are specified from the beginning.

Table 6.1: Controller coefficients table.

Control Action	N	q_{5i}	q_{4i}	q_{3i}	q_{2i}	q_{1i}	q_{0i}
P	1	0	0	K	0	0	1
PD	1	0	KT_d	K	0	0	1
PI	1	0	K	KT_i	0	1	0
PID	1	KT_d	K	KT_i	0	1	0
Lag (β>1)	1	0	KT	K	0	βT	1
Lead (0<α<1)	1	0	KT	K	0	αT	1
First Order Filter	1	0	0	K	0	T	1
Second Order Filter	1	0	0	$K\omega^2$	1	$2\zeta\omega$	ω^2

It is possible that for certain data sets $|W_S|$, $|W_T|$, G, ω; no solutions to the solution procedure outlined above exist. Nonexistence of a solution for a specific frequency ω could be because of nonexistence of a positive Δ_M in equation **(6.36)** or nonexistence of a positive solution $|L|$ in equation **(6.35)**. Nonexistence of a solution usually results from a weight $|W_S|$ or $|W_T|$ that is too restrictive. The solution procedure, which is programmed in an interactive fashion, results in no solution points in this case. Then, the user will know that his mixed sensitivity requirement at that frequency was too restrictive and has the choice of relaxing this requirement. Note that solutions might exist at all individual frequencies, however; their intersection in Step M6 resulting in the overall solution region, might still be empty. In that case, the user must change the sensitivity and complementary sensitivity weights at the problematic frequencies.

6.5 Case Study: High-Speed Atomic Force Microscope (AFM) Scanner Position Control

In this part of the Chapter 6, the high speed atomic force microscope (AFM) scanner which is designed and modelled in [95] is utilized as a numerical example to explain the methodology of the multi-objective parameter space approach for SISO repetitive controller design. The second order and fourth order mathematical models of this high speed AFM scanner are given in [95]. In this example, the fourth order model is

used because it includes the first mode of the piezoelectric stack in the vertical direction. The transfer function of the AFM scanner is given by

$$G(s)=\frac{K\left(s^2+2\zeta_2\omega_2 s+\omega_2^2\right)}{\left(s^2+2\zeta_1\omega_1 s+\omega_1^2\right)\left(s^2+2\zeta_3\omega_3 s+\omega_3^2\right)}\left[nm/V\right] \qquad \textbf{(6.42)}$$

where $K=1\times10^{12}$ *nm/V* includes the power amplifier and sensor gain. The system seen in **(6.42)** has two resonant frequencies and one anti-resonant frequency. The numerical values of these frequencies are given as $f_1=40.9$ *kHz*, $f_2=41.6$ *kHz* and $f_3=120$ *kHz* and can be seen in Figure 6.8. The numerical values of the relative damping coefficients are given as $\zeta_1=0.016$, $\zeta_2=0.016$ and $\zeta_3=0.17$.

The dynamic compensator $b(s)$ is chosen as a pure time advance as

$$b(s)=b_p(s)e^{\tau_b s}=e^{3\times10^{-6}s} \qquad \textbf{(6.43)}$$

The low-pass filter $q(s)$ is chosen as

$$q(s)=q_p(s)e^{\tau_q s}=\frac{a_0}{s^2+a_1 s+a_0}e^{7.5\times10^{-6}s} \qquad \textbf{(6.44)}$$

The parameters of $q_p(s)$ given in equation **(6.44)** are chosen as $q_{51}=q_{41}=0$, $q_{21}=1$, $q_{31}=q_{01}=a_0$ and $q_{11}=a_1$ in the general form **(6.39)** in order to obtain unity d.c. gain. Phase advance is also added to this low-pass filter for phase cancellation. Thus, a decrease in the steady state error is aimed. The regions in the $q_{01}-q_{11}$ controller parameter space are computed for three cases which are respectively the nominal performance at low frequencies ($W_T=0$), mixed sensitivity at intermediate frequencies and robust stability at high frequencies ($W_S=0$).

The sensitivity constraints are specified at a set of discrete frequencies. The periodic input command of the high speed AFM scanner has a period of 0.0005 *sec*. The specific numerical values of the chosen weights used in the computation of the controller parameters are seen in Table 6.2. The frequencies corresponding to the weights in Table 6.2 are shown with dots in the Bode magnitude plot of Figure 6.8. The overall region calculated for nominal performance, mixed sensitivity and stability robustness can be seen in Figure 6.9.

Table 6.2: Desired sensitivity upper bounds at τ_d=0.0005sec.

Frequency Range	*k*	*f=k/τ_d (kHz)*	W_S	W_T
Low (NP)	1	2	500	0
Low (NP)	2	4	225	0
Low (NP)	3	6	115	0
Low (NP)	4	8	75	0
Intermediate (RP)	40	80	3.3	0.001
Intermediate (RP)	50	100	4.5	0.045
Intermediate (RP)	55	110	4.5	0.001
Intermediate (RP)	60	120	1.5	0.005
Intermediate (RP)	70	140	1.5	0.01
High (RS)	80	160	0	0.05
High (RS)	90	180	0	0.05
High (RS)	100	200	0	0.05

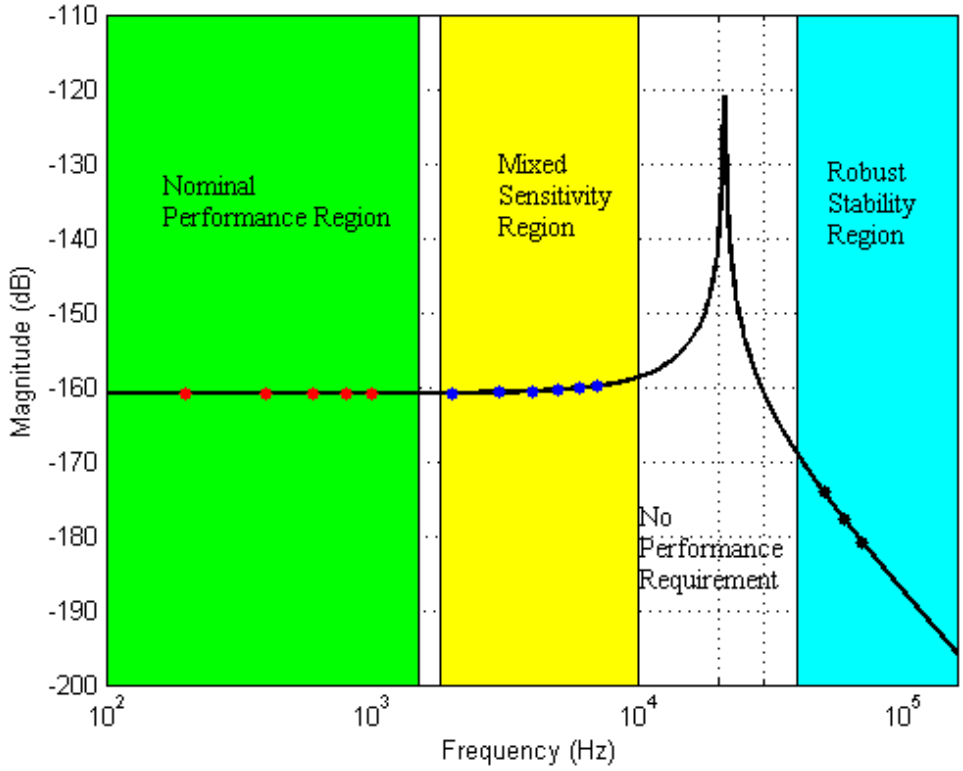

Figure 6.8 : The Bode magnitude plot of high speed AFM – scanner with the mapping frequencies for the nominal performance, robust performance and robust stability.

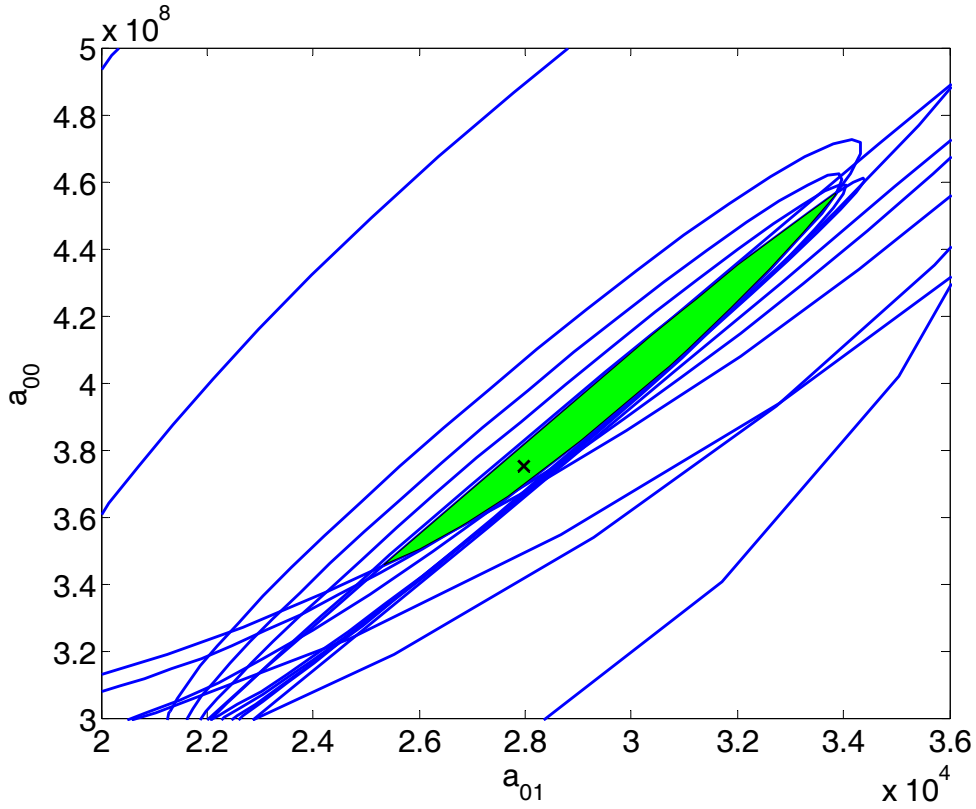

Figure 6.9 : The region where nominal performance, mixed sensitivity and robust stability are all satisfied.

The mathematical model of the high-speed AFM scanner cannot be fitted very well for frequencies above 160 *kHz*. A uniform weight for the robust stability requirement for frequencies above this value is chosen here as $|T| < 0.05$ for $f \geq 160\,kHz$. This corresponding discontinuous weight W_T has been shown graphically with red-colored cross sign in Figure 6.8. The relative multiplicative error $\left|(G - G_n)/G_n\right|$ has to be below the weight specified in the stability robustness considerations given in Figure 6.8. The intersection of the regions, which are calculated in order for the nominal performance, the mixed sensitivity and the robust stability requirements, in the $q_{01} - q_{11}$ controller parameter space is filled with green colour. The designation procedure is concluded by choosing a point in the $q_{01} - q_{11}$ controller parameter plane given in Figure 6.9. The solution within this region is chosen arbitrarily in this example and is point is marked with a cross in Figure 6.9. The simulation results for triangular wave input with the period 2 kHz and amplitude can be seen in Figures 6.10 and 6.11. These results show the effectiveness of the repetitive controller in decreasing the steady state error while tracking a periodic input signal.

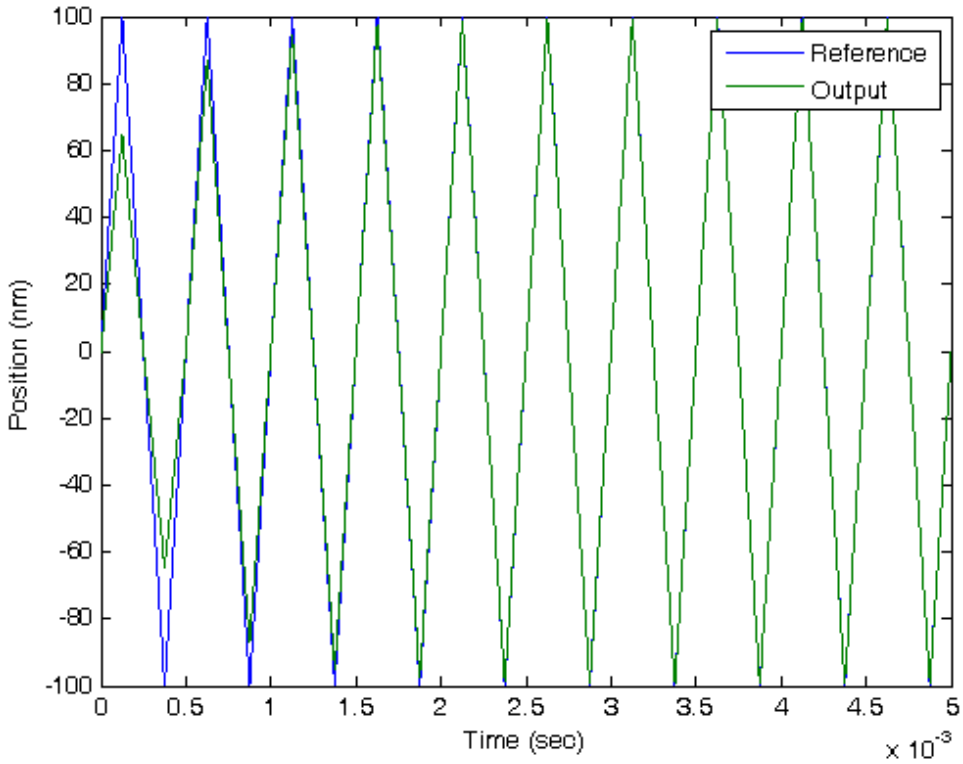

Figure 6.10 : Simulation results for triangular wave input at 2 *kHz*.

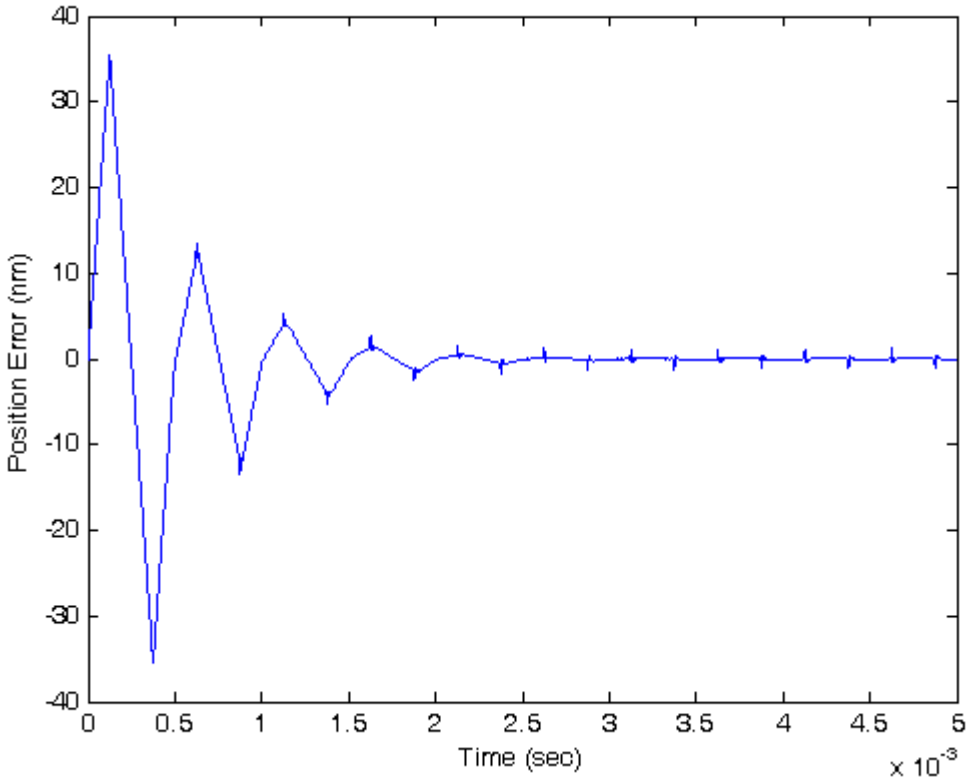

Figure 6.11 : Simulation results for triangular wave input at 2 *kHz*.

6.6 COMES Toolbox: Repetitive Control System Design

In addition to abovementioned method, MATLAB-based toolbox that implements parametric robust control methods is presented in this study. The technique behind it is based on mapping a frequency domain mixed sensitivity bound into the chosen repetitive controller parameter plane. The procedure leads to graphical solution regions (2-D plots with color filling showing where the specifications are met) in controller parameter space. The aim is to design a user-friendly toolbox with graphical user interface (GUI), which hides all calculations from the user as much as possible. Hence, the user can focus on analyzing the graphical results rather than do the all complicated calculations. This MATLAB-based toolbox has two built-in functions on servohydraulic material testing machine position control and high speed AFM scanner position tracking system.

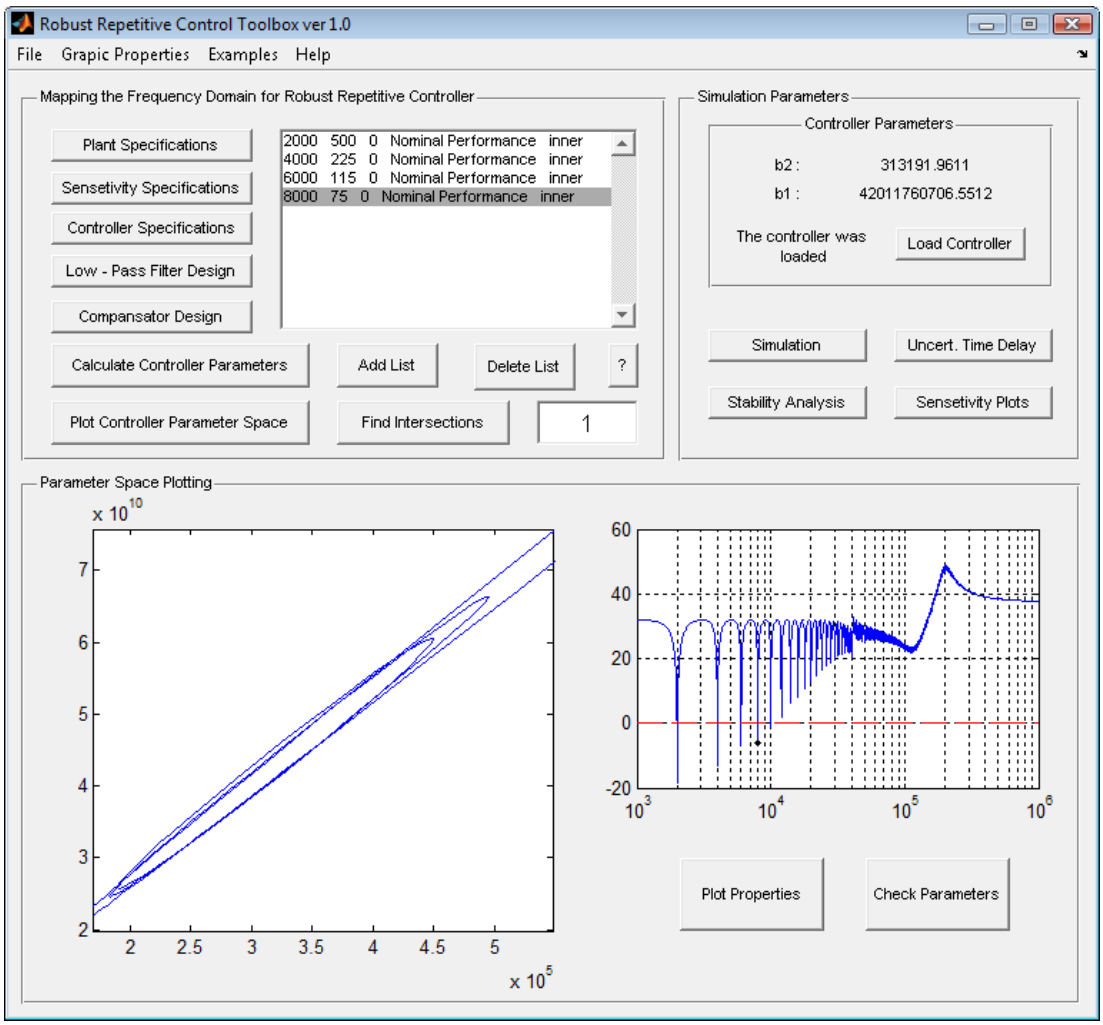

Figure 6.12 : Main window of repetitive control system design part of COMES toolbox.

6.7 Chapter Summary and Concluding Comments

A multi-objective parameter space repetitive controller design procedure for satisfying a mixed sensitivity objective was presented here. The main idea was to use a simple easily implementable structure for the repetitive controller filters and compute solution regions in the chosen controller parameter space where frequency domain specifications on the nominal performance at low frequencies (W_T=0), mixed sensitivity at intermediate frequencies and robust stability at high frequencies (W_S=0) are satisfied. The abovementioned method is well suited to the structure of a repetitive control system with discrete frequencies of interest and the computations were also quite fast. The proposed method is successfully applied to the infinite dimensional nature of the repetitive control system with its inherent time delay. The effectiveness of the proposed method was demonstrated by carrying out a design and simulation study for high speed AFM scanner position control problem.

7. CONCLUSION AND RECOMMENDATIONS

The main purpose of this research was to develop an interactive computer program for MATLAB in order to design controllers for mechatronic systems. This toolbox brings together many different control strategies like classical control, preview control, model regulator control and repetitive control. Some of these control techniques include robust design and others do not include that. The toolbox offers the users the option to choose one of these control strategies to build a controlled mechatronic system without making many extensive calculations required for various design.

One of the main contributions of this thesis is the development of practical tools for understanding the fundamental concepts in robust design based on parameter space approach and reducing the design time of control systems by using this toolbox. The design procedure leads to graphical solution region in controller parameter space instead of preview control design. The aim was to design a user-friendly toolbox with graphical user interface (GUI), which hides all calculations from the user as much as possible. Thus, the user is able to focus on analyzing the graphical results rather than doing all of complicated calculations.

Summaries of the material presented in each chapter were provided at the end of respective chapters. Here, we will give again some brief information on each chapter.

The second chapter was devoted to the analytical solution procedure to design classical control systems like lead, lag, lead-lag compensator in the frequency domain. The analytical solution technique mentioned in this chapter is based on the analytical solution of phase margin design. Therefore, only unique controller parameters can be determined in order for the desired crossover frequency and phase margin. In addition, the controller parameters can be calculated very fast thanks to this procedure. The results obtained using this method can be compared with those using the root-locus methodology so as to demonstrate effectiveness of design procedure.

The third chapter introduced robust design methodology based on mapping Hurwitz stability, *D*-stability and the frequency domain specifications of weighted sensitivity minimization and gain/phase margin bound to the chosen controller parameter plane. Multi-objective solutions are easily obtained by forming graphical intersections of several single-objective solutions in parameter space. Hurwitz stability, *D*-stability, the mixed sensitivity frequency domain bound and gain/phase margin bound can be combined to obtain a final overall solution region. The effectiveness of this multi-objective design procedure was tested by applying to the automated path following problem.

The fourth chapter was dedicated to the discrete-time preview based feedforward control systems such as ZPET, PTC and OPTC. The ZPET, PTC and OPTC methods were formulated to handle systems with NMP zeros here. In addition, these methods were compared with each other. Moreover, an evolutionary optimization algorithm was used in order to determine the OPTC's parameters which minimize the cost function given in this chapter. To demonstrate the performance of these preview control systems, an example from the literature was utilized.

The fifth chapter dealt with a multi-objective parameter space model regulator design procedure with mixed sensitivity performance requirement. The application of a robust model regulator design based on mapping frequency domain criteria to controller parameter space to the vehicle yaw stability control problem has been presented in this chapter. The effectiveness of the proposed method was illustrated by means of carrying out a design and simulation study for robust yaw stability control problem.

The sixth chapter was devoted to a multi-objective parameter space repetitive controller design procedure for satisfying a mixed sensitivity objective. The main idea of this methodology developed in this study is to use a simple and easily implementable structure for repetitive controller filters and compute solution regions in the chosen controller parameter space where frequency domain specifications on the nominal performance at low frequencies, mixed sensitivity at intermediate frequencies and robust stability at high frequencies are satisfied. By using the method explained in this work, low order and physically meaningful robust repetitive controllers can be designed and implemented for plants that possibly include time

delay, poles on the imaginary axis and for discontinuous weights. Additionally the proposed method was compared with the existing method by giving some example.

REFERENCES

[1] **Url-1** <*http://en.wikipedia.org/wiki/Mechatronics*>, accessed at 24.09.2009.

[2] **Isermann R.,** 2005. Mechatronic Systems Fundamentals, Springer Verlag: London, UK.

[3] **Jia L. and Schaufelberger W.,** 1995. Software for Control Engineering Education, Verlag der Fachvereine an der ETH-Zürich, Zürich.

[4] **Johansson M., Gäfvert M. and K.J. Åström KJ.,** 1998. Interactive tools for education in automatic control, *IEEE Transactions on Interactive Learning,* pp. 33-40.

[5] **Azemi A. and Yaz E.E.,** 1997. Using MATLAB in a graduate electrical engineering optimal control course, *IEEE Frontiers in Education Conference,* pp. 13-17.

[6] **Sienel W., Bünte T. and Ackermann J.,** 1996. PARADISE – Parametric robust analysis and design interactive software environment: A Matlab-based robust control toolbox, *IEEE International Symposium on Computer-Aided Control System Design,* pp. 380-385, Dearborn MI.

[7] **Sakabe K., Yanami H., Anai H. and Hara S.,** 2004. A MATLAB toolbox for robust control synthesis by symbolic computation, *SICE Annual Conference in Sapporo,* pp. 1968-1973, Japan.

[8] **Hyodo N., Hong M., Yanami H., Anai H. and Hara S.,** 2006. Development of a MATLAB toolbox for parametric robust control – algorithms and functions –, *ISICE-ICASE International Joint Conference,* pp. 2856-2861, Busan, Korea.

[9] **Balas G.J., A.K. Packard A.K., Safonov M.G. and Chiang R.Y.,** 2004. Next generation of tools for robust control, *Proceedings of the 2004 American Control Conference,* pp. 5612-5615, Boston, Massachusetts.

[10] **Vivero O. and Liceago-Castro J.,** 2008. MIMO toolbox for Matlab, *Annual IEEE Student Paper Conferece,* pp. 1-5, Aalborg, Denmark.

[11] **Boyle J.M., Ford M.P. and Maciejowski J.M.,** 1989: A multivariable toolbox for use with matlab, *IEEE Control System Magazine*, Vol. **9**, No. 1, pp. 59-65.

[12] **Campa G., Davini M. and Innocenti M.,** 2000. MVTOOLS: Multivariable systems toolbox, *Proceedings of the 2000 International Symposium on Computer-Aided Control System Design,* pp. 163-167, Anchorage, Alaska, USA.

[13] **Ogata K.,** 1990. Modern Control Engineering, Prentice Hall: New York, USA.

[14] **Thaler G. and Brown R.,** 1953. Servomechanism Analysis, McGraw-Hill: New York, USA.

[15] **Del Toro V. and Parker S.,** 1960. Principles of Control Systems Engineering, McGraw-Hill: New York, USA.

[16] **D'Azzo J. and Houpis C.,** 1966. Feedback Control System Analysis and Synthesis, McGraw-Hill: New York, USA.

[17] **Watkins B.,** 1969. Introduction to Control Systems, Macmillan: New York, USA.

[18] **Dorf R.,** 1974. Modern Control Systems, Addison-Wesley: Reading, MA, UK.

[19] **Ross E., Warren T. and Thaler G.,** 1960. Design of servo compensation based on the root locus approach, *AIEE Transactions on Application to Industry*, Vol. **79**, pp. 272-277.

[20] **Wakeland W.,** 1967. Analytic technique for root locus compensation with quadratic factors, *IEEE Transactions on Automatic Control,* Vol. **AC-12**, pp. 631-632.

[21] **Wakeland W.,** 1967. New analytic technique for root locus compensation, *Proceedings of First Asilomar Conference of Circuits and Systems,* pp. 562-572.

[22] **Wakeland W.,** 1975. Bode compensator design, *IEEE Transactions on Automatic Control,* Vol. **AC-21**, pp. 771-773.

[23] **Mitchell J.R,** 1977. Comments on "Bode compensator design", *IEEE Transactions on Automatic Control,* Vol. **AC-22**, pp. 869-870.

[24] **Ackermann J., Blue P., Bünte T., Güvenç L., Kaesbauer D., Kordt M., Mühler M., Odenthal D.,** 2002. Robust Control: The Parameter Space Approach, Springer Verlag: London, UK.

[25] **Djaferis T.E.,** 1991. Representations of controllers that achieve robust performance for systems with real parameter uncertainty, *Systems and Control Letters,* Vol. **16**, pp. 329-339.

[26] **Saeki M.,** 1994. A design method of the optimal PID controller for a two disc type mixed sensitivity problem, *Transactions on the Inst. of Sys. Contr. Info. Eng.,* Vol. **7**, No. 12, pp. 520-527.

[27] **Besson V. and Shenton A.T.,** 1997. Interactive control system design by a mixed H-infinity parameter space method, *IEEE Transactions on Automatic Control,* Vol. **42**, pp. 946-955.

[28] **Bünte T.,** 1998. Beitraege zur robusten lenkregelung von personenkraftwegen, Ph.D: Dissertation, RWTH Aachen, VDI Fortschritt-Bericht, Reiche 12, Nr. 366, VDI-Verlag, Düsseldorf.

[29] **Odenthal D. and Blue P.,** 2000. Mapping of H-infinity design specifications into parameter space, *Proceedings of 3rd IFAC Symposium on Robust Control Design,* Prague.

[30] **Saeki M. and Hirayama D.,** 1996. Parameter space design method of PID controller for robust sensitivity minimization problem, *Transactions on the Society of Instrument and Control Engineers,* Vol. **32**, No. 12, pp. 1612-1619.

[31] **Saeki M. and Kimura J.,** 1998. Design method of robust PID controller and CAD system, *Proceedings of the 11th IFAC Symposium on System Identification,* Vol. **3**, pp. 1587-1593.

[32] **Saeki M.,** 2006. Fixed structure PID controller design for standard H-infinity control problem, *Automatica,* Vol. **42**, No. 1, pp. 93-100.

[33] **Besson V. and Shenton A.T.,** 1999: An interactive parameter space method for robust performance in mixed sensitivity problems, *IEEE Transactions on Automatic Control,* Vol. **44**, pp. 1272-1276.

[34] **Güvenç L. and Ackermann J.,** 2001. Links between the parameter space and frequency domain methods of robust control, *International Journal of Robust and Nonlinear Control,* Vol. **11**, No. 15, pp. 1435-1453.

[35] **Ackermann J., Guldner J., Sienel W., Steinhauser R. and Utkin V.I,** 1995. Linear and nonlinear controller design for robust automatic steering, *IEEE Transactions on Control Systems Technology,* Vol. **3**, No. 1, pp. 132-143.

[36] **Cannon R.H. and Schmitz E.,** 1984. Initail experiments on the control of a flexible manipulator, *International Journal of Robotics Research,* Vol. **3**, pp. 62-75.

[37] **Tomizuka M.,** 1987. Zero phase error tracking algorithm for digital control, *ASME Journal of Dynamic Systems, Measurement and Control,* Vol. **109**, No. 1, pp. 65-68.

[38] **Haack B. and Tomizuka M.,** 1991. The effect of adding zeros to feedforward controllers, *ASME Journal of Dynamic Systems, Measurement and Control,* Vol. **113**, No. 1, pp. 6-10.

[39] **Manq C.H. and Xia Z.,** 1990. Characterization and compensation of discrete-time nonminimum phase zeros to feedforward controllers, *Proceedings of ASME Symposium on Robotics Research,* DSC-Vol. **26**, pp. 15-23, New York.

[40] **Aksun Güvenç B. and L. Güvenç L.,** 1999. Optimal precision tracking control of discrete time nonminimum phase systems, *Proceedings of European Control Conference*.

[41] **Güvenç L., Harib K. and Srinivasan K.,** 1995. Extended precision tracking control of discrete-time nonminimum phase systems, *Proceedings of ASME International Mechanical Engineering Congress and Exposition,* DSC-Vol. **57**-1, pp. 151-158, San Fransisco.

[42] **Gross E., Tomizuka M. and Messner W.,** 1994. Cancellation of discrete time unstable zeros by feeedforward control *ASME Journal of Dynamic Systems, Measurement and Control,* Vol. **116**, No. 1, pp. 33-38.

[43] **Åström K.J., Hagender P. and Sternby J.,** 1984. Zeros of sampled systems, *Automatica,* Vol. **20**, pp. 31-38.

[44] **Aksun Güvenç B. and Güvenç L.,** 2001. Characterization and compensation of complex nonminimum phase zeros for preview control, *IEEE Mediterranean Conference on Control and Automation*.

[45] **Fu Y. and Dumont G.A.,** 1989. Choice of sampling to ensure minimum-phase behavior *IEEE Transactions on Automatic Control,* Vol. **34**, No. 5, pp. 560-563.

[46] **Ishitobi M.,** 1992. Conditions for stable zeros of sampled systems, *IEEE Transactions on Automatic Control,* Vol. **37**, No. 10, pp. 1558-1561.

[47] **Tsao T.C. and M. Tomizuka M.,** 1994. Robust adaptive and repetitive digital control and application to a hydraulic servo for noncircular machining, *ASME Journal of Dynamic Systems, Measurement and Control,* Vol. **116**, No.1, pp. 24-32.

[48] **Ohnishi K.,** 1987. A new servo method in mechatronics, *Transactions on Japanese Electrical Engineers,* Vol. **107-D**, pp. 83-86.

[49] **Umeno, T. and Hori, Y.,** 1991. Robust Speed Control of DC Servomotors Using Modern Two Degrees-of-Freedom Controller Design , *IEEE Transactions on Industrial Electronics*, Vol **38**, No. 5, pp. 363-368.

[50] **Kempf C.J. and Kobayashi S.,** 1999. Disturbance observer and feedforward design for a high-speed direct-drive positioning table, *IEEE Transactions on Control Systems Technology*, Vol. **7**, No. 5, pp. 513-526.

[51] **Güvenç L. and Srinivasan K.,** 1994. Friction compensation and evaluation for a force control application, *Mechanical Systems and Signal Processing,* Vol. **8**, No. 6, pp. 623-638.

[52] **Aksun Güvenç B., Bünte T., Odenthal D. and Güvenç L.,** 2004. Robust two degree of freedom vehicle steering compensator design, *IEEE Transactions on Control Systems Technology,* Vol. **12**, No. 4, pp. 627-636.

[53] **Bünte T., Odenthal D., Aksun Güvenç B. and Güvenç L.**, 2002. Robust vehicle steering control based on the disturbance observer, *IFAC Annual Reviews in Control,* part 1, Vol. **26**, pp. 139-149.

[54] **Karaman S., Öncü S., Güvenç L., Ersolmaz Ş.S., Çetin E., Kanbolat A.,** 2006. Robust Velocity Scheduled Yaw Stability Control of a Light Commercial Vehicle, *IEEE Intelligent Vehicles Symposium*, Tokyo.

[55] **Öncü S., Karaman S., Güvenç L., Ersolmaz S., Öztürk E., Çetin E., Sinal M.,** 2007. Robust Yaw Stability Controller Design for a Light Commercial Vehicle Using a Hardware in the Loop Steering Test Rig, *IEEE Intelligent Vehicles Symposium*, Istanbul.

[56] **Francis B.A. and Wonham W.M.,** 1975. The internal model principle for linear multivariable regulators, *Applied Mathematics and Optimization*, Vol. **2**, pp. 170-194.

[57] **Inoue T., Iwai S., and Nakano M.,** 1981. High accuracy control of a proton synchrotron magnet power supply, Proceedings *of 8th IFAC World Congress*, Part 3, pp. 3137-3142.

[58] **Cheng Y.Q., Moore K.L., Yu J. and Zhang T.,** 2004. Iterative learning control and repetitive control in hard disk drive industry – a tutorial.

[59] **Moon J.H., Lee M.N., and Chung M.,** 1998. Repetitive control for the track-following servo system of an optical disk drive, *IEEE Transactions on Control Systems Technology*, Vol. **6**, No. 5, pp. 663-667.

[60] **Omata T., Hara S., and Nakano M.,** 1987. Nonlinear repetitive control with application to trajectory control of manipulators, *Journal of Robotic Systems*, Vol. **4**, No. 5, pp.631-652.

[61] **Sadegh N., Horowitz R., Kao W.W., and Tomizuka M.,** 1990. A unified approach to the design of adaptive and repetitive controllers for robotic manipulators, *ASME Journal of Dynamical Systems, Measurement and Control*, Vol. **112**, No. 4, pp. 618-629.

[62] **Kobayashi F., Hara S., and Tanaka H.,** 1990. Reduction of motor speed fluctuation using repetitive control, *Proceedings of 29th IEEE Conference on Decision and Control*, pp. 1697-1702.

[63] **Fung R.F., Huang J.S., and Chien C.C.,** 2000. Design and application of a continuous repetitive controller for rotating mechanisms, *International Journal of Mechanical Sciences*, Vol. **42**, No. 9, pp. 1805-1819.

[64] **Shaw F.R., and Srinivasan K.,** 1993. Discrete-time repetitive control systems design using the regeneration spectrum, *ASME Journal of Dynamical Systems, Measurement and Control*, Vol. **115**, No. 2A, pp. 228-237.

[65] **Garimella S.S., and Srinivasan K.,** 1996. Application of repetitive control to eccentricity compensation in rolling, *ASME Journal of Dynamical Systems, Measurement and Control*, Vol. **118**, No. 4, pp. 657-664.

[66] **Tinghsu S., Hattori S., Ishida M., and Hori T.,** 2002. Suppression control method for torque vibration of AC motor utilizing repetitive controller with fourier transform, *IEEE Transactions on Industry Application*, Vol. **38**, No. 5, pp. 1316-1325.

[67] **Rech C., Pinheriro H., and Grundling H.,** 2003. Comparison of digital control techniques with repetitive integral action for low cost PWM inverters, *IEEE Transactions on Power Electronics*, Vol. **18**, No. 1, pp. 401-410.

[68] **Zhang K., Kang Y., and Xiong J.,** 2003. Direct repetitive control of SPWM inverter for UPS purpose, *IEEE Transactions on Power Electronics*, Vol. **18**, No. 3, pp. 784-792.

[69] **Zhou K., and Wang D.,** 2003. Digital repetitive controlled three-phase PWM rectifier, *IEEE Transactions on Power Electronics*, Vol. **18**, No. 1, pp. 309-316.

[70] **Choi G.S., Lim Y.A., and Choi G.H.,** 2002. Tracking position control of piezoelectric actuators for periodic reference inputs, *Mechatronics*, Vol. **12**, No. 5, pp. 669-684.

[71] **Choi G.H., Jong H.O., and Choi G.S.,** 1999. Repetitive tracking control of a course-fine actuator, *Proceedings of IEEE/ASME International Conference Advanced Intelligent Mechatronics*, pp. 335-340.

[72] **Hara S., Yamamoto Y., Omata T. and Nakano M.,** 1988. Repetitive control systems: A new type servo system for periodic exogenous signals, *IEEE Transactions on Automatic Control,* Vol. **33**, pp. 657-667.

[73] **Srinivasan K., and Shaw F.R.,** 1991. Analysis and design of repetitive control systems using the regeneration spectrum, *ASME Journal of Dynamical Systems, Measurement and Control*, Vol. **113**, No. 2, pp. 216-222.

[74] **Tomizuka M., Tsao T.C., and Chew K.K.,** 1989. Analysis and synthesis of discrete-time repetitive controllers," *ASME Journal of Dynamical Systems, Measurement and Control*, Vol. **111**, No. 3, pp. 353-358.

[75] **Srinivasan K., Özbay H., and Jung I.S.,** 1995. A design procedure for repetitive control systems, *Proceedings of ASME International Mechanical Engineer's Congress and Exposition*, pp. 581-593.

[76] **Özbay H.,** 1993. H_∞ optimal controller design for a class of distributed parameter space, *International Journal of Control*, Vol. **58**, No. 4, pp. 739-782.

[77] **Peery T. and Özbay H.,** 1997. H_∞ optimal repetitive controller design for stable plants," *ASME Journal of Dynamical Systems, Measurement and Control*, Vol. **119**, No. 3, pp. 541-547.

[78] **Roh C.L. and Chung M.J.,** 1995. Design of repetitive control system for an uncertain plant," *Electronics Letter*, Vol. **31**, No. 22, pp. 1959-1960.

[79] **Weiss G. and Häfele M.,** 1999. Repetitive control of MIMO systems using H_∞ design, *Automatica*, Vol. **35**, pp. 1185-1199.

[80] **Weiss G., Zhong Q.Z., Green T.C. and Liang J.,** 2004. H_∞ repetitive control of DC-AC converters in microgrids, *IEEE Transactions on Power Electronics*, Vol. **19**, No.1, pp. 219-230.

[81] **Zhong Q.C., Liang J., Weiss G., Feng C. and Green T.C.,** 2006. H_∞ control of the neutral point in four-wire three-phase DC-AC converters, *IEEE Transactions on Industrial Electronics*, Vol. **53**, No. 5.

[82] **Doh T.Y. and Chung M.J.,** 2003. Repetitive control design for linear system with time-varying uncertainties, *IEEE Proceedings of Control Theory Applications,* Vol. **150**, pp. 427-432.

[83] **Güvenç L.,** 1996. Stability and performance robustness analysis of repetitive control systems, *ASME Journal of Dynamical Systems, Measurement and Control*, Vol. **118**, No. 3, pp. 593-597.

[84] **Li J. and Tsao T.C.,** 1998. Robust performance repetitive control design using structured singular values, *Proceedings of ASME International Mechanical Engineer's Congress and Exposition.*

[85] **Aksun Güvenç B. and Güvenç L.,** 2006. Robust repetitive controller design in parameter space, *ASME Journal of Dynamical Systems, Measurement and Control*, Vol. **128**, pp. 406-413.

[86] **Omata T., Hara S., and Nakano M.,** 1985. Synthesis of repetitive control systems and its applications, *Proceedings of IEEE Conference on Decision and Control,* pp. 1387-1392.

[87] **Sadegh N.,** 1991. Synthesis and stability analysis of repetitive controllers, *Proceedings of American Control Conference,* pp. 2634-2639.

[88] **Hara S.,** 1988. Repetitive control system: a new type of servo for periodic exogenous signals, *IEEE Transactions on Automatic Control,* Vol. **33**, No. 7, pp. 659-668.

[89] **Hara S. and Yamamoto Y.,** 1985. Stability of repetitive control systems, *Proceedings of IEEE Conference on Decision and Control,* pp. 326-327.

[90] **Silva G.J., A. Datta A., Bhattacharya S.P.,** 2005. PID Controllers for Time-delay Systems, Boston: Birkhäuser.

[91] **El'sgol L.E.,** 1966. Introduction to the theory of differential equations with deviating argument, Translated by R. J. McLaughlin Holden-day, San Francisco.

[92] **Srinivasan K. and Nachtigal C.L.,** 1978. Analysis and design of machine tool chatter control systems using regeneration spectrum, *ASME Journal of Dynamical Systems, Measurement and Control*, Vol. **100**, pp. 191-200.

[93] **Bartalucci B. and Lucci G.G.,** 1969. Grinding process instability, *ASME Journal of Engineering and Industry*, Vol. **19**, pp. 597-606.

[94] **Broberg H.L. and Molyet R.G.,** 1994. A new approach to phase cancellation in repetitive control, *Proceedings of Industry Applications Society Annual Meeting,* Vol. **3**, pp. 1766-1770.

[95] **Schitter G., Åström K.J., DeMartini B.E., Thurner P.J., Turner K.L. and Hansma P.K.,** 2007. Design and modelling of a high-speed AFM-scanner, *IEEE Transactions on Control Systems Technology*, Vol. **15**, No. 5, pp. 906-915.

APPENDICES

APPENDIX A: Some mathematical inferences on analytical solution procedure in frequency-domain

APPENDIX A.1: Lead Compensator Design

APPENDIX A.2: PD Controller Design

APPENDIX A.3: Lag Compensator Design

APPENDIX A.4: PI Controller Design

APPENDIX A.5: PID Controller Design

APPENDIX B: Nonlinear Single Track Model

APPENDIX C: Some mathematical inferences on characteristics polynomial of repetitive control systems

APPENDIX A.1

In order to demonstrate the general use of the analytical solution procedure in frequency domain, the procedure is applied to a time-delayed control system. The transfer function of plant is defined as

$$G(s) = G_p(s)e^{-\tau_d s} \quad \textbf{(A.1)}$$

The phase lead compensator is used to control the system. It is given by

$$C(s) = K_c\alpha\frac{\tau s+1}{\alpha\tau s+1} = K_c\alpha C_p(s) \quad \textbf{(A.2)}$$

The controller transfer function without controller gain (unity gain) is

$$C_p(s) = \frac{\tau s+1}{\alpha\tau s+1} \quad \textbf{(A.3)}$$

The desired gain margin of open-loop control system is given by

$$\left|C_p\left(j\omega_{gc1}\right)\left[K_c\alpha G_p\left(j\omega_{gc1}\right)H\left(j\omega_{gc1}\right)\right]\right| = 1 \quad \textbf{(A.4)}$$

The phase of open-loop control system is obtained as

$$\theta = \angle\left(C_p\left(j\omega_{gc1}\right)\right) = \pi + \phi_m + \tau_d\omega - \angle\left(G_p\left(j\omega_{gc1}\right)H\left(j\omega_{gc1}\right)\right) \quad \textbf{(A.5)}$$

From equation (A.4), the statement (A.6) is written

$$\left|C_p\left(j\omega_{gc1}\right)\right| = \frac{1}{K_c\alpha\left|G_p\left(j\omega_{gc1}\right)H\left(j\omega_{gc1}\right)\right|} \quad \textbf{(A.6)}$$

The controller frequency response is calculated as

$$C\left(j\omega_{gc1}\right) = \left|C\left(j\omega_{gc1}\right)\right|e^{j\theta} \quad \textbf{(A.7)}$$

By using equations **(A.6)** and **(A.7)**, the statement seen below is obtained.

$$\frac{1+j\tau\omega_{gc1}}{1+j\alpha\tau\omega_{gc1}} = \frac{1}{K_c\alpha\left|G_p\left(j\omega_{gc1}\right)H\left(j\omega_{gc1}\right)\right|}\left(\cos\theta + j\sin\theta\right) \quad \textbf{(A.8)}$$

The mathematical interferences on statement **(A.8)** are given in equations **(A.9)** and **(A.10)**.

$$K_c\alpha\left|G_p\left(j\omega_{gc1}\right)H\left(j\omega_{gc1}\right)\right|\left(1+j\tau\omega_{gc1}\right) = \left(1+j\alpha\tau\omega_{gc1}\right)\left(\cos\theta+j\sin\theta\right) \quad \textbf{(A.9)}$$

$$K_c\alpha\left|G_p\left(j\omega_{gc1}\right)H\left(j\omega_{gc1}\right)\right|\left(1+j\tau\omega_{gc1}\right) = \left(\cos\theta-\alpha\tau\omega_{gc1}\sin\theta\right)+j\left(\alpha\tau\omega_{gc1}\cos\theta+\sin\theta\right) \quad \textbf{(A.10)}$$

We seperate the statement **(A.10)** into real and imaginary parts which are given by equations **(A.11)** and **(A.12)**.

$$\mathrm{Re}:\cos\theta-\alpha\tau\omega_{gc1}\sin\theta = K_c\alpha\left|G_p\left(j\omega_{gc1}\right)H\left(j\omega_{gc1}\right)\right| \quad \textbf{(A.11)}$$

$$\mathrm{Im}:\alpha\tau\omega_{gc1}\cos\theta+\sin\theta = K_c\alpha\left|G_p\left(j\omega_{gc1}\right)H\left(j\omega_{gc1}\right)\right|\tau\omega_{gc1} \quad \textbf{(A.12)}$$

By solving these two equations, we obtained the two controller parameters seen in **(A.13)** and **(A.14)**.

$$\frac{1}{\alpha\tau} = \frac{\sin\theta}{\cos\theta-K_c\alpha\left|G_p\left(j\omega_{gc1}\right)H\left(j\omega_{gc1}\right)\right|}\omega_{gc1} \quad \textbf{(A.13)}$$

$$\frac{1}{\tau} = \frac{\sin\theta}{\dfrac{1}{K_c\alpha\left|G_p\left(j\omega_{gc1}\right)H\left(j\omega_{gc1}\right)\right|}-\cos\theta}\omega_{gc1} \quad \textbf{(A.14)}$$

APPENDIX A.2

Here, PD controller being the special case of lead compensator is investigated using analytical solution procedure in frequency-domain. The controller transfer function, which is used to control the system **(A.1)**, is given by

$$C(s) = K_p(\tau_d s + 1) = K_d s + K_p \qquad \textbf{(A.15)}$$

The desired gain margin of open-loop control system is given by

$$\left| C(j\omega_{gc1}) \left[G_p(j\omega_{gc1}) H(j\omega_{gc1}) \right] \right| = 1 \qquad \textbf{(A.16)}$$

The phase of open-loop control system is obtained as

$$\theta = \angle\left(C_p(j\omega_{gc1}) \right) = \pi + \phi_m + \tau_d \omega - \angle\left(G_p(j\omega_{gc1}) H(j\omega_{gc1}) \right) \qquad \textbf{(A.17)}$$

From equation **(A.16)**, the statement **(A.18)** is written

$$\left| C(j\omega_{gc1}) \right| = \frac{1}{\left| G_p(j\omega_{gc1}) H(j\omega_{gc1}) \right|} \qquad \textbf{(A.18)}$$

The controller frequency response is calculated as

$$C(j\omega_{gc1}) = \left| C(j\omega_{gc1}) \right| e^{j\theta} \qquad \textbf{(A.19)}$$

By using equations **(A.16)** and **(A.17)**, the statement seen below is obtained.

$$K_p + jK_d\omega_{gc1} = \frac{1}{\left| G_p(j\omega_{gc1}) H(j\omega_{gc1}) \right|} (\cos\theta + j\sin\theta) \qquad \textbf{(A.20)}$$

From the equation **(A.20)**, we obtain the statement seen below.

$$\left| G_p(j\omega_{gc1}) H(j\omega_{gc1}) \right| (K_p + jK_d\omega_{gc1}) = (\cos\theta + j\sin\theta) \qquad \textbf{(A.21)}$$

We seperate the statement **(A.21)** into real and imaginary parts which are given by equations **(A.22)** and **(A.23)**.

$$\mathrm{Re}: K_p \left| G_p(j\omega_{gc1}) H(j\omega_{gc1}) \right| = \cos\theta \qquad \textbf{(A.22)}$$

$$\mathrm{Im}: K_d \left| G_p(j\omega_{gc1}) H(j\omega_{gc1}) \right| \omega_{gc1} = \sin\theta \qquad \textbf{(A.23)}$$

By solving these two equations, we obtained the two controller parameters seen in **(A.24)**, **(A.25)** and **(A.26)**.

$$K_p = \frac{\cos\theta}{\left|G_p\left(j\omega_{gc1}\right)H\left(j\omega_{gc1}\right)\right|} \quad \textbf{(A.24)}$$

$$K_d = \frac{\sin\theta}{\left|G_p\left(j\omega_{gc1}\right)H\left(j\omega_{gc1}\right)\right|\omega_{gc1}} \quad \textbf{(A.25)}$$

$$\tau_d = \frac{\tan\theta}{\omega_{gc1}} \quad \textbf{(A.26)}$$

APPENDIX A.3

In Appendix A.3, we investigate the design of lag compensator by utilizing analytical solution procedure in frequency-domain. The phase lag compensator is used to control the system. It is given by

$$C(s) = K_c\beta \frac{\tau s + 1}{\beta\tau s + 1} = K_c\beta C_p(s) \quad \textbf{(A.27)}$$

The controller transfer function without controller gain (unity gain) is

$$C_p(s) = \frac{\tau s + 1}{\beta\tau s + 1} \quad \textbf{(A.28)}$$

The desired gain margin of open-loop control system is given by

$$\left| C_p\left(j\omega_{gc1}\right)\left[K_c\beta G_p\left(j\omega_{gc1}\right)H\left(j\omega_{gc1}\right)\right]\right| = 1 \quad \textbf{(A.29)}$$

The phase of open-loop control system is obtained as

$$\theta = \angle\left(C_p\left(j\omega_{gc1}\right)\right) = \pi + \phi_m + \tau_d\omega - \angle\left(G_p\left(j\omega_{gc1}\right)H\left(j\omega_{gc1}\right)\right) \quad \textbf{(A.30)}$$

From equation **(A.29)**, the statement **(A.31)** is written

$$\left|C_p\left(j\omega_{gc1}\right)\right| = \frac{1}{K_c\beta\left|G_p\left(j\omega_{gc1}\right)H\left(j\omega_{gc1}\right)\right|} \quad \textbf{(A.31)}$$

The controller frequency response is calculated as

$$C\left(j\omega_{gc1}\right) = \left|C\left(j\omega_{gc1}\right)\right| e^{j\theta} \quad \textbf{(A.32)}$$

By using equations **(A.29)** and **(A.30)**, the statement seen below is obtained.

$$\frac{1 + j\tau\omega_{gc1}}{1 + j\beta\tau\omega_{gc1}} = \frac{1}{K_c\beta\left|G_p\left(j\omega_{gc1}\right)H\left(j\omega_{gc1}\right)\right|}\left(\cos\theta + j\sin\theta\right) \quad \textbf{(A.33)}$$

The mathematical interferences on statement **(A.33)** are given in equations **(A.34)** and **(A.35)**.

$$K_c\beta\left|G_p\left(j\omega_{gc1}\right)H\left(j\omega_{gc1}\right)\right|\left(1 + j\tau\omega_{gc1}\right) = \left(1 + j\beta\tau\omega_{gc1}\right)\left(\cos\theta + j\sin\theta\right) \quad \textbf{(A.34)}$$

$$K_c\beta\left|G_p\left(j\omega_{gc1}\right)H\left(j\omega_{gc1}\right)\right|\left(1+j\tau\omega_{gc1}\right)$$
$$=\left(\cos\theta-\beta\tau\omega_{gc1}\sin\theta\right)+j\left(\beta\tau\omega_{gc1}\cos\theta+\sin\theta\right) \quad \textbf{(A.35)}$$

We seperate the statement **(A.35)** into real and imaginary parts which are given by equations **(A.36)** and **(A.37)**.

$$\mathrm{Re}:\cos\theta-\beta\tau\omega_{gc1}\sin\theta=K_c\beta\left|G_p\left(j\omega_{gc1}\right)H\left(j\omega_{gc1}\right)\right| \quad \textbf{(A.37)}$$

$$\mathrm{Im}:\beta\tau\omega_{gc1}\cos\theta+\sin\theta=K_c\beta\left|G_p\left(j\omega_{gc1}\right)H\left(j\omega_{gc1}\right)\right|\tau\omega_{gc1} \quad \textbf{(A.38)}$$

By solving these two equations, we obtained the two controller parameters seen in **(A.39)** and **(A.40)**.

$$\frac{1}{\beta\tau}=\frac{\sin\theta}{\cos\theta-K_c\beta\left|G_p\left(j\omega_{gc1}\right)H\left(j\omega_{gc1}\right)\right|}\omega_{gc1} \quad \textbf{(A.39)}$$

$$\frac{1}{\tau}=\frac{\sin\theta}{\dfrac{1}{K_c\beta\left|G_p\left(j\omega_{gc1}\right)H\left(j\omega_{gc1}\right)\right|}-\cos\theta}\omega_{gc1} \quad \textbf{(A.40)}$$

APPENDIX A.4

Here, PI controller being the special case of lag compensator is investigated using analytical solution procedure in frequency-domain. The controller transfer function, which is used to control the system **(A.1)**, is given by

$$C(s) = \frac{K_p}{s}\left(s + {}^{1}\!\!\diagup\!\!{}_{\tau_i}\right) = \frac{K_p s + K_i}{s} \qquad \textbf{(A.41)}$$

The desired gain margin of open-loop control system is given by

$$\left|C\left(j\omega_{gc1}\right)\left[G_p\left(j\omega_{gc1}\right)H\left(j\omega_{gc1}\right)\right]\right| = 1 \qquad \textbf{(A.42)}$$

The phase of open-loop control system is obtained as

$$\theta = \angle\left(C_p\left(j\omega_{gc1}\right)\right) = \pi + \phi_m + \tau_d\omega - \angle\left(G_p\left(j\omega_{gc1}\right)H\left(j\omega_{gc1}\right)\right) \qquad \textbf{(A.43)}$$

From equation **(A.42)**, the statement **(A.44)** is written

$$\left|C\left(j\omega_{gc1}\right)\right| = \frac{1}{\left|G_p\left(j\omega_{gc1}\right)H\left(j\omega_{gc1}\right)\right|} \qquad \textbf{(A.44)}$$

The controller frequency response is calculated as

$$C\left(j\omega_{gc1}\right) = \left|C\left(j\omega_{gc1}\right)\right|e^{j\theta} \qquad \textbf{(A.45)}$$

By using equations **(A.42)** and **(A.43)**, the statement seen below is obtained.

$$\frac{K_i + jK_p\omega_{gc1}}{j\omega_{gc1}} = \frac{1}{\left|G_p\left(j\omega_{gc1}\right)H\left(j\omega_{gc1}\right)\right|}\left(\cos\theta + j\sin\theta\right) \qquad \textbf{(A.46)}$$

From the equation **(A.20)**, we obtain the statement seen below.

$$\left|G_p\left(j\omega_{gc1}\right)H\left(j\omega_{gc1}\right)\right|\left(K_i + jK_p\omega_{gc1}\right) = j\omega_{gc1}\left(\cos\theta + j\sin\theta\right) \qquad \textbf{(A.47)}$$

$$\left|G_p\left(j\omega_{gc1}\right)H\left(j\omega_{gc1}\right)\right|\left(K_i + jK_p\omega_{gc1}\right) = \left(-\omega_{gc1}\sin\theta + j\omega_{gc1}\cos\theta\right) \qquad \textbf{(A.48)}$$

We seperate the statement **(A.48)** into real and imaginary parts which are given by equations **(A.49)** and **(A.50)**.

$$\mathrm{Re}: K_i\left|G_p\left(j\omega_{gc1}\right)H\left(j\omega_{gc1}\right)\right| = -\omega_{gc1}\sin\theta \qquad \textbf{(A.49)}$$

$$\mathrm{Im}: K_p \omega_{gc1} \left| G_p\left(j\omega_{gc1}\right) H\left(j\omega_{gc1}\right) \right| = \omega_{gc1} \cos\theta \qquad \textbf{(A.50)}$$

By solving these two equations, we obtained the two controller parameters seen in **(A.50)**, **(A.51)** and **(A.52)**.

$$K_p = \frac{\cos\theta}{\left| G_p\left(j\omega_{gc1}\right) H\left(j\omega_{gc1}\right) \right|} \qquad \textbf{(A.51)}$$

$$K_i = -\frac{\sin\theta}{\left| G_p\left(j\omega_{gc1}\right) H\left(j\omega_{gc1}\right) \right|} \omega_{gc1} \qquad \textbf{(A.52)}$$

$$\frac{1}{\tau_i} = -\tan\theta\, \omega_{gc1} \qquad \textbf{(A.53)}$$

APPENDIX A.5

Here, PID controller being the special case of lead-lag compensator is investigated using analytical solution procedure in frequency-domain. The controller transfer function, which is used to control the system **(A.1)**, is given by

$$C(s)=\frac{K_p}{s}\left(\tau_d s^2+s+{}^{1}\!/\!_{\tau_i}\right)=\frac{K_d s^2+K_p s+K_i}{s} \qquad \textbf{(A.54)}$$

The desired gain margin of open-loop control system is given by

$$\left|C\left(j\omega_{gc1}\right)\left[G_p\left(j\omega_{gc1}\right)H\left(j\omega_{gc1}\right)\right]\right|=1 \qquad \textbf{(A.55)}$$

The phase of open-loop control system is obtained as

$$\theta=\angle\left(C_p\left(j\omega_{gc1}\right)\right)=\pi+\phi_m+\tau_d\omega-\angle\left(G_p\left(j\omega_{gc1}\right)H\left(j\omega_{gc1}\right)\right) \qquad \textbf{(A.56)}$$

From equation **(A.55)**, the statement **(A.57)** is written

$$\left|C\left(j\omega_{gc1}\right)\right|=\frac{1}{\left|G_p\left(j\omega_{gc1}\right)H\left(j\omega_{gc1}\right)\right|} \qquad \textbf{(A.57)}$$

The controller frequency response is calculated as

$$C\left(j\omega_{gc1}\right)=\left|C\left(j\omega_{gc1}\right)\right|e^{j\theta} \qquad \textbf{(A.58)}$$

By using equations **(A.55)** and **(A.56)**, the statement seen below is obtained.

$$\frac{\left(K_i-K_d\omega_{gc1}^2\right)+jK_p\omega_{gc1}}{j\omega_{gc1}}=\frac{1}{\left|G_p\left(j\omega_{gc1}\right)H\left(j\omega_{gc1}\right)\right|}\left(\cos\theta+j\sin\theta\right) \qquad \textbf{(A.59)}$$

From the equation **(A.20)**, we obtain the statement seen below.

$$\left|G_p\left(j\omega_{gc1}\right)H\left(j\omega_{gc1}\right)\right|\left[\left(K_i-K_d\omega_{gc1}^2\right)+jK_p\omega_{gc1}\right]=j\omega_{gc1}\left(\cos\theta+j\sin\theta\right) \qquad \textbf{(A.60)}$$

$$\left|G_p\left(j\omega_{gc1}\right)H\left(j\omega_{gc1}\right)\right|\left[\left(K_i-K_d\omega_{gc1}^2\right)+jK_p\omega_{gc1}\right]=\left(-\omega_{gc1}\sin\theta+j\omega_{gc1}\cos\theta\right) \qquad \textbf{(A.61)}$$

We seperate the statement **(A.61)** into real and imaginary parts which are given by equations **(A.62)** and **(A.63)**.

$$\mathrm{Re}:\left(K_i - K_d\omega_{gc1}^2\right)\left|G_p\left(j\omega_{gc1}\right)H\left(j\omega_{gc1}\right)\right| = -\omega_{gc1}\sin\theta \qquad \textbf{(A.62)}$$

$$\mathrm{Im}: K_p\omega_{gc1}\left|G_p\left(j\omega_{gc1}\right)H\left(j\omega_{gc1}\right)\right| = \omega_{gc1}\cos\theta \qquad \textbf{(A.63)}$$

By solving these two equations, we obtained the two controller parameters seen in **(A.64)** and **(A.65)**.

$$K_i - K_d\omega_{gc1}^2 = -\frac{\sin\theta}{\left|G_p\left(j\omega_{gc1}\right)H\left(j\omega_{gc1}\right)\right|}\omega_{gc1} \qquad \textbf{(A.64)}$$

$$K_p = \frac{\cos\theta}{\left|G_p\left(j\omega_{gc1}\right)H\left(j\omega_{gc1}\right)\right|} \qquad \textbf{(A.65)}$$

We have three independent variables and just two equations. For this reason, we should eliminate the one of independent variables. If we define $K_d=\alpha K_i$, the number of independent variables can reduce.

$$K_i = \frac{\sin\theta}{\left(\alpha\omega_{gc1}^2 - 1\right)\left|G_p\left(j\omega_{gc1}\right)H\left(j\omega_{gc1}\right)\right|}\omega_{gc1} \qquad \textbf{(A.66)}$$

APPENDIX B

The nonlinear single track model, also called the bicycle model is shown in Figure B.1. The single track vehicle model captures the lateral dynamics of a road vehicle quite accurately in handling maneuvers where lateral acceleration does not exceed 0.3g.

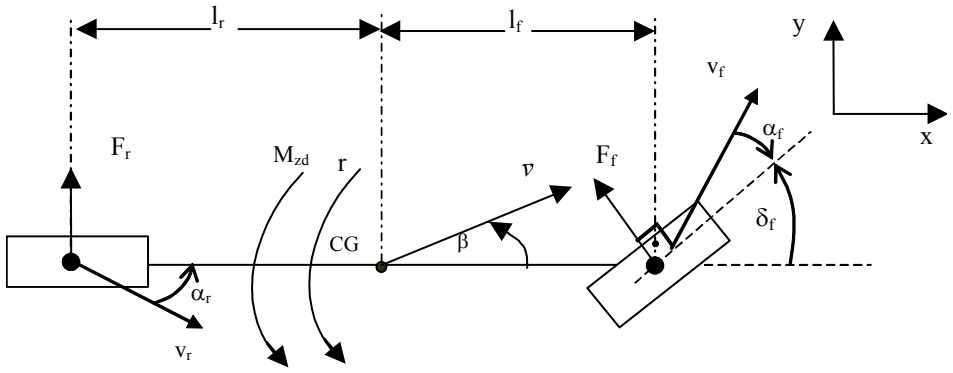

Figure B.1: Geometry of the single track vehicle model.

The nomenclature used in defining the major variables and geometric parameters of the single track are given in Table B.1.

The nonlinear single track model is characterized by the force coordinate transformation due to steering angle projection given by [6]:

$$\begin{bmatrix} \sum F_x \\ \sum F_y \\ \sum M_z \end{bmatrix} = \begin{bmatrix} -\sin\delta_f & -\sin\delta_r \\ \cos\delta_f & \cos\delta_r \\ l_f\cos\delta_f & -l_r\cos\delta_r \end{bmatrix} \begin{bmatrix} F_f \\ F_r \end{bmatrix} \qquad \textbf{(B.1)}$$

the dynamics equations

$$\begin{bmatrix} mv(\dot{\beta}+r) \\ m\dot{v} \\ I_z\dot{r} \end{bmatrix} = \begin{bmatrix} -\sin\beta & \cos\beta & 0 \\ \cos\beta & \sin\beta & 0 \\ 0 & 0 & 1 \end{bmatrix} \begin{bmatrix} \sum F_x \\ \sum F_y \\ \sum M_z \end{bmatrix} \qquad \textbf{(B.2)}$$

and the equations of kinematics/geometry

$$\tan\beta_f = \tan\beta + \frac{l_f r}{v\cos\beta} \qquad \textbf{(B.3)}$$

$$\tan \beta_r = \tan \beta - \frac{l_r r}{v \cos \beta} \qquad \textbf{(B.4)}$$

Table B.1: Steering system parameters.

Parameter	Explanation
F_f (F_r)	Lateral wheel force at front (rear) wheel
M_{zd}	Yaw disturbance moment
r	Yaw rate
β	Chassis side slip angle at vehicle centre of gravity
α_f (α_r)	Front (rear) tire side slip angle
V	Vehicle speed at centre of gravity point
l_f (l_r)	Distance from front (rear) axle to centre of gravity
δ_f	Front wheel steering angle
m	The mass of the vehicle
I_z	The moment of inertia wrt a vertical axis through the centre of gravity
c_f (c_r)	Front (rear) wheel cornering stiffness
μ	Road friction coefficient

The tire longitudinal forces F_f and F_r are nonlinear functions of the corresponding side slip angles α_f and α_r. F_f and F_r also depend on the friction characteristics between the road and the tires. The nonlinear single track model is illustrated in the top part of the block diagram of Figure B.2 while its linearized version is shown in the bottom part of the same figure.

The nonlinear single track model is linearized assuming small steering angles δ_f and small side slip angle β. The tire force characteristics are linearized as

$$F_f(\alpha_f) = \mu C_{f0} \alpha_f = C_f \alpha_f, \quad F_r(\alpha_r) = \mu C_{r0} \alpha_r = C_r \alpha_r \qquad \textbf{(B.5)}$$

with the tire cornering stiffnesses C_f, C_r the road-tire friction coefficient μ and the tire side slip angles given by

$$\alpha_f = \delta_f - \left(\beta + \frac{l_f}{v} r \right) \qquad \textbf{(B.6)}$$

$$\alpha_r = -\left(\beta - \frac{l_r}{v} r \right) \qquad \textbf{(B.7)}$$

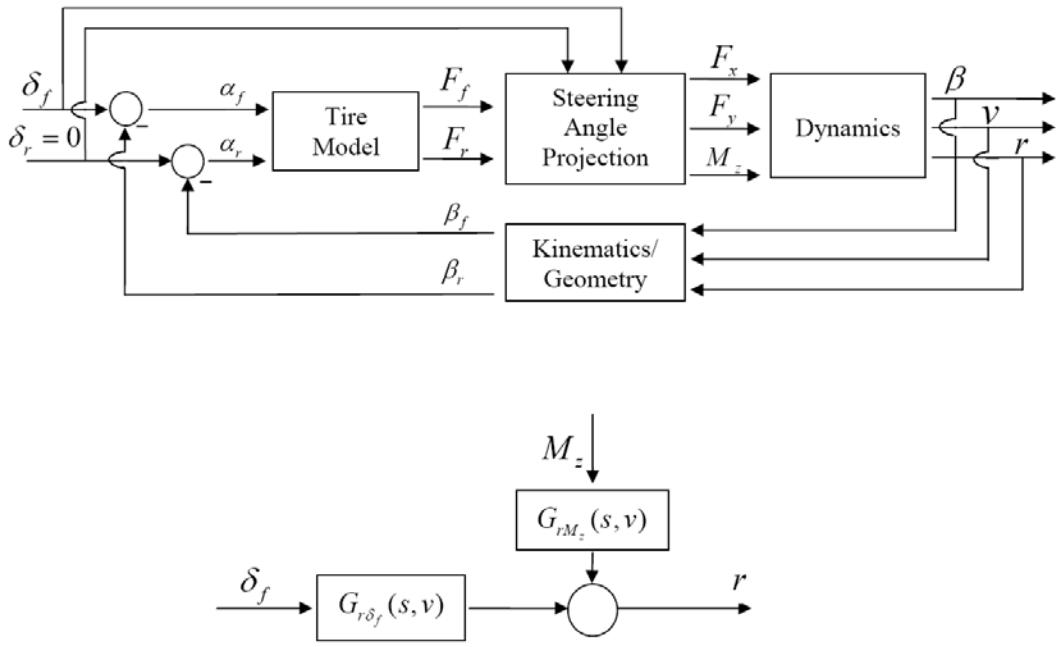

Figure B.2 : Nonlinear (top) and linearized (bottom) single track model block diagrams.

Note that C_{f0} and C_{r0} in **(B.5)** are the nominal values for dry road ($\mu = \mu_n = 1$) of the tire cornering stiffnesses. The transfer function from the front wheel steering angle δ_f to the yaw rate r is given by:

$$G_{r\delta_f}(s,v) = \frac{r(s)}{\delta_f(s)} = \frac{b_1(v)s + b_0(v)}{a_2(v)s^2 + a_1(v)s + a_0(v)} \qquad \textbf{(B.8)}$$

with

$$\begin{aligned} b_0 &= c_f c_r (l_f + l_r) v \\ b_1 &= c_f l_f m v^2 \\ a_0 &= c_f c_r (l_f + l_r)^2 + (c_r l_r - c_f l_f) m v^2 \\ a_1 &= (c_f (I_z + l_f^2 m) + c_r (I_z + l_r^2 m)) v \\ a_2 &= I_z m v^2 \end{aligned} \qquad \textbf{(B.9)}$$

$G_{r\delta f}(s,v)$ in **(B.8)** is also called the steering wheel input response transfer function here. The d.c. gain of the nominal single track model **(B.8)** is

$$K_n(v) = \lim_{s \to 0} G_{r\delta_f}(s,v)\Big|_{\mu=\mu_n=1} \qquad \textbf{(B.10)}$$

at the chosen longitudinal speed v and for $\mu = \mu_n = 1$.

APPENDIX C

The transfer function of the repetitive controller given in Figure 6.1 is obtianed below

$$G_c(s) = 1 + \frac{b(s)q(s)e^{-\tau_d s}}{1 - q(s)e^{-\tau_d s}} \qquad \textbf{(C.1)}$$

By making some mathematical operations, the statement seen in equation **(C.2)** is obtained as

$$G_c(s) = \frac{1 - qe^{-\tau_d s} + bqe^{-\tau_d s}}{1 - e^{-\tau_d s}} = \frac{1 + (b-1)qe^{-\tau_d s}}{1 - qe^{-\tau_d s}} \qquad \textbf{(C.2)}$$

The transfer function of closed loop system is obtained below.

$$G(s) = \frac{G_c(s)G_p(s)}{1 + G_c(s)G_p(s)} \qquad \textbf{(C.3)}$$

By inserting the statement of repetitive controller obtained in equation **(C.2)** into equation **(C.3)**, the statements seen in equation **(C.4)** and **(C.5)** are figured out.

$$G(s) = \frac{\dfrac{1 + (b-1)qe^{-\tau_d s}}{1 - qe^{-\tau_d s}} G_p(s)}{1 + \dfrac{1 + (b-1)qe^{-\tau_d s}}{1 - qe^{-\tau_d s}} G_p(s)} \qquad \textbf{(C.4)}$$

$$\begin{aligned} G(s) &= \frac{\left[1 + (b-1)qe^{-\tau_d s}\right]G_p(s)}{1 - qe^{-\tau_d s} + \left[1 + (b-1)qe^{-\tau_d s}\right]G_p(s)} \\ &= \frac{\left[1 + (b-1)qe^{-\tau_d s}\right]G_p(s)}{1 + G_p(s) - \left[1 + G_p(s) - bG_p(s)\right]qe^{-\tau_d s}} \end{aligned} \qquad \textbf{(C.5)}$$

At the end of the mathematical operations, the transfer function seen below is found out.

$$G(s) = \frac{\left(1 + (b-1)qe^{-\tau_d s}\right)\dfrac{G_p(s)}{1 + G_p(s)}}{1 - q\left(1 - b\dfrac{G_p(s)}{1 + G_p(s)}\right)e^{-\tau_d s}} \qquad \textbf{(C.6)}$$

$$G(s)=\frac{\left(1-(1-b)qe^{-\tau_d s}\right)G_{cl}}{1-\underbrace{q(1-bG_{cl})}_{R(\omega)}e^{-\tau_d s}} \quad \textbf{(C.7)}$$

The characteristic polynomial is seen of system is seen in equation **(C.7)**.

$$\delta(s)=1-q(s)\left(1-b(s)\frac{G_p(s)}{1+G_p(s)}\right)e^{-\tau_d s} \quad \textbf{(C.8)}$$

CURRICULUM VITA

Candidate's full name: Burak DEMİREL

Place and date of birth: İstanbul, 20/12/1984

Permanent Address: İ.T.Ü. Makina Fakültesi, İnönü Caddesi, No: 87, Oda No: 241, Gümüşsuyu, İstanbul, 34437

Universities and Colleges attended:

İstanbul Technical University

B.Sc. Mechanical Engineering (2002-2007)

İstanbul Technical University

B.Sc. Control Engineering (2004-2009)

İstanbul Technical University

M.Sc. Mechatronics Engineering (2007-2009)

Publications:

- **Demirel B.**, Erol O. K., and Eksin İ., Enhancing the Big Bang Big Crunch Optimization Method via Local Search Initialization Algorithm, *Advances in Engineering Software* (*to be submitted*)
- **Demirel B.**, Güvenç L., Parameter Space Design of Repetitive Controllers for Satisfying a mixed sensitivity Performance Requirement, *IEEE Transactions on Automatic Control* (*to be submitted*).
- **Demirel B.**, Emirler M.T., Sönmez Ü., and Yörükoğlu A., Compliant Force Generator Mechanism Synthesis for a Required Impact and Contact Force, *ASME Journal of Mechanism and Robotics* (*to be submitted*).
- **Demirel B.**, Emirler M.T., Yörükoğlu A., Koca N., and Sönmez Ü., 2008: Compliant Impact Generator for Required Impact and Contact Force, ASME International Mechanical Engineering Congress and Exposition, Boston, MA, October 31 – November 06.